

Spatial characteristics of brightness and apparent-contrast perception

Citation for published version (APA):

du Buf, J. M. H. (1987). *Spatial characteristics of brightness and apparent-contrast perception*. [Phd Thesis 1 (Research TU/e / Graduation TU/e), Industrial Engineering and Innovation Sciences]. Technische Universiteit Eindhoven. <https://doi.org/10.6100/IR272991>

DOI:

[10.6100/IR272991](https://doi.org/10.6100/IR272991)

Document status and date:

Published: 01/01/1987

Document Version:

Publisher's PDF, also known as Version of Record (includes final page, issue and volume numbers)

Please check the document version of this publication:

- A submitted manuscript is the version of the article upon submission and before peer-review. There can be important differences between the submitted version and the official published version of record. People interested in the research are advised to contact the author for the final version of the publication, or visit the DOI to the publisher's website.
- The final author version and the galley proof are versions of the publication after peer review.
- The final published version features the final layout of the paper including the volume, issue and page numbers.

[Link to publication](#)

General rights

Copyright and moral rights for the publications made accessible in the public portal are retained by the authors and/or other copyright owners and it is a condition of accessing publications that users recognise and abide by the legal requirements associated with these rights.

- Users may download and print one copy of any publication from the public portal for the purpose of private study or research.
- You may not further distribute the material or use it for any profit-making activity or commercial gain
- You may freely distribute the URL identifying the publication in the public portal.

If the publication is distributed under the terms of Article 25fa of the Dutch Copyright Act, indicated by the "Taverne" license above, please follow below link for the End User Agreement:

www.tue.nl/taverne

Take down policy

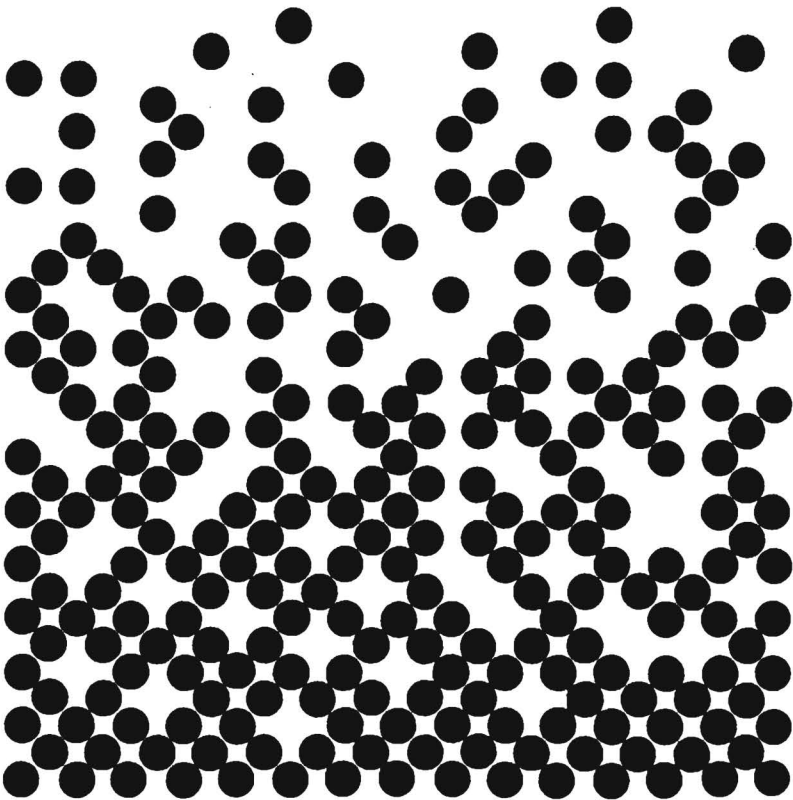
If you believe that this document breaches copyright please contact us at:

openaccess@tue.nl

providing details and we will investigate your claim.

Spatial Characteristics of Brightness and Apparent-contrast Perception

J.M.H. du Buf



Spatial characteristics of brightness and apparent-contrast perception

Proefschrift

ter verkrijging van de graad van doctor aan de
Technische Universiteit Eindhoven, op gezag van de
rector magnificus, prof. dr. F.N. Hooge, voor een
commissie aangewezen door het college van dekanen in
het openbaar te verdedigen op dinsdag 3 november 1987
te 16.00 uur

door

Johannes Martinus Hubertina du Buf

geboren te Venlo

Dit proefschrift is goedgekeurd door de promotoren

Prof. Dr. Ir. J.A.J. Roufs

en

Prof. Dr. H. Bouma

Dit onderzoek werd uitgevoerd aan het Instituut voor Perceptie Onderzoek (IPO) te Eindhoven, en werd financieel gesteund door de Stichting Biofysica van de Nederlandse Organisatie voor Zuiver Wetenschappelijk Onderzoek (ZWO).

Met dank aan de leden van de Visuele Groep, alle stagiairs en studentassistenten in het bijzonder, voor hun steun en medewerking.

Hein's Law:

Problems worthy of attack prove their worth by hitting back.

Riddle's Constant:

There are coexisting elements in frustration phenomena which separate expected results from achieved results.

Paul Dickson

The official rules

Dell Publishing Co., Inc., New York, 1978

Contents

1	Introduction	1
2	Brightness matching and scaling compared	7
3	Large-field asymmetry in brightness and apparent-contrast perception	31
4	Brightness and apparent-contrast perception of incremental and decremental disks with varying diameter	49
5	Brightness and apparent-contrast perception of blurred disks and circular cosine gratings	71
6	Detection symmetry and asymmetry	87
7	Apparent contrast of noise gratings	101
8	On modelling spatial vision at threshold level	117
	References	147
	Summary	157
	Samenvatting	160
	Curriculum vitae	165

1 Introduction

Despite the fact that psychologists and psychophysicists started to investigate perception more than a century ago and despite the vast amount of available literature, our present insight into the neural mechanism that is able to map the external world into its perceived image shows quite some unsolved gaps¹. This also holds for achromatic spatial vision, the specific part of vision research this thesis is addressed to.

Much effort has been invested in vision at threshold level. This type of research has resulted in several detection models. Quantitative indeed, but with limited validity. Most of these are dedicated to the detection of simple one-dimensional patterns such as sinewave gratings with varying spatial frequency. They are assumed to be composed of multiple line spread functions named channels. Although line spread functions under certain conditions can be reduced to point spread functions mathematically, thus enabling an analysis of more local or two-dimensional patterns, physiological data on retinal receptive field profiles suggest that a conscious choice for modelling based on radially symmetric spread functions may be propitious.

Suprathreshold perception, important with regard to our performance in everyday visual tasks, has received less attention, probably because of the nonlinearities that hamper a straight-forward application of linear system theory to vision. This difficulty is reflected by the availability of - to our knowledge - only a single spatial model that is able to describe data on threshold as well as suprathreshold perception of sinewave-like gratings. Furthermore, this model is merely an extension of the one-dimensional detection models: it consists of line spread functions cascaded by nonlinear amplitude transfer functions.

History

The evolution of visual psychophysics can be illustrated by following two apparently independent paths which correspond to different experimental methods. The first one is the measurement of sensation strengths directly attributed to some physical amplitude. It is usually performed by keeping the spatial properties of the stimulus in study invariable although the procedure can be repeated for different spatial parameters. This method involves the use of scaling techniques such as magnitude estimation. The second method is based on matching the sensation strengths of stimuli differing in their spatial properties, including the determination of detection thresholds as a special case. Matching by adjusting the physical

¹Recent and profound expositions are presented by De Valois and De Valois (1980), Julesz and Schumer (1981) and Kelly and Burbeck (1984).

amplitude of test stimuli until their sensation strength equals that of a fixed reference stimulus, as a function of the spatial property, can be repeated for different amplitudes of the reference. Although the method of directly matching is commonly applied, it should be emphasized that a point of subjective equality does not exist: there is merely a bounded amplitude interval characterized by an incremental and a decremental just noticeable difference. Consequently, matching can be considered as a special case of threshold detection.

Early manuscripts written by Fechner, Plateau and Brentano date from around 1870. In these the exact nature of the brightness-luminance relationship was discussed. For a concise historic review see Stevens (1961). Fechner's logarithmic relation, often referred to as Weber-Fechner's law, has been preferred for quite a long period, though the plea seems to be settled now in favour of Stevens' power relation (Marks, 1974; Stevens, 1975). Both can be brought into relation with just noticeable differences (JND's). They can be derived from measured JND's in the physical domain, if these data are combined with appropriate assumptions with respect to JND's in the sensory domain and Fechnerian integration is applied. The latter assumptions, which state that JND's in perceived brightness are constant (Fechner) or proportional to the brightness level that they are superimposed on (Brentano), can be questioned, although Ekman (1956) seems to have established the empirical generality of Brentano's conjecture². Despite the fact that Fechner himself (in 1860!) recognized the two alternative possibilities, the arisen controversy between Fechnerians and Stevens supporters has led to quite some discussion in mathematical psychology (Luce and Edwards, 1958; Ekman, 1964; Wagenaar, 1975). Anyhow, a major role in the acceptance of Stevens' power law was played by the availability of the psychophysical method of magnitude estimation. Although similar methods were applied before - Hipparchus (150 B.C.) introduced a 6-point category scale of stellar magnitudes, while Richardson (1929) used a 100-point category scale in judging coloured papers - scaling experiments became en vogue after 1953 when Stevens (1975) proposed to use a single standard. Magnitude estimation was thought to enable fast and direct determinations of the so-called Stevens exponents. Its validity could be demonstrated by the general agreement with respect to the brightness perception of aperiodic stimuli. Such patterns are, amongst others, circular fields with certain diameter and homogeneous luminance (disks) which can be presented with varying duration against a large background. Experimental results indicate that the Stevens exponent varies between 0.33 for a large, long-duration disk and 1 for a small, short-duration one. These values relate to perceived brightness at a dark background (Mansfield, 1973). In addition, the Stevens exponent of a large, long-duration stimulus is reported to increase

²Stevens (1966) proposed Brentano's conjecture, being the subjective counterpart of Weber's law, to be called Ekman's law.

from 0.33 at a dark background to approximately 0.5 at photopic background levels (Stevens and Stevens, 1960; Onley, 1961; Warren, 1976). But how about periodic stimulus patterns? Contrary to the disk situation, no general agreement has been reached with respect to the apparent-contrast perception of sinewave gratings. All types of Stevens relations have been reported: linear and nonlinear, frequency-independent and frequency-dependent (Franzén and Berkley, 1975; Cannon, 1980; Gottesman et al., 1981; Biondini and Mattiello, 1985; Cannon, 1985; Quinn, 1985). Indeed, there appears to exist some literature in which the validity of magnitude estimation as a scaling method is questioned. One reason for the rejection of magnitude estimation consists of the nonlinear and individual way in which subjects handle numbers, i.e. map the magnitude of for instance perceived brightness into decimal numbers (Curtis, 1970; Saunders, 1972; Bartleson and Breneman, 1973). It was demonstrated that subjects can be classed within several groups, each having quite different response scales. The commonly practiced approach of averaging the experimental results obtained by large groups of subjects is supposed to determine the final result in advance on account of the composition of the group. Another reason to question the validity of magnitude estimation is based on the observation that responses are biased by the interval of the stimuli and the position of the standard within this interval (Poulton, 1979; Teghtsoonian, 1973).

The evolution of research based on matching experiments and the determination of detection thresholds illustrates the rise and fall of the application of linear system theory to vision. The notion that, in analogy to passive optics, our visual system can be regarded as a simple linear spatial filter predominated this type of research for several decades. Selwyn (1948) and Schade (1948) found that the modulation depth of a sinewave grating, required for detection, increased for lower frequencies. This differentiating action was soon contributed to the neural processing, and the reciprocal threshold curve for sinewave gratings, the contrast sensitivity function or CSF, was regarded to reflect the bandpass modulation transfer function of the visual system. Convolution with a line spread function, being the CSF's Fourier transform, was adopted to explain detection thresholds of other one-dimensional patterns (DePalma and Lowry, 1962; Campbell and Robson, 1968; Campbell et al., 1969). The CSF and its line spread function were even brought into relation with the Mach-band phenomenon, which can be observed from suprathreshold luminance edges (Lowry and DePalma, 1961a,b; Ratliff, 1965). The application of such straight-forward considerations in modelling spatial vision came to an end in consequence of two independent though simultaneous developments.

Matching data, as a suprathreshold supplement to detection thresholds, became available. Hanes (1951) measured iso-brightness curves of disk-shaped stimuli, with varying diameter, presented against a dark background. His experiment

was repeated by Glezer (1965) and by Hay and Chesters (1972), and extended to incremental disks on higher background levels by Higgins and Rinalducci (1975). The one-dimensional alternative, i.e. matching of sinewave gratings with varying spatial frequency, was also considered (Watanabe et al., 1968; Georgeson and Sullivan, 1975). The modulation-threshold curve of gratings, if presented against a photopic background, suggests a band-pass characteristic, while apparent iso-contrast curves tend to show a low-pass characteristic for increasing reference levels. These data conclusively demonstrate the fundamental nonlinearity of our visual system. Moreover, grating data appear to conflict with disk data, since the latter suggest an exactly opposite behaviour of the visual system: low-pass at threshold and band-pass at suprathreshold levels (Higgins and Rinalducci, 1975). It is therefore not surprising that simple nonlinear parametric models, in which the shape of a point spread function is derived in such a way that for instance disk data are fitted, do not simultaneously agree with grating data (Furukawa and Hagiwara, 1978).

The second development was inaugurated by physiologically achieved insight. It was shown that the retina of primates and vertebrate animals contains a structured set of receptive fields, each with an excitative centre and an inhibitive surround. These fields sample the retinal image and transmit the information thus coded to similar though more elongated, almost one-dimensional fields in the visual cortex. The existence of such fields was also psychophysically verified. Blakemore and Campbell (1969) found that preadaptation raises the detection thresholds of gratings in a narrow frequency band, while Bagrash (1973) demonstrated the same effect for disk-shaped stimuli. As a result of this knowledge, confirmed by many other psychophysical studies (e.g Olzak and Thomas, 1986), a system of size- or frequency-selective mechanisms was incorporated into detection models (MacLeod and Rosenfeld, 1974; Legéndy, 1975; Wilson and Bergen, 1979; Bergen et al., 1979; Jaschinsky-Kruza and Cavonius, 1984). In addition, the perceived contrast of suprathreshold gratings was also demonstrated to depend on preadaptation (Blakemore et al., 1973) and a single multiple channel model that is able to predict threshold as well as suprathreshold grating perception has been advanced (Swanson et al., 1984).

Scope

Some issues of the present thesis emerged directly from the foregoing. The first is the consistency between scaling data on the one hand and matching data on the other (chapter 2). If Stevens' power relation is accepted as a valid description of the relation between a physical and its perceived entity, then a combination of the magnitude estimation data obtained with two different stimuli should agree with direct matching results. The proof of this hypothesis depends also on the

validity of matching data (transitivity). Besides, Stevens exponents determined by magnitude estimation should agree with those obtained by applying other scaling techniques. Bisection and fractionation are perhaps scaling techniques less obscured by the way subjects handle numbers.

More complicated is the simultaneous explanation of matching and detection data obtained with fairly different types of stimulus patterns, such as periodic and aperiodic ones, by using multichannel models dominating contemporary research (chapters 5 and 8). A quantitative comparison of different data sets is enabled provided that they are measured under equal experimental conditions (monocular foveal viewing, hue, background level, temporal modulation of the spatial patterns). It should be obvious that the construction of a nonlinear single or multiple channel model from a single set of matching curves at various reference levels is merely a straight-forward (although nonlinear) data fitting problem. If these data refer to a one-dimensional periodic stimulus type, such as sinewave gratings, the prediction of data on similar stimuli might be a rather insensitive test. The ultimate test would be the prediction of two-dimensional aperiodic data, obtained by matching for instance disks with varying diameter.

Evidence is found for the existence of antagonistic centre-on and centre-off receptive fields, which at least suggests the possibility that luminance increments and decrements are processed or transmitted by different, perhaps even asymmetrical, neural networks. This intriguing idea invites for a psychophysical verification by matching incremental disks with varying diameter as well as decremental ones, all presented against the same background (chapters 3 and 4). Besides, the results of this experiment should be brought into relation with the perception of sinewave gratings, since these consist of simultaneously presented luminance increments and decrements (chapters 5 and 6).

This connects to one of the main points of this thesis: the influence of different perceptual attributes that can be used as a matching criterion (chapters 3, 4 and 5). The Mach-band effect, a well-known phenomenon with one-dimensional luminance edges, can also be observed from disk-shaped stimuli, be it less pronounced. This observation leads to the introduction of an exact definition of the subject's task. Matching either the local brightness in the centre of disks with varying diameter or the brightness maximum at the inner edge is expected to render different results. In addition, the global perception of a nonuniform brightness pattern as a whole, which involves the apparent or brightness contrast, can be considered. Observing a luminous disk against a homogeneous and vast background, one feels that the way in which the disk contrasts with its surround can be judged directly, without looking at spatial details, and that this percept is as dominant as the brightnesses of disk and surround separately. A similar observation holds for gratings, where positive phases contrast with negative ones. Matching either the brightness extremes or the apparent contrast of sinewave gratings with vary-

ing frequency provides us with information about the nature of apparent-contrast perception, and its relation with brightness perception in particular. A similar approach can be applied to blurred edges. Degrading the edge sharpness, by accurately changing the luminance profile, provides additional information about brightness and apparent contrast in relation to luminance gradients.

All experiments proposed so far involve deterministic stimulus types. Results obtained with these fairly abstract stimuli, and eventually derived models in particular, should be applicable to everyday perception of complex scenes, which only exceptionally contain such patterns. The large gap between abstract, deterministic stimuli and complex scenes may be bridged by studying the apparent-contrast perception of noise gratings (chapter 7). Such patterns, to be defined by their amplitude spectrum in the frequency domain, provide a stochastic brightness pattern. As for deterministic brightness patterns, it may be expected that they evoke an unambiguous apparent-contrast sensation which dominates the fuzzy and unimportant local brightness information.

Finally, there is one point which needs to be emphasized. All data to be presented have been gathered by using a single subject. Experimental effort can be utilized by following two strategies: either many subjects with few experimental conditions or few subjects with many conditions. The first approach emphasizes the study of the ensemble behaviour. Here a conscious choice for the second approach has been made: as the key problem addressed concerns the difference and relation between different but related perceptual attributes, as well as the modelling of threshold and suprathreshold spatial vision, the quantitative comparison of various experimental results is of importance. Since the data reflect the visual processing of a single subject, this means that care should be exercised in generalizing. However, all chapters include, by way of precaution, experiments that allow for a comparison with already published results. These data, where comparable, show that the subject is rather representative.

2 Brightness Matching and Scaling Compared

Abstract

The perception of brightness increments of disk-shaped stimuli, with various diameters and durations presented against a uniform, photopic background, has been studied. Both brightness matching and scaling methods, i.e. magnitude estimation, bisection and fractionation, have been applied by the same subject. Transitivity was shown to hold reasonably well for brightness matching. Matching and scaling, in particular bisection and fractionation, are mutually consistent in the sense that the exponents of Stevens' power functions, which describe brightness increments as a function of luminance increments, in case of scaling, and the ratios of these exponents in case of matching, correspond. Differences between scaling results were attributed to differences in the strategy of the subject. Results indicate that brightness exponents for large, long duration stimuli as well as small, short duration stimuli are affected by the background level. Furthermore, exponents of small stimuli are shown to depend on the position in the fovea. Lastly, it is suggested that the just noticeable brightness difference in sequential observation is proportional to the luminance increment of the stimulus to be judged.

2.1 Introduction

The compressive, nonlinear relation between (subjective) brightness B and (physical) luminance L is usually assumed to obey Stevens' law: $B = k(L - L_{threshold})^\beta$. This relation has often been studied for stimuli presented against a dark background (e.g. Mansfield, 1973; Marks, 1974; Stevens, 1975). Because of its rapidity and simplicity, mainly magnitude estimation has been used, the results being averaged over large groups of subjects. In magnitude estimation experiments, subjects are instructed to generate numbers rating the perceived brightness, i.e. in ratio with an internal or external reference. During the last decades, the validity of magnitude estimation as a scaling method has been doubted because of the nonlinear way in which subjects handle numbers (Poulton, 1968; Curtis et al., 1968; Saunders, 1972; Bartleson and Breneman, 1973; Wagenaar, 1975). Relatively few investigations concerned with brightness perception have relied on alternative scaling methods such as bisection and fractionation, where subjects are asked to consider subjective intervals rather than absolute magnitudes. Moreover, brightness exponents determined by bisection and fractionation are reported to vary across subjects and reference intervals (Stewart et al., 1967). A further problem arises from the frequent use of a dark background, where superimposed high-luminance stimuli disturb the state of adaptation. Besides, everyday observation takes place at photopic levels of illumination. There is substantial evidence that brightness exponents tend to increase at higher background levels (Stevens and Stevens, 1960;

Onley, 1961; Warren, 1976): the generally accepted brightness exponent of $\beta = 1/3$ for large, long duration fields presented against a dark background tends towards $\beta = 1/2$ at photopic backgrounds.

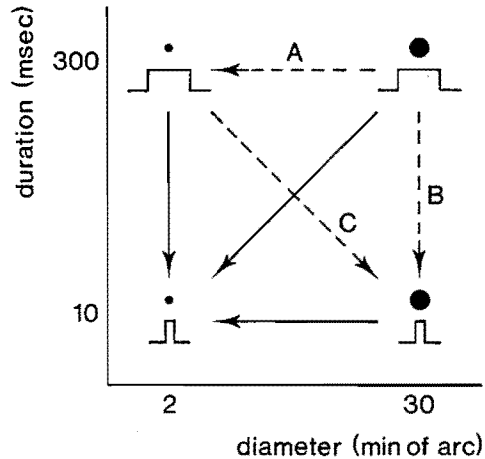


Figure 1: A schematic reproduction of the stimuli. Stimulus combinations are denoted by arrows, in order to define test and reference stimuli in the matching experiments unambiguously. These arrows point towards references.

The present study is concerned with the relation between brightness and luminance increments presented against a photopic background. Diameters and durations of the stimuli were chosen outside the spatio-temporal domain that is known to produce a suprathreshold Broca-Sulzer effect¹ (Rinalducci and Higgins, 1971; Higgins and Rinalducci, 1975), and such that the largest differences in exponent values are expected (Mansfield, 1973); see Fig. 1. Instead of using a large group of subjects, we emphasized a *within subject* comparison of different scaling methods. Brightness matches were performed as a further test on the consistency of the scaling results. Different scaling methods should, within experimental inaccuracy, yield equal brightness exponents for the same stimuli. Moreover, if mutual transitivity of brightness matches is perfect, exponent ratios measured by matching should equal the ratios of exponents as obtained by scaling. This transitivity, meaning that if the brightness of stimulus X equals that of stimulus Y , and the brightness of stimulus Y equals that of stimulus Z , than the brightnesses of stimuli X and Z should also be equal, can be studied easily. To test the foregoing hypotheses, we performed four experiments successively: matching, magnitude estimation, bisection and fractionation. In these experiments the foveal position of

¹Broca and Sulzer (1902) found that the brightness of a flashed stimulus is maximum for a certain duration. This duration is larger than the Bloch domain, indicating pure integration for short durations, but smaller than long durations for which the brightness does not depend on duration. A similar transition domain has been found for stimuli with varying diameter.

the stimuli was kept unchanged. An additional fifth experiment was performed to study the influence of the position of the stimuli within the fovea.

2.2 Apparatus

In all experiments a four-channel monoptic Maxwellian-view optical system was used. Two channels provided stimuli, while the other channels were used for background field and for fixation points. Light sources were Sylvania R1131C glow-modulator tubes which had to be linearized and stabilized by a $V(\lambda)$ corrected feedback system, which means that the photopic spectral sensitivity of the visual system has been taken into account. These tubes were driven by pulse generators in connection with logarithmic attenuators. The colour of the light approximated white. This was achieved by putting neutral density filters and a cyan filter (Kodak gelatine type CC50C) into the lightpaths. At the beginning of experimental sessions the calibration was checked by means of a $V(\lambda)$ corrected photomultiplier. All observations were done by a single subject, a corrected astigmatic myope. Stimuli were viewed by means of an ocular using the right eye. An artificial pupil 2 mm in diameter, equipped with an entoptic guiding system to check the centering of the pupils was used (Roufs, 1963). The background luminance was 32 cd.m^{-2} (100 Td) throughout all experiments.

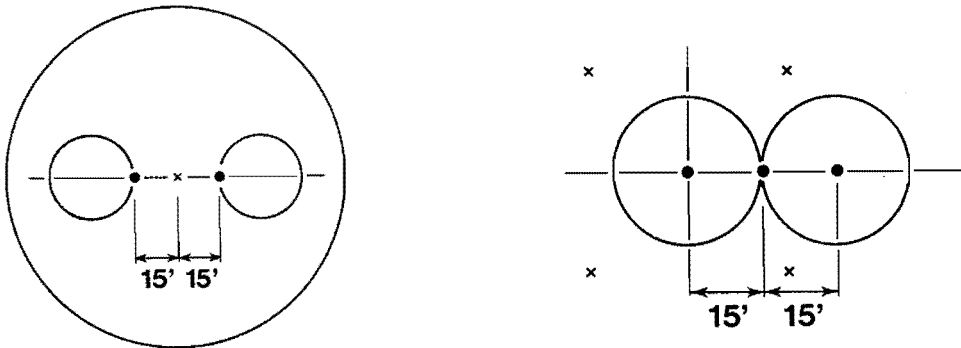


Figure 2: Left panel: Visual field of the right eye, not drawn to scale, in experiments 1 to 4. The stimuli, 2 (●) or 30 (○) min. of arc in diameter, could be presented on either side of the fixation point (×) on the horizontal meridian. Right panel: The additional retinal positions of the 2 and 30 min. of arc stimuli in experiment 5, where the imaginary centre indicated by four points (×) was fixated.

The stimuli presented were circular luminance increments, with diameters of 2 or 30 min. of arc, situated on the horizontal meridian. In experiments 1 to 4, the retinal position of the stimuli was unchanged, by keeping a distance of 15 min. of arc between the fixation point and the edges of the stimuli (see the left panel of Fig. 2). In brightness matching, the two stimuli were presented on either side of

the fixation point. In magnitude estimation each time a reference was presented prior to the test stimulus. This reference, with equal size and duration as the test stimulus, was mirrored with respect to the fixation point. In bisection and fractionation experiments reference and test stimuli were also identical, but were generated sequentially at the same position in the temporal visual field. In order to explore the effect of the stimulus position in the fovea, the retinal positions in accordance with the right panel of Fig. 2 were considered in experiment 5.

Both the small and large stimuli were presented with two durations, 10 or 300 msec, while stimulus pairs (i.e. test and references) were generated sequentially in all experiments. An interstimulus interval of at least 500 msec was regarded, as well as a delay of 300 msec between the control of a start button and the release of the first stimulus. Sequences of stimulus presentations were separated by intervals of approximately 1.5 seconds.

Prior to the experiments, two series of introductory measurements were performed. The first series concerned a check on the absence of meta-contrast effects. This effect means that detection of a test stimulus is possibly influenced by the presence of another stimulus, in space as well as time separated from the test stimulus (e.g. Vrolijk, 1986). To this end thresholds of stimuli were measured with and without the presence of a high-luminance perturbing stimulus. No significant influence of the perturbing stimulus was found at the selected spatio-temporal distances of the stimuli. The second series was a check on the correct calibration of the channels of the optical system. To this end identical stimuli, i.e. with equal diameter and duration, were matched in brightness at various luminance increments. Given a correct calibration, the resulting luminance increments of the two stimuli should be equal. This control experiment provided the result expected; see Results in section 2.3.

2.3 Experiment 1: Brightness Matching

Theory

In order to generalize Stevens' relation for a dark background (e.g. Onley, 1961), we postulate that the brightness B of a stimulus presented against a photopic, uniform background with retinal illuminance E_b and corresponding brightness B_b can be written as $B = B_b + \Delta B$. In the expression for the brightness increment

$$\Delta B = k(\varepsilon - \varepsilon_{thr})^\beta ; \varepsilon \geq \varepsilon_{thr} \quad (1)$$

ε is an increment in retinal illuminance that has to exceed a certain threshold increment ε_{thr} in order that a brightness difference with the background can be perceived. In brightness matching, the increment in retinal illuminance of a test stimulus is varied until its perceived brightness equals that of a reference with a fixed increment. It can be derived that $\Delta B_T = \Delta B_R$ leads to

$$\log(\varepsilon_T - \varepsilon_{T,thr}) \propto \frac{\beta_R}{\beta_T} \log(\varepsilon_R - \varepsilon_{R,thr}) \quad (2)$$

where subscripts T and R stand for test and reference respectively. The exponent ratio β_R/β_T of eq. (2) can be determined by performing brightness matches between test and reference increments at various reference levels. The slope of a graph, describing eq. (2) in $\log(\varepsilon - \varepsilon_{thr})$ coordinates, equals the ratio of the exponents.

Methods

Brightness matches were performed for all six stimulus combinations based on the two diameters and the two durations as explained in the foregoing. These combinations are represented by the arrows in Fig. 1, where arrows point in the direction of chosen reference stimuli. In the first series of three stimulus combinations, the 2'-10msec stimulus acted as the reference (the solid arrows in Fig. 1). The luminance increment of the reference was varied across a number of fixed values, chosen prior to the experiments. The luminance increment of a test stimulus was determined by the method of constant stimuli, using equal numbers of trials with 'brighter than the reference' and 'darker than the reference' as criteria. Taking the mean of these determinations might still imply a brightness difference with respect to the point of subjective equality, reflected by a just noticeable difference in retinal illuminance $\delta\varepsilon$. However, our control experiment on matching equal stimuli learned that $\delta\varepsilon/\varepsilon < 0.04$ and that deviations found are of the same order of magnitude as the standard deviations of the measurements².

At least five reference levels were considered for each of the stimulus combinations, excluding threshold measurements. All brightness matches and threshold determinations were done eight times. Each determination consisted of two series of ten presentations with observational probabilities between 10% and 90%. The geometric mean of the 50% values of the eight log-ogives was computed in terms of log incremental retinal illuminance. The total number of stimulus presentations thus exceeded $(5+1) \times 8 \times 2 \times 10 = 960$ for any combination. To compensate for nonstationary effects (drift) in the observations, measurements were performed in randomized and counterbalanced blocks.

Results

The results of the matching experiment are given in Figs. 3 and 4. In Fig. 3, where the 2'-10msec stimulus was used as the reference, we see that the measured curves approximate linearity on a log-log scale for suprathreshold levels of retinal

²A Weber fraction of 0.14 is reported in case of a 50'-4msec disk presented against a dark background (Cornsweet, 1970).

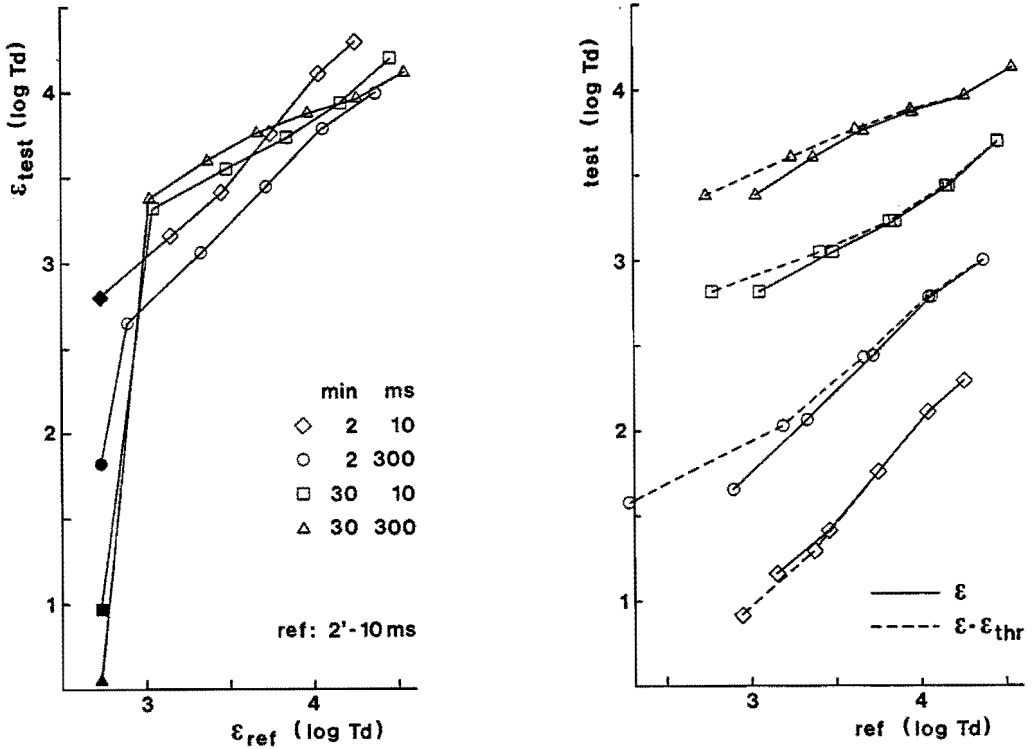


Figure 3: Brightness matching in which the 2'-10msec stimulus was used as reference. Left panel: Detection thresholds are given by solid symbols, matching data by open symbols. The diamond graph reflects a test experiment in which identical stimuli, i.e. 2'-10msec, were matched to check the calibration. The symbol size approximates the standard deviation of individual measurements. Right panel: Influence of threshold correction applied to the matching data. Curves have been vertically shifted to avoid clutter.

illuminance. This justifies the assumption of a Stevens relation between brightness and retinal illuminance increments in accordance with eq. (1). The influence of threshold correction is illustrated in the right panel of fig. 3. This correction has an appreciable effect only for the lowest matching results. It should be mentioned, however, that the low-level brightness matches are possibly influenced by hue shifts caused by the glowmodulator tubes. The least-mean-square slopes of all threshold corrected matching results, ignoring the lowest matching points, which are thus thought to reflect exponent ratios in accordance with eq. (2), are given in Fig. 8 for a direct comparison with exponents measured by means of scaling methods treated further on. Also given in Fig. 3 are the matching results of an experiment to test the identity of the channels with identical, i.e. 2'-10msec, stimuli. These results approximate the expected graph with slope 1 through the origin indeed.

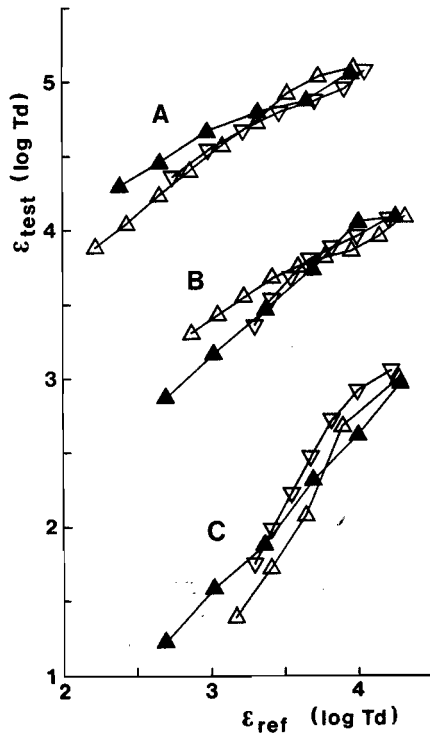


Figure 4: Brightness matches for stimulus combinations A, B and C as defined in Fig. 1. Solid symbols are directly measured values; open symbols reflect independent predictions, computed from two other stimulus combinations and indicated by the \triangle and ∇ curves, to check the transitivity. To avoid overlap, the A and C curves have been vertically shifted by 1 and -1 log unit respectively.

The matching results of the remaining stimulus combinations, which corre-

spond to the dashed arrows labelled A, B and C in Fig. 1, are presented in Fig. 4, and the least-mean-square slopes in Fig. 8. Since we intend to study the consistency between matching and scaling methods, the mutual transitivity of the matching results is of interest. For this purpose independent predictions, based on matching results obtained with other stimulus combinations, are plotted together with directly measured data. Regarding stimulus combination A for instance, see Fig. 1, the brightness of the 30'-300msec test stimulus can be directly compared with the brightness of the 2'-300msec reference stimulus. An independent prediction can be computed by using the matching curves obtained with stimulus combinations B and C. Alternatively, the matching curves obtained with the stimulus combinations 30'-300msec versus 2'-10msec and 2'-300msec versus 2'-10msec can be used. This procedure of predicting matching curves can be applied for all stimulus combinations of course. Predictions are presented in Fig. 4 by the open symbol curves, while directly measured data are presented by solid symbol curves. We must conclude that transitivity is fair but not perfect, and the maximum deviation of 0.3 log unit is much smaller than the transitivity error of 1 log unit reported by Higgins and Rinalducci (1975). This implies that a small inaccuracy in the measured exponent ratios has to be accepted.

2.4 Experiment 2: Magnitude Estimation

Theory

In magnitude estimation the subject is asked to generate numbers M proportional to the perceived brightness increment ΔB : $M \propto \Delta B$. After substitution in eq. (1) it follows that

$$\log M \propto \beta \log(\varepsilon - \varepsilon_{thr}). \quad (3)$$

Performing magnitude estimations at several luminance increments enables us to obtain the exponent β - it equals the slope of the $\log(M)$ versus $\log(\varepsilon - \varepsilon_{thr})$ graph.

Methods

All four stimuli of Fig. 1 were used in the magnitude estimation experiment. At each of six luminance increments, the geometric mean of 20 estimates was computed. The task of the subject was to estimate the magnitude of the brightness increment in proportion to a reference increment. References, taken 100 by definition, were equal in size and duration to the test stimuli. Their luminance increments were chosen such that their brightnesses were the same, and accordingly derived from the matching results. Luminance increments of test stimuli were presented in randomized and counterbalanced blocks, with the restriction that the brightest and dimmest stimuli never succeeded each other. Reference and

test stimuli were presented sequentially on either side of the fixation point, with an interstimulus interval of 500 msec.

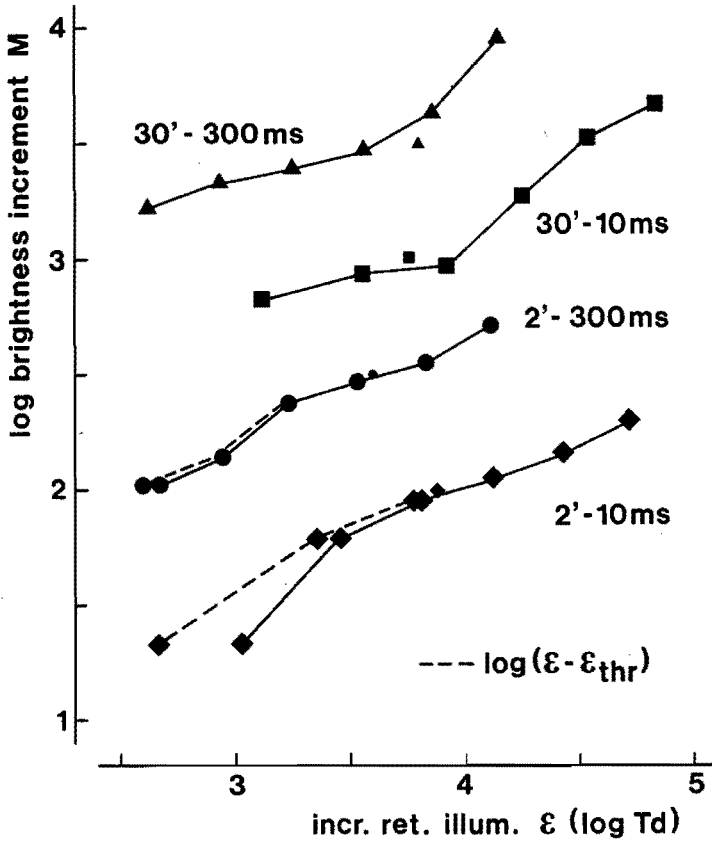


Figure 5: Magnitude estimation of brightness increments (solid curves). The size of the large symbols approximates the standard deviation of individual estimates. Small symbols refer to reference increments, $M=100$ by definition. The influence of threshold correction is demonstrated by the dashed curves. Curves have been vertically shifted by multiples of 0.5 log unit.

Results

The results of all magnitude estimations are shown in Fig. 5. Threshold correction according to eq. (3) has only an appreciable effect on the linearity and slope in case of the small stimuli. Results of these small stimuli approximate the expected linearity, while those of the large stimuli do not. For the latter the slope of the

curves changes for retinal illuminances above and beneath that required for an equal brightness with the reference. We must therefore assume that this effect reflects a change in strategy of the subject in the evaluation of magnitudes. The number of measured points is rather small for an accurate determination of the slopes (exponents) above and below references. Least-mean-squares slopes have therefore been computed over the entire measured range. These slopes are presented in Table 5 for a direct comparison with the bisection and fractionation results.

2.5 Experiment 3: Bisection

Theory

Bisection is a scaling method in which three stimuli, differing only in luminance, are presented to the subject. Two stimuli, one with a high and the other with a low brightness, define a reference interval. The luminance of the third stimulus is varied until its brightness intersects the reference interval in equal parts. In this case we may write $B_M = 0.5(B_H + B_L)$, or $\Delta B_M = 0.5(\Delta B_H + \Delta B_L)$, with subscripts M(idway), H(igh) and L(ow). Equation (1) substituted, it follows that

$$(\varepsilon_M - \varepsilon_{thr})^\beta = \frac{1}{2} [(\varepsilon_H - \varepsilon_{thr})^\beta + (\varepsilon_L - \varepsilon_{thr})^\beta] \quad (4)$$

Since ε_H and ε_L are fixed, while ε_M and ε_{thr} can be measured, it is possible to solve for the exponent. However, in repeated measurements a number of bisection points $\{\varepsilon_{M,i}\}$ with $i = 1, \dots, n$ is determined. Substitution of the geometric mean of these bisection points in eq. (4) might yield a reliable exponent, because it is hard to distinguish the psychophysical power law from the logarithmic law according to Weber-Fechner on given intervals. Note that taking the geometric mean of bisection points emphasizes the idea of a logarithmic law, and might result in an error if the exponent of a power law is computed. Fagot (1963) argued that a first order approximation of the transformed distribution of measured bisection points, leading to linear averaging in the sensory domain, is to be preferred. Approximating the (threshold corrected) distribution $\{\varepsilon_{M,i} - \varepsilon_{thr}\}$ by its mean $\bar{\varepsilon}_M$ and standard deviation s would thus lead to

$$\bar{\varepsilon}_M + (\beta - 1) \frac{s^2}{2\bar{\varepsilon}_M} = \left[\frac{1}{2} (\varepsilon_H^\beta + \varepsilon_L^\beta) \right]^{1/\beta} \quad (5)$$

in which ε_H and ε_L are also threshold corrected values. From this the exponent β can be solved numerically by iterative successive substitution.

Methods

Sequences of three stimuli, with equal size, duration and retinal position, were presented to the subject on any trial. First and third ones were references, the middle one the test. The task of the subject was to decide whether the brightness of the test stimulus was either above or below halfway the reference interval. It is known that a sequential presentation results in a hysteresis effect (Stevens, 1961). This implies that sequences of stimuli have to be presented in both ascending and descending orders of brightness, the results being averaged to eliminate the bias. Because of the time consuming character of these experiments, bisections were performed for only two of the stimuli: the 2'-10msec and the 30'-10msec ones. For each of these stimuli, the method of successive interval halving was adopted first. This means that a large brightness interval is divided into two, subjectively equal, subintervals. These subintervals are each divided into still smaller intervals and so on. In this way, seven bisection intervals were observed for both stimuli. Each bisection point was determined by means of a double staircase method, in which 8 reversals were achieved. Thus, 16 reversals were obtained, since this procedure was followed in both ascending and descending orders of reference and test sequences. As may be seen from Table 1, the spread of the resulting brightness exponents was rather large for the 2'-10msec stimulus, possibly caused by lack of experience of the subject since we started these experiments with this stimulus. Therefore additional bisection experiments were performed for this stimulus, with various reference intervals and extending the number of staircase reversals to 32.

Results

Reference values and results of the first series of bisections, in which the method of successive interval halving was adopted, are shown in Table 1. The bisection exponents were computed by applying eq. (5). From this we can see that the spread in the computed exponents is quite large. Note that negative exponent values imply a bisection point below the geometric mean of the references (Fagot, 1963). Results of the 30'-10msec stimulus show two extreme values of the exponent. Excluding these by applying the inequality of Bienayme-Chebyshev, we find

$$\bar{\beta}_{30'-10msec} = 0.52 ; s(\bar{\beta}) = 0.06 \quad (6)$$

Results of the additional bisections performed for the 2'-10msec stimulus are presented in Table 2, showing a significant decrease in spread of the computed exponents with respect to the first bisections (Table 1). By taking all significant exponents for this stimulus within the Bienayme-Chebyshev range as stated above, i.e. $0.15 \leq \beta \leq 0.52$, we obtain

$$\bar{\beta}_{2'-10msec} = 0.35 ; s(\bar{\beta}) = 0.05 \quad (7)$$

	$\epsilon_H - \epsilon_{thr}$	$\epsilon_L - \epsilon_{thr}$	$\overline{\epsilon_M - \epsilon_{thr}}$	s	β
2'-10 msec	16.40	0.18	3.75	1.20	0.32
	3.61	0.18	1.30	0.85	0.28
	16.40	3.61	8.25	4.30	-0.73
	16.40	7.02	9.20	1.35	-2.54
	7.02	3.61	5.00	0.75	-0.30
	3.61	1.30	2.20	0.60	-0.25
	1.30	0.18	1.00	0.40	2.44
30'-10 msec	19.90	0.34	4.75	0.65	0.30
	4.89	0.34	2.05	0.35	0.58
	19.90	4.89	11.40	2.55	0.55
	19.90	12.00	16.30	2.85	2.34
	12.00	4.89	8.25	1.45	0.66
	4.90	2.18	3.25	0.40	-0.12
	2.18	0.34	1.05	0.10	0.51

Table 1: Successive interval bisections. All increments in retinal illuminance are given in 10^3 Trolands. First column: stimulus diameter and duration. Second column: threshold corrected reference intervals. Third column: linear means and standard deviations of threshold corrected bisection points. Fourth column: computed exponents.

	$\epsilon_H - \epsilon_{thr}$	$\epsilon_L - \epsilon_{thr}$	$\overline{\epsilon_M - \epsilon_{thr}}$	s	β
2'-10 msec	19.50	1.90	6.85	1.35	0.15
	17.20	0.73	6.40	2.35	0.49
	20.70	1.74	8.05	2.45	0.36
	19.80	1.75	7.55	2.10	0.30
	20.40	4.82	11.45	2.60	0.52

Table 2: Additional bisections for the 2'-10msec stimulus, where 32 staircase reversals were determined.

2.6 Experiment 4: Fractionation

Theory

Fractionation is here regarded as a special case of bisection. By taking the background brightness B_b as the lowest reference, bisection would lead to $B_M = 0.5(B_H + B_b)$ or in case of increments $\Delta B_M = 0.5\Delta B_H$. Substitution of eq. (1) provides an explicit solution of the exponent

$$\beta = \frac{\log \frac{1}{2}}{\log[(\varepsilon_M - \varepsilon_{thr})/(\varepsilon_H - \varepsilon_{thr})]} \quad (8)$$

As in case of bisection, one may substitute the geometric mean of the n fractionation points $\{\varepsilon_{M,i}\}$. Alternatively, Fagot's (1963) approach based on a first order approximation of the transformed distribution would lead to

$$\beta = \frac{\log \frac{1}{2}}{\log\{\bar{\varepsilon}_M + (\beta - 1)\frac{s^2}{2\bar{\varepsilon}_M}\}/\{\varepsilon_H\}} \quad (9)$$

in which ε_H is the threshold corrected value of the reference increment. Since fractionation experiments are to be performed at several values of the reference increment $\{\varepsilon_{H,j}\}$, with $j = 1, \dots, m$, a direct normalization of all fractionation results may be applied. Approximating the distribution of the normalized results $\{x_{i,j}\}$ with

$$x_{i,j} = \frac{\varepsilon_{M,i} - \varepsilon_{thr}}{\varepsilon_{H,j} - \varepsilon_{thr}}; \quad i = 1, \dots, n; \quad j = 1, \dots, m \quad (10)$$

by its mean \bar{x} and standard deviation s_x we obtain

$$\bar{\beta} = \frac{\log \frac{1}{2}}{\log[\bar{x} + (\bar{\beta} - 1)\frac{s_x^2}{2\bar{x}}]} \quad (11)$$

Since

$$\beta = \frac{\log \frac{1}{2}}{\log x}; \quad 0 \leq x \leq 1 \quad (12)$$

and therefore

$$\frac{d\beta}{dx} = \frac{-\log \frac{1}{2}}{\ln 10} \cdot \frac{1}{x(\log x)^2} \approx \frac{0.13}{x(\log x)^2} \quad (13)$$

we arrive at an estimation of the standard deviation of the mean exponent:

$$s(\bar{\beta}) = \frac{s_x}{\sqrt{N}} \cdot \left[\frac{d\beta}{dx} \right]_x \approx \frac{s_x}{\sqrt{N}} \cdot \frac{0.13}{\bar{x}(\log \bar{x})^2} \quad (14)$$

Here N is the total number of fractionation experiments performed. If n equals the number of repeated fractionations at each of m reference intervals, it is obvious that $N = nm$.

Methods

All four stimuli were used in this experiment. Stimulus presentations were sequential, similar to the bisection experiment, except that sequences of only two stimuli, a test and a reference, were presented on any trial. The task of the subject was to decide whether the brightness of the test stimulus was larger or smaller than half the reference interval. Four reference intervals were considered. These were chosen in such a way that the reference luminance increments differed by about a factor of 2. At any of the reference intervals, the geometric mean of sixteen 50% points, achieved by the method of constant stimuli as mentioned before, was computed. Alternatively, the 16 resulting fractionation points were processed following the computational methods as described in the foregoing section.

Results

The results of the fractionation experiment are presented in Table 3. To compare the influence of the various computational methods, exponents were calculated in three different ways. Firstly, exponents were computed on the basis of the geometric mean of the fractionation points. Using this most simple method, the linear mean of dB settings of a logarithmic attenuator can be determined. The corresponding threshold corrected increment in retinal illuminance is substituted in eq. (8). Secondly, Fagot's approach was used by applying eq. (9) for each reference interval individually. Thirdly, Fagot's method was applied to all normalized results by using eqs. (10) - (14). As may be observed from Table 3, the method applied has no significant influence. This means that any sophistication is superfluous and that substitution of the geometric mean in eq. (8), the simplest method by far, will do as well. We may also conclude that the reference interval has no systematic influence upon resulting exponents, contrary to the results obtained by Stewart et al. (1967), but our fractionation exponents are also substantially higher than our bisection exponents.

2.7 Experiment 5: Influence Foveal Position

Methods

In experiments 1 to 4 the foveal position, relative to the fixation point, of the stimuli was unchanged. Since a distance of 15 min. of arc was kept between the fixation point and the edges of the stimuli, this means that the centres of the 2' and 30' stimuli were positioned at eccentricities of 16' and 30' respectively (on the horizontal meridian). To study the influence of this position in the fovea on the brightness exponents of the stimuli used, additional scaling experiments were performed. In these the eccentricity of the centres was chosen to be 0' and 30' for

	$\epsilon_H - \epsilon_{thr}$	Geometric		Fagot's approach			Fagot's approach normalized values
		$\epsilon_M - \epsilon_{thr}$	β	$\overline{\epsilon_M - \epsilon_{thr}}$	s	β	
2'-10 msec	18.50	6.67	0.68	6.97	1.85	0.70	$\overline{x} = 0.348$ $s_x = 0.078$ $\overline{\beta} = 0.65$ $s(\overline{\beta}) = 0.02$
	9.48	3.10	0.62	3.23	0.61	0.64	
	4.37	1.30	0.57	1.32	0.20	0.57	
	1.87	0.68	0.68	0.65	0.10	0.65	
		$\overline{\beta} = 0.64$		$\overline{\beta} = 0.64$		$s(\overline{\beta}) = 0.03$	
30'-10 msec	22.40	9.32	0.79	9.49	1.50	0.81	$\overline{x} = 0.472$ $s_x = 0.067$ $\overline{\beta} = 0.92$ $s(\overline{\beta}) = 0.02$
	12.10	5.60	0.91	5.62	0.55	0.91	
	5.65	2.56	0.87	2.61	0.25	0.89	
	2.74	1.46	1.11	1.46	0.15	1.11	
		$\overline{\beta} = 0.92$		$\overline{\beta} = 0.93$		$s(\overline{\beta}) = 0.06$	
2'-300 msec	21.80	9.29	0.81	9.37	1.30	0.82	$\overline{x} = 0.449$ $s_x = 0.063$ $\overline{\beta} = 0.87$ $s(\overline{\beta}) = 0.02$
	11.20	5.25	0.92	5.20	0.70	0.90	
	5.45	2.41	0.85	2.43	0.30	0.86	
	2.53	1.16	0.89	1.16	0.20	0.89	
		$\overline{\beta} = 0.87$		$\overline{\beta} = 0.87$		$s(\overline{\beta}) = 0.02$	
30'-300 msec	26.30	13.50	1.04	13.70	1.30	1.07	$\overline{x} = 0.535$ $s_x = 0.100$ $\overline{\beta} = 1.11$ $s(\overline{\beta}) = 0.04$
	13.50	8.70	1.58	8.81	1.10	1.65	
	6.60	3.01	0.88	2.99	0.50	0.87	
	3.01	1.54	1.04	1.54	0.20	1.03	
		$\overline{\beta} = 1.14$		$\overline{\beta} = 1.15$		$s(\overline{\beta}) = 0.17$	

Table 3: Fractionation results. All increments are given in 10^3 Trolands. The number of performed fractionations at each of the 4 reference intervals was 16. Second column: threshold corrected references. Third column: geometric means of fractionation points with computed exponents. Fourth column: linear means and standard deviations with exponents computed by applying Fagot's approach to each reference interval individually. Last column: Fagot's approach applied to all reference-normalized fractionation results.

the 2' stimuli, and 0' for the 30' stimuli, as shown in the right panel of fig. 2. Both the small and the large stimuli were presented with 10 and 300msec durations. The scaling method applied was fractionation, following the same methods as in experiment 4.

	eccentricity centre-stimulus		
	0'	15'	30'
2'- 10 msec	0.97	0.65*	0.68
30'- 10 msec	0.95		0.92*
2'-300 msec	0.62	0.87*	0.98
30'-300 msec	0.98		1.11*

Table 4: Fractionation exponents obtained at various positions in the fovea, on the horizontal meridian in the temporal visual field; see the right panel of Fig. 2. Exponents labelled by an asterisk were previously determined in experiment 4.

Results

Since reference intervals and the computational methods used were exactly the same as in the fractionation experiments described before, only the resulting exponents are presented in Table 4. These exponents were computed by applying eqs. (10) and (11). It is likely that fractionation exponents of large stimuli are not affected by the foveal position, in contrast to the exponents of small stimuli. The exponent of the 2'-10msec stimulus decreases rapidly with eccentricity, while the exponent of the 2'-300msec stimulus increases.

2.8 Discussion

On the Visibility Level

In Fig. 6 the matching results are presented in a somewhat different way. By shifting the curves of Fig. 3 over $\log(\varepsilon_{thr})$, thresholds are now positioned in the origin. This presentation corresponds to the definition of the visibility level (VL) as advocated by the CIE (1981): if contrast is defined as

$$C = \frac{E - E_b}{E_b} = \frac{\varepsilon}{E_b} \quad (15)$$

with E and E_b the retinal illuminances of the stimulus and the background respectively, than visibility level is next introduced as

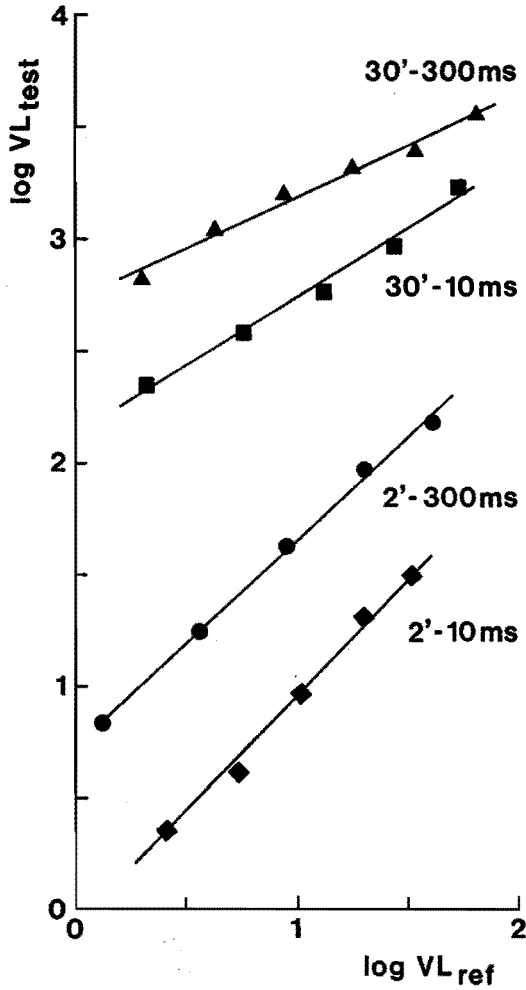


Figure 6: Matching data of the left panel of Fig. 3 converted into log visibility level (VL) coordinates. The 2'-10msec stimulus was the reference, and solid diamond symbols reflect matches of identical, i.e. 2'-10msec, stimuli.

$$VL = \frac{C}{C_{thr}} = \frac{\varepsilon}{\varepsilon_{thr}} \quad (16)$$

By drawing a line parallel to the ordinate in Fig. 6, representing a constant brightness of the reference, we can see that equal brightness stimuli have different visibility levels. Although an equal brightness of stimuli, with different dimensions and durations superimposed on the same background, does not automatically mean an equal brightness contrast, the results make one question whether equal visibility levels imply that they are also equally visible. Since the visibility level is advised as a parameter in the performance of visual tasks, further research on this issue seems necessary. Similar problems arise of course if other contrast formulas, for instance E/E_b , which is often used to describe the contrast of characters on VDU's, are applied.

Magnitude Estimation Re-examined

From Fig. 4 we have already concluded that the mutual transitivity of matching results was not perfect and, therefore, that a certain inaccuracy in the measured exponent ratios must be accepted. A similar conclusion, based on the nonlinearity of graphs as shown in Fig. 5, holds for magnitude estimation results. As stated in the introduction, circumstantial evidence has been obtained that scaling results are influenced by the nonlinear number handling of subjects. Since we have both matching and estimation data at our disposal, it is possible to visualize the influence of the number handling in two ways. The first consists of a construction of matching curves by reprocessing the estimation data. Intersecting the estimation curves of Fig. 5 for some value of the estimated brightness increment, we obtain the corresponding increments in retinal illuminance of the four stimuli. These increments in retinal illuminance should thus agree with values resulting from directly matching test stimuli with, for instance, a 2'-10msec reference. Doing this for several values of the estimated brightness increment, we can construct matching curves from estimation curves. The result of this procedure is presented in the left panel of Fig. 7, together with least-squares approximations of the directly measured matching results. Graphs are given in log visibility levels in order to avoid clutter. This presentation therefore agrees with that of Fig. 6. If all magnitude estimations were influenced by a single, additional exponent describing the nonlinear number of handling of the subject (Curtis, 1970), which would be eliminated by the procedure as explained above, the constructed matching curves are expected to overlap the measured matching curves. The left panel of Fig. 7 shows that the hypothesis of a single power function, which relates perceived brightness increments to numbers, must be rejected. In view of the pronounced nonlinearity of the estimation data for the large stimuli (Figs. 5 and 7), which coincides with the reference levels used, it is more likely that the subject applied different strate-

gies in computing the brightness magnitudes above and below these references. It is curious that the subject applied different strategies only in case of large stimuli, and not in case of small stimuli.

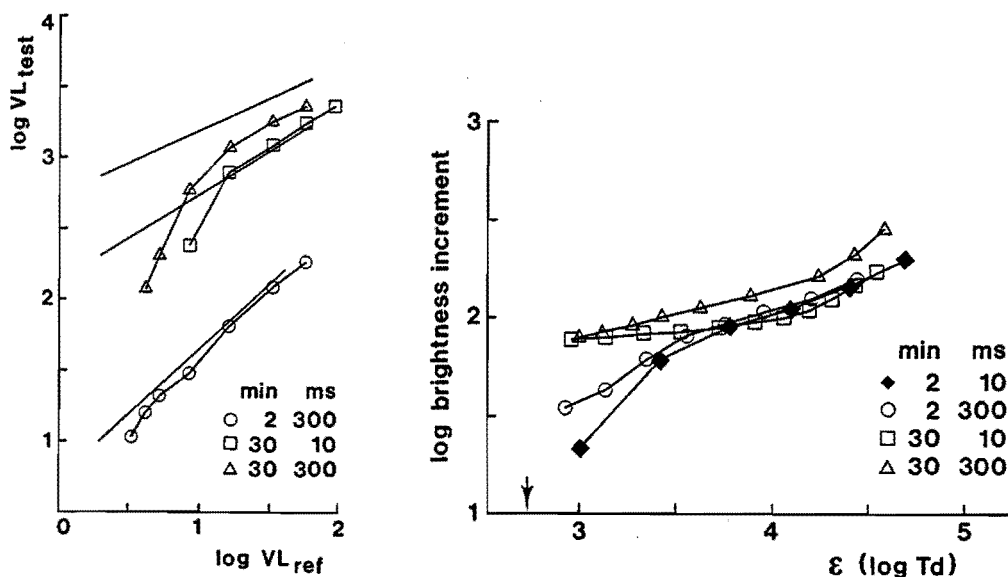


Figure 7: Reprocessed matching and estimation data. Left panel: Matching curves (open symbols) computed from magnitude estimation results. Straight lines are duplicated from Fig. 6. Right panel: By means of matching curves projected estimation results of the non 2'-10msec stimuli (open symbols). Directly measured estimates of the 2'-10msec stimulus are given by solid symbols, and the detection threshold by the arrow. For explanation see text.

The second way of reprocessing obtained data is based on a projection of estimation results by means of matching results. For a certain value of the estimated brightness increment, the corresponding increment in retinal illuminance can be obtained by intersecting the estimation curve of Fig. 5. This increment in retinal illuminance corresponds to an increment in retinal illuminance of the 2'-10msec stimulus, which can be obtained by intersecting the matching curve of Fig. 3. Doing this for several values of the estimated brightness increment and for the non 2'-10msec stimuli, we can project the estimation curves of the non 2'-10msec stimuli onto the estimation curve of the 2'-10msec stimulus. Again, this way of reprocessing provides a measure of the consistency of matching and estimation data. The right panel of Fig. 7, which gives both measured estimates for the 2'-10msec stimulus and reprocessed estimates for the other stimuli, indicates that measured and projected curves largely overlap indeed. Deviations are found for the two large stimuli, at low levels in particular, which confirm the conclusion with respect to the different strategies applied by the subject.

Scaling Methods Compared

A comparative summary of measured brightness exponents is presented in Table 5. On the one hand, we see that the exponents of the 2'-10msec stimulus, as measured by magnitude estimation and bisection, agree (the magnitude estimation exponent of the 30'-10msec stimulus is not very reliable). On the other hand, fractionation exponents are significantly larger than bisection exponents, despite the similarity of these scaling methods. Roughly speaking:

$$\beta_f \approx 1.8 \beta_b \quad (17)$$

If our fractionation exponents are divided by 1.8, see the last column of Table 5, the corrected fractionation exponent of the 2'-300msec stimulus even agrees with the magnitude estimation exponent (again, the magnitude estimation exponent of the 30'-300msec stimulus is not quite reliable).

	magnitude estimation β_m	bisection β_b	fractionation β_f	$\frac{\beta_f}{1.8}$
2' - 10 msec	0.36	0.35	0.65	0.36
30' - 10 msec	≈ 0.52	0.52	0.92	0.51
2' - 300 msec	0.45		0.87	0.48
30' - 300 msec	≈ 0.42		1.11	0.62

Table 5: Summary of scaling exponents. For the last column see text.

The ratio of eq. (17) has been found before: averaging the exponents reported by Stewart et al. (1967) yields a ratio of 2, thereby ignoring the significance of differences over subjects as well as reference intervals. Contrary to their finding, we obtained no systematic relation between reference intervals and resulting exponents (Tables 1, 2 and 3). The absence of such an interval bias confirms the hypothesis of a unique, stimulus-dependent value of the brightness exponent. The factor of 1.8 between bisection and fractionation exponents can perhaps be explained by considering the strategies used by the subject. Although instructed to consider intervals in both experiments, the subject reported that he was aware of applying two different strategies. In bisections, with a clearly bounded reference interval defined by two reference stimuli, he compared brightness differences. In fractionations, with one of the references equal to the background (zero increment), he actually performed computations of brightness increments: multiplication or division by a factor of 2. This explanation of the different exponents is equivalent to the extensively discussed discrepancy between the handling of interval and ratio scales (e.g. Marks, 1974).

Consistency between Matching and Scaling

The hypothesis that each stimulus has a unique brightness exponent β leads to the expectation that measured exponent ratios (matching) and measured exponents (scaling) are in mutual agreement. In practice, however, the proof of the validity of this hypothesis is hampered by experimental error of course. We have seen that the transitivity of the matching results is fair but not perfect, and the scaling results, including fractionation exponents divided by 1.8, seem to agree for most stimuli. Combining all ten measured results, i.e. the six exponent ratios obtained by matching and the four exponents obtained by fractionation, we arrive at the scheme presented in Fig. 8. This figure is meant to visualize the mutual consistency between matching and scaling results. Directly measured values are those not given between parentheses: fractionation exponents in the corners and exponent ratios alongside the arrows. Independent predictions, based on other stimuli or stimulus combinations, are given between parentheses. Taking the short duration stimuli for instance, the exponent ratio computed from the fractionation results is $\beta_{ref}/\beta_{test} = 0.36/0.51 = 0.70$ since arrows point towards reference stimuli. This ratio of 0.70 approximates the directly measured ratio (matching) of 0.61. The same procedure holds for the exponents themselves, where three predictions, each based on a ratio and an exponent of a different stimulus, are presented. It may be seen that the mutual consistency is reasonable, be it that the matching result of the long duration stimuli is somewhat too low.

Rounding off the averaged measured and predicted values (excluding the predictions which involve the matching result of the long duration stimuli) we obtain the values in the left column of Table 6. This enables us to compare the present simple fractional exponents for stimuli presented against a photopic background with those obtained by Mansfield (1973), representing typical data found against a dark background. The exponents obtained for the 30'-10msec and 2'-300msec stimuli are identical, and the comparison with Mansfield's data suggests that they are unaffected by the background level. In contrast, the exponent of the 2'-10msec stimulus is decreased while that of the 30'-300msec stimulus is increased. The latter result confirms the data of Stevens and Stevens (1960), Onley (1961) and Warren (1976).

Just Noticeable Brightness Differences

Analyzing the fractionation results, we noticed a curious relation between the fractionation exponents β_f and the slopes of the $\log(s)$ versus $\log(\bar{\epsilon}_M)$ graphs, i.e. graphs of standard deviations versus geometric means of fractionation points for all reference intervals. These data are given in Fig. 9 together with least-squares approximations. As shown in Table 7, the slope of each curve approximates

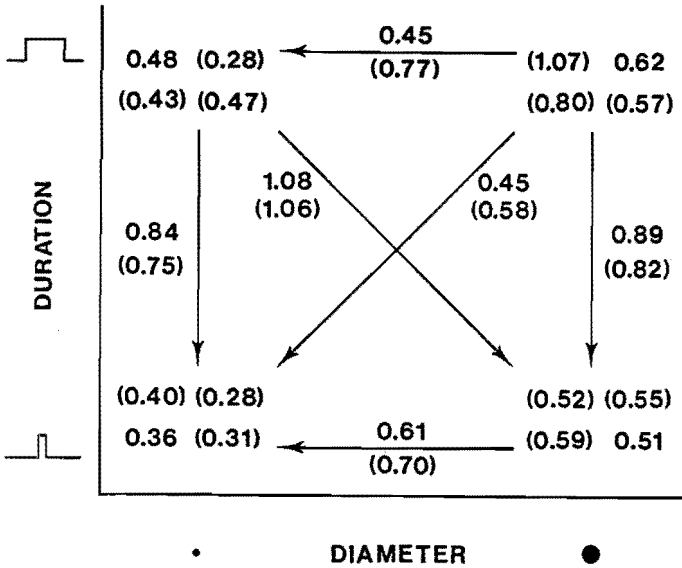


Figure 8: Scheme of brightness exponents and exponent ratios. Corrected fractionation exponents are given in the corners and exponent ratios, as measured by matching, alongside the arrows (arrows point towards references). Values between parentheses are not directly measured but computed predictions based on independently measured values; see text. Values not given between parentheses are directly measured.

	photopic background β	dark background β
2'- 10 msec	$1/3$	1
30'- 10 msec	$1/2$	$1/2$
2'-300 msec	$1/2$	$1/2$
30'-300 msec	$2/3$	$1/3$

Table 6: Exponents rounded off. The last column gives simple fractional exponents for stimuli presented against a dark background, taken from Mansfield (1973).

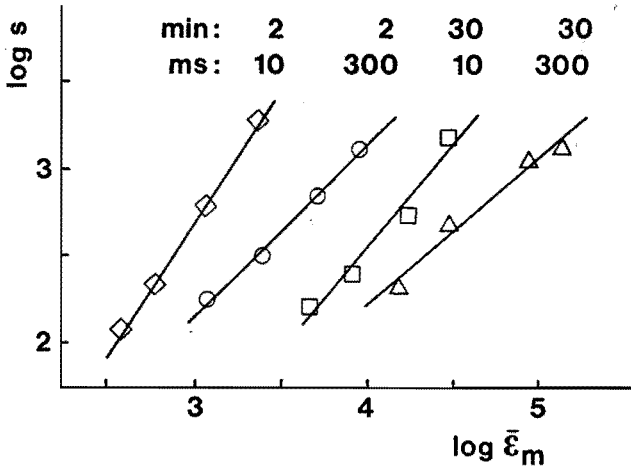


Figure 9: Standard deviation versus mean increment in retinal illuminance of fractionation points with least-squares approximations. Data have been horizontally shifted by multiples of 0.5 log unit in order to avoid overlap.

	$\frac{d \log s}{d \log \bar{\epsilon}_m}$	$2 - \frac{d \log s}{d \log \bar{\epsilon}_m}$	β_f
2'- 10 msec	1.52	0.48	0.65
30'- 10 msec	1.17	0.83	0.92
2'-300 msec	0.98	1.02	0.87
30'-300 msec	0.84	1.16	1.11

Table 7: Least-squares slopes from Fig. 9 brought into relation with fractionation exponents.

$(2 - \beta_f)$. This correspondence possibly implies a deviant proposal for the just noticeable brightness difference: an alternative to Fechner's and Brentano's postulates that the just noticeable brightness difference is either constant or proportional to the absolute brightness level (e.g. Stevens, 1961)³. Assume, according to Crozier's law (e.g. Roufs, 1974), that the just noticeable difference of sequential increments in retinal illuminance is proportional to the standard deviation of the measured distribution: $\delta\varepsilon = k_1 s$. The corresponding just noticeable brightness difference is

$$\begin{aligned} \delta B &= k_2(\varepsilon + \delta\varepsilon)^\beta - k_2\varepsilon^\beta \\ &= k_2\varepsilon^\beta \left(1 + \frac{k_1 s}{\varepsilon}\right)^\beta - k_2\varepsilon^\beta \\ &\approx k_2\varepsilon^\beta \left(1 + \beta \frac{k_1 s}{\varepsilon}\right) - k_2\varepsilon^\beta \\ &= \frac{k_1 k_2 \beta s}{\varepsilon^{1-\beta}} \end{aligned} \tag{18}$$

Only the assumption that $\delta B = k_3 \varepsilon$ will lead to the relation required. By substituting in eq. (18), it follows that

$$s = k_3 \varepsilon \cdot \frac{\varepsilon^{1-\beta}}{k_1 k_2 \beta} = k \varepsilon^{2-\beta} \tag{19}$$

Hence,

$$\frac{d(\log s)}{d(\log \varepsilon)} = 2 - \beta \tag{20}$$

We see that the assumption $\delta B \propto \varepsilon$ can explain the achieved fractionation results. Curiously, our postulate holds the midway between those made by Fechner and Brentano, $\delta B = K$ and $\delta B \propto \Delta B \propto \varepsilon^\beta$ respectively, where the latter is applied to brightness increments instead of to absolute brightnesses.

³Stevens (1966) proposed Brentano's assumption, being the subjective counterpart of Weber's law, to be called Ekman's law.

3 Large-field Asymmetry in Brightness and Apparent-Contrast Perception

Abstract

Experiments have been performed on the quasistatic perception of brightness and apparent contrast of a foveal one degree disk, presented either as a luminance increment or as a decrement against a 300 cd.m^{-2} background. Results suggest that the perceptual attributes of brightness and apparent (or subjective) contrast are to be distinguished. They are consistent with the assumption that brightness increments and decrements can both be described by a Stevens power function of the respective luminance increments and decrements. Apparent contrast can, apart from applying the usual physical contrast formulas, also be described as a power function of the luminance difference with the background.

For an equal brightness difference with respect to the background, luminance increments are more effective than decrements. However, for an equal apparent contrast with respect to the surround, it is found that luminance increments and decrements, up to 100 cd.m^{-2} , are about equally effective; for higher values luminance decrements are more effective than increments.

3.1 Introduction

Relatively few studies have been concerned with the relation between the perception of brightness and darkness¹. Some of these studies are concerned with the temporal behaviour of the visual system (Magnussen and Glad, 1975; White et al., 1980) or with physiology (Krüger and Fischer, 1975). More work has been done with respect to the brightness of stimuli as influenced by the luminance of the surround (Stevens, 1961; Horeman, 1965; Saunders, 1972; Bodmann et al., 1979). As for the spatial suprathreshold Broca-Sulzer effect for incremental disks (Higgins and Rinalducci, 1975), only a single study is known to us that reports a spatial Broca-Sulzer effect for decremental disks (Björklund and Magnussen, 1979).

Moreover, all studies report in terms of brightness. In judging brightness (or darkness) attention has to be focussed quite intensively to a precisely defined point in the visual field. This would imply that brightness is a strictly *local* perceptual attribute. Irrespective of the complexity of a perceived brightness pattern, there also exists a simultaneously perceived and unambiguous impression of the *global* apparent (or subjective) contrast. It seems as if this percept is predominantly an edge effect, i.e. strongly related to luminance transitions and consequently brightness transitions. The question arises whether equal-brightness stimuli, if

¹Darkness is often referred to if the stimulus brightness is lower than the background or surround brightness. Hence, brightness is used in case of luminance increments and darkness in case of decrements, although in both situations the absolute brightness can be judged.

presented against the same background/surround, do also have an equal apparent contrast with the surround; whether apparent contrast can be directly related to some property of the brightness pattern. An indication of this duality between brightness and apparent contrast is reported by Georgeson and Sullivan (1975) who matched the apparent contrast of sinewave gratings with varying spatial frequency. Some evidence has been found that the apparent contrast of sinewave gratings is directly related to differences between local brightness extremes (Arend et al., 1981; Arend and Lange, 1980).

A next question considers the symmetry or asymmetry in the perception of brightness and darkness, and the symmetry or asymmetry in apparent contrast. Burkhardt et al. (1984), who used 1.4 degree single bars, reported contrast symmetry. It is beyond any doubt that the perceptual attribute of apparent contrast was used as a criterion in their experiments. Contrary to this conclusion, Magnussen and Glad (1975) reported a significant asymmetry between the perception of brightness and darkness of temporal stimuli. However, as for most studies, they performed experiments in which either brightness or darkness were matched, the results being compared on a 'log relative luminance' scale. Following this procedure, no conclusion can be drawn as to the relation between the magnitudes of brightness and darkness sensation.

In order to address these questions, we have performed experiments on the perception of both brightness and apparent contrast of disks with varying diameter, presented either as a luminance increment or as a decrement against a fixed background. In order to restrict the vast number of possible stimulus combinations, we partitioned the experiments in three distinct groups:

1. The study of the (a)symmetry of the brightness difference and the apparent contrast with respect to the background, using large fields 1 degree in diameter.
2. The effect of stimulus diameter on the brightness and apparent contrast of *incremental* disks.
3. The effect of stimulus diameter on the brightness and apparent contrast of *decremental* disks.

The results reported here deal only with the first group, the 1° disk asymmetry. The other groups will be presented in chapter 4. Further experiments on the brightness and apparent contrast of blurred disks and circular cosine gratings will be presented in chapter 5. In order to enable a quantitative combination of the various results afterwards, we kept the experimental conditions constant as much as possible, including a background of 300 $cd.m^{-2}$, quasistatic temporal envelopes of the spatial stimuli, monocular viewing and the same subject to perform all observations.

As stated by Burkhardt et al. (1984), the judgment of the apparent contrast of incremental and decremental stimuli is a task that subjects perform very easily. This would imply that, in our situation, the apparent contrast of incremental and decremental 1° disks can be compared directly. However, for brightness no such direct comparison between increments and decrements is possible, if the state of the system is kept constant by keeping the background luminance constant. Judgment of brightness differences has been applied more often (Curtis, 1970; Curtis and Rule, 1972; Arend et al., 1981) and was shown to be useful. Therefore we also performed experiments in which the brightness difference with respect to the background was taken as a criterion. In order to obtain insight into the consistency of these measurements, we introduced a second stimulus, a non-contiguous annulus of width 0.5 degree. Both disk and annulus can be presented either as a luminance increment or as a decrement. This makes a total of 6 stimulus combinations, see Fig. 1. It should be emphasized that these stimulus combinations were presented sequentially, in order to avoid simultaneous contrast effects. All combinations are to be considered twice: once to measure the attribute brightness (or brightness difference with respect to the background) and once to measure the attribute apparent contrast with respect to the steady surround.

3.2 Apparatus and Methods

Stimuli were generated by means of a specially developed circular CRT device, with spiral scan and a white phosphor, the maximum luminance being about 2000 cd.m^{-2} . A deflection unit provides x and y driver signals to write 256 spiral turns in progressive scans, having a frame frequency of 150 Hz. The z-modulation input, to be synchronized with the frame and spiral turn timing, is corrected turnwise by means of an EPROM-driven μDAC to compensate for the nonuniform velocity of the beam. The z modulation input is provided for by a control unit, based on a microprocessor system that is linked with a mainframe computer. The control unit provides three channels; each of these enables us to generate an independent stimulus in space (the 256 spiral turns) as well as time (the envelope of the spirals in 6.6 msec samples). In addition, the overall modulation in luminance of each channel is controlled by independent, software-programmable, digital attenuators. Thus, within the restriction of radial symmetry, a wide variety of stimuli and stimulus combinations can be generated under software control.

Disks and annuli were generated as luminance increments as well as decrements on a homogeneous background field of 300 cd.m^{-2} ; see Fig. 1. All stimuli had quasi-static temporal envelopes, that consisted of three contiguous time functions of 300 msec each, i.e. a constant plateau, flanked by two error-functions truncated at 1% of their asymptotic tails, thus avoiding typical transient phenomena. Sequential pairs of stimuli were presented in various combinations, avoiding order

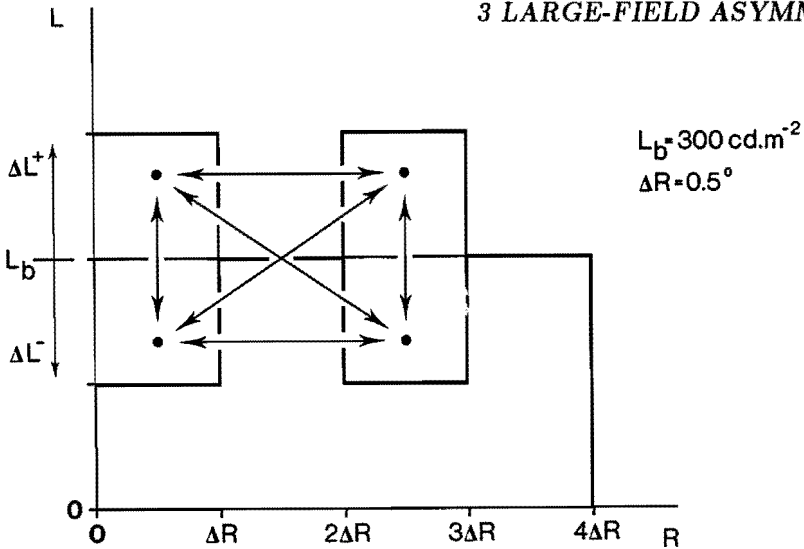


Figure 1: A schematic reproduction (cross section) of the circular stimuli and the stimulus combinations used in the experiments. The centre of the 4 degree diameter background field was fixated. Both the 1 degree disk and the 0.5 degree annulus could be presented as a luminance increment or as a decrement. Stimulus combinations were always presented sequentially.

effects by changing the order of test and reference. This was mainly done because the apparatus did not allow for a simultaneous presentation of for instance an incremental and a decremental disk. However, sequential presentation has the advantage that the subject is not forced to compare separated stimuli simultaneously. An interstimulus interval of 500 msec was used as well as a delay of 300 msec between the control of a start button, used in self-release, and the first stimulus. All observations were performed by a well-trained subject (JDB). This subject, astigmatic myope with a corrected-to-normal vision, observed with the right eye and with natural pupil (approx. 3 mm in diameter).

All stimulus combinations, as indicated by the arrows in Fig. 1, were judged in two experiments using different perceptual attributes as a criterion. The first experiment involved comparing the brightness on the flat plateaus: i.e. the centre of the disks and the middle of the annuli. If test and reference were of the same polarity, for instance an incremental disk and an incremental annulus, the absolute brightnesses of these could be matched. At different polarities, for instance an incremental disk and a decremental annulus, the brightness differences with respect to the steady background level had to be matched. The second experiment involved comparing the apparent contrast of any stimulus with its surrounding background.

In all matching experiments the method of constant stimuli was used, a 50% point being computed from two series of 10 test-reference sequences with observational probabilities between 10% and 90%. Both 'larger than the reference' and

'smaller than the reference' were used as criteria, with equal number of trials, in order to avoid systematic deviations from the point of subjective equality due to just noticeable differences. This was done 8 times, for all stimulus combinations and matching criteria, in randomized blocks, although experiments on brightness and apparent contrast were performed in separate sessions. The geometric mean of the 8 resulting 50% points was computed for any of the reference levels. Additional detection experiments, following the same method, were performed to measure the thresholds of the 4 stimuli.

3.3 Results

The results of all matching experiments, i.e. on both brightness and apparent contrast, are combined in Figs. 2 and 3, in the form of graphs giving log threshold corrected luminance increments and decrements. Fig. 2 presents the results obtained with equal stimulus polarities, obtained by matching the absolute brightnesses of for instance an incremental disk and an incremental annulus, and by matching the apparent contrasts of these stimuli. There is no significant difference between incremental and decremental presentations, nor between the results using brightness or apparent contrast as a criterion.

The first sequel is that brightness decrements, similar to increments, can be described by a Stevens relation, i.e.

$$\Delta B \propto (\Delta L - \Delta L_{thr})^\beta \quad (1)$$

when ΔL , that is the luminance increment or decrement with respect to the steady background L_b , exceeds a threshold increment or decrement ΔL_{thr} . Using log threshold corrected luminance differences, linear graphs are to be expected for matching results. Giving subscripts T and R to test and reference stimuli,

$$\Delta B_T \propto (\Delta L_T - \Delta L_{T,thr})^{\beta_T} \quad (2)$$

$$\Delta B_R \propto (\Delta L_R - \Delta L_{R,thr})^{\beta_R} \quad (3)$$

matching of brightness or brightness differences ($\Delta B_T = \Delta B_R$) leads to

$$\log(\Delta L_T - \Delta L_{T,thr}) \propto \frac{\beta_R}{\beta_T} \log(\Delta L_R - \Delta L_{R,thr}) \quad (4)$$

Thus, putting log threshold corrected luminance increments or decrements of a test and a reference stimulus on ordinate and abscissa respectively, the slope of the matching results will correspond to the exponent ratio β_R/β_T . This ratio of Stevens exponents turns out to be independent of the stimulus polarity for the disk-annulus combination. The second sequel is that this exponent ratio approximates 0.8 and not 1. Since all possible sequences of stimuli and test-reference exchanges

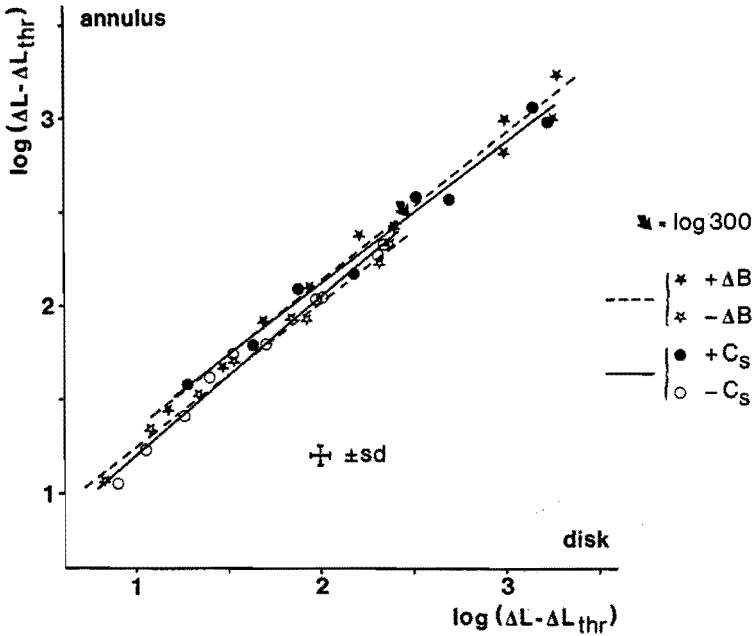


Figure 2: Matching stimuli with equal polarities, i.e. either increments or decrements. Both axes are given in log threshold corrected luminance increments or decrements, expressed in $cd.m^{-2}$. Straight lines are least-squares approximations. Since a 300 cd.m^{-2} background was used, the maximum luminance decrement corresponds to $\log(300) = 2.48$; this maximum is indicated by the small arrow.

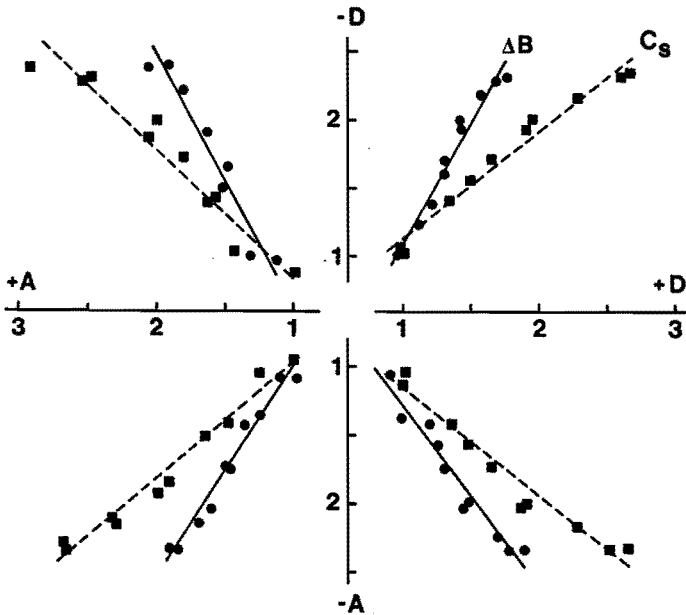


Figure 3: Matching results obtained with opposite stimulus polarities. Stimuli are denoted by +D (incremental disk), -D (decremental disk), +A (incremental annulus) and -A (decremental annulus). Same coordinates as in Fig. 2. Least-squares approximations have been drawn through the data.

have been considered, showing no measurable differences due to metacontrast, this leads to the suggestion that the unequal Stevens exponents reflect the area and retinal position of the stimuli. However, detection thresholds do not reflect this influence, for it was found that threshold luminance increments and decrements of all 4 stimuli were equal (4.8 cd.m^{-2}). The third sequel is that apparent contrast, similar to brightness, can possibly be described by a Stevens relation directly based on luminance increments and decrements instead of by one of the usual luminance-contrast formulas; see also Discussion. In addition, the results obtained here can be regarded as a verification of the generally accepted hypothesis that equal brightness stimuli also have an equal apparent contrast with their surrounding background. As will be shown in the following chapter, this only holds for large fields!

In Fig. 3 the results obtained with opposite stimulus polarities are presented. The striking difference between the brightness and apparent-contrast results obtained here is the first indication that the percepts of brightness and apparent contrast are distinct. Concentrating on the main goal of this study, the 1° disk asymmetry, it follows that $\beta^+ \approx 1.8 \beta^-$ if the Stevens brightness exponent of the incremental disk is symbolized by β^+ and that of the decremental disk by β^- . For an equal brightness difference with respect to the background the luminance increment required is smaller than the luminance decrement. A similar asymmetry was found in on- and off-centre neurons in the cat's visual system (Krüger and Fischer, 1975).

The contrast-matching results relate approximately linearly in log threshold corrected coordinates. This would imply that the nonlinear relation between apparent contrast and luminance increments or decrements can also be described by means of a Stevens relation, similar to brightness, though with other exponents. The exponent ratio for incremental versus decremental disks approximates 0.8, about half the ratio obtained for brightness. However, a more accurate consideration of the apparent-contrast results shows that for large values there is a significant deviation from a straight line. For smaller luminance increments and decrements, up to 100 cd.m^{-2} , the matching data approximate a straight line with slope 1 through the origin. This means that stimuli with equal luminance increments and decrements are perceived with an equal apparent contrast. The threshold correction applied has no influence on this conclusion, since thresholds of all 4 stimuli are equal and about 5 cd.m^{-2} . For larger luminance values, a systematic departure towards luminance increments is found. This result is examined below, where a direct relation is sought between apparent and physical contrast, by using a contrast formula.

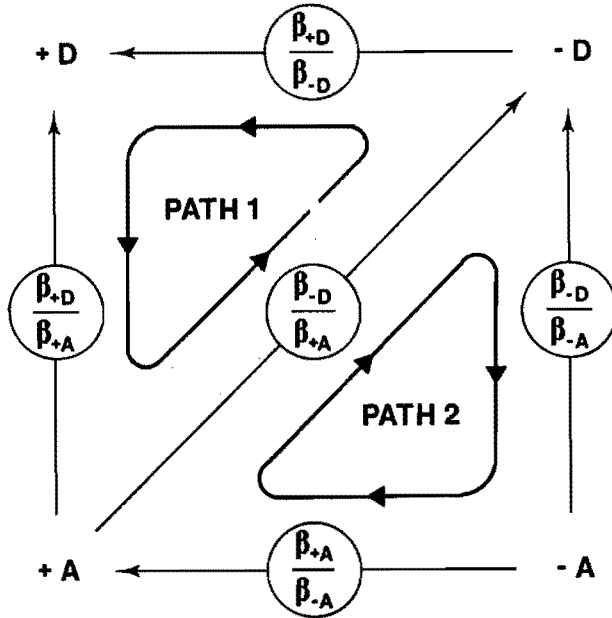


Figure 4: Stimulus combinations and exponent ratios. Stimuli are denoted by +D (incremental disk), -D (decremental disk), +A (incremental annulus) and -A (decremental annulus). Arrows point towards assumed references in order to define exponent ratios unambiguously.

3.4 Discussion

The Relation between Apparent Contrast and Brightness

In Figs. 2 and 3 it is shown that matching of brightness and brightness differences with respect to the steady background leads to linear graphs in log threshold corrected luminance increments and decrements. The slopes of these graphs equal the ratios of the Stevens exponents as illustrated in figs. 4 and 5. In order to define the exponent ratios unambiguously, the direction of the arrows has been chosen arbitrarily, but in such a way that they point in the direction of 'reference' stimuli, in correspondence with eq. (4). However, least-mean-square slopes (exponent ratios) will be obscured by measurement error. Since all possible stimulus combinations have been considered, we can study the mutual transitivity of all results; see also chapter 2. This is demonstrated in Fig. 4. Concentrating on the exponent ratio of the incremental annulus (+A) and decremental disk (-D), the least-squares slope of the matching results would equal β_{-D}/β_{+A} . In a full consistent or transitive system of exponent ratios, independent predictions for this ratio can be computed. Following path 1 of Fig. 4, one can derive that repeated application of eq. (4) leads to

$$\frac{\beta_{-D}}{\beta_{+A}} \cdot \frac{\beta_{+D}}{\beta_{-D}} \cdot \frac{\beta_{+A}}{\beta_{+D}} = 1 \quad (5)$$

Therefore, it follows that

$$\frac{\beta_{-D}}{\beta_{+A}} = \frac{\beta_{-D}}{\beta_{+D}} \cdot \frac{\beta_{+D}}{\beta_{+A}} \quad (6)$$

and consequently for path 2

$$\frac{\beta_{-D}}{\beta_{+A}} = \frac{\beta_{-D}}{\beta_{-A}} \cdot \frac{\beta_{-A}}{\beta_{+A}} \quad (7)$$

Combining the directly measured β_{-D}/β_{+A} and the independently predicted values following eqs. 6 and 7, we obtain a new estimation of the exponent ratio for this stimulus combination:

$$\frac{\beta_{-D}}{\beta_{+A}} := \frac{1}{3} \left\{ \frac{\beta_{-D}}{\beta_{+A}} + \frac{\beta_{-D}}{\beta_{+D}} \cdot \frac{\beta_{+D}}{\beta_{+A}} + \frac{\beta_{-D}}{\beta_{-A}} \cdot \frac{\beta_{-A}}{\beta_{+A}} \right\} \quad (8)$$

Applying this averaging procedure for all 6 stimulus combinations, it even appeared that successive substitution converged rapidly into a full consistent scheme of exponent ratios. The data on brightness, both least-squares slopes and successive substitution results, are presented in the top row of Fig. 5. Following any closed path in the top-right panel, taking into account the directions of the arrows, the product of the exponent ratios equals 1. It should be pointed out that in the procedure mentioned above two exponent ratios have been kept fixed. These were the ratios obtained by matching equal-polarity stimuli: β_{+D}/β_{+A} and β_{-D}/β_{-A} . In this situation we were able to compare the absolute brightness of the stimuli and the results were found to be very reliable and almost identical (Fig. 2).

This same procedure was applied to the apparent-contrast results. In Fig. 3 we saw that, to a first order approximation, the matching results obtained with apparent contrast are also to be represented by a linear graph in log threshold corrected luminance increments and decrements. This would suggest that apparent contrast C_S is a power function of the brightness difference ΔB and thus of the luminance difference ΔL with respect to the background L_b :

$$C_S \propto (\Delta B)^\alpha \propto (\Delta L - \Delta L_{thr})^{\alpha\beta} \quad (9)$$

The least-squares slopes of the apparent contrast matching results, equal to $(\alpha\beta)$ -ratios, are given in the middle-left panel of fig. 5, while the results of the successive substitution process are presented in the middle-right panel. From all available exponent ratios, i.e. both β 's and $(\alpha\beta)$'s, it is possible to compute the ratios of the brightness-to-apparent-contrast exponents α . These are given in the bottom row of Fig. 5. As can be seen, the α -ratios have only two distinct values. For

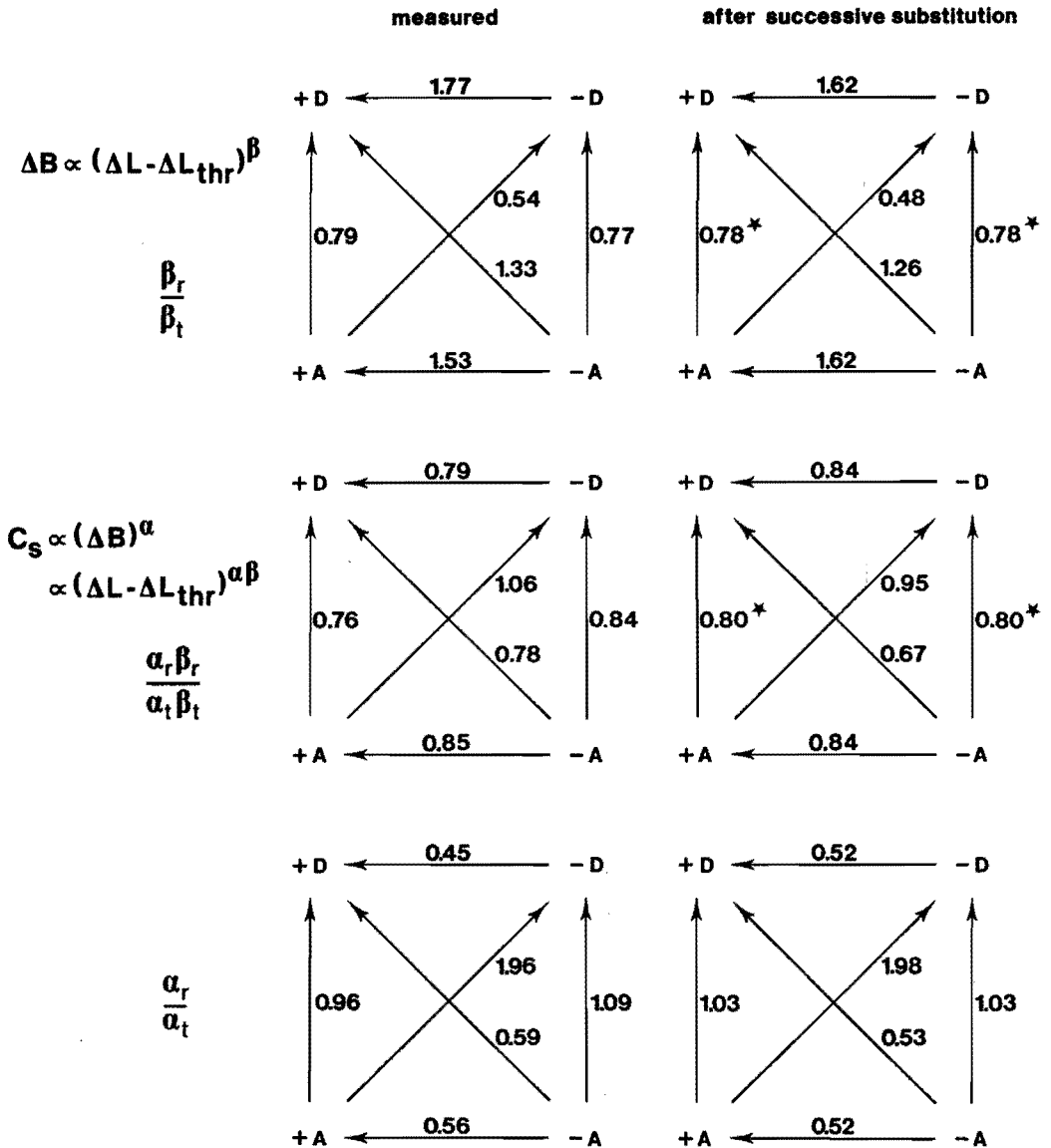


Figure 5: Ratios of Stevens exponents for brightness (top row), apparent contrast (middle row) and their interrelation (bottom row). Measured values are given in the left column, while the results of a successive substitution process are given in the right column. For details see text.

stimuli with equal polarities this value is 1 and for stimuli with opponent polarities it is 0.5 (or 2 in the opposite direction). This means that the measured difference between brightness and apparent contrast, caused by the stimulus polarity, is rather consistent.

Since matching only provides us with exponent ratios, the values of the separate exponents of the stimuli are still unknown. However, reported results from scaling experiments on large, long-duration fields presented against photopic backgrounds are available. From earlier experiments (see chapter 2) we concluded that the brightness exponent of an incremental 30' diameter - 300 msec duration stimulus on a 100 Td background approximates 2/3. Similar values, about 1/2, are reported by Stevens and Stevens (1960), Onley (1961) and Warren (1976). Note that these exponents deviate from those measured against a dark background, which are often found to be 1/3 (e.g. Mansfield, 1973). Assuming the brightness exponent of an incremental quasistatic 1° disk to be 1/2, all other brightness exponents can be computed on the basis of Fig. 5. Such a computation is not only applicable in case of brightness but also in case of apparent contrast of course. The latter case would involve scaling of apparent contrast rather than brightness. Magnitude estimations on the apparent contrast of decremental 1.4 degree bars were performed by Burkhardt et al. (1984). Their results indicate that the apparent contrast of decremental bars is a power function of the (Michelson) luminance contrast (see also next section) with an exponent of 0.83. Approximating the Michelson contrast, which is defined as $(L_{max} - L_{min}) / (L_{max} + L_{min})$, for luminance decrements not too large, suggests that the apparent contrast of decremental bars is a power function of the luminance decrement with an exponent of 0.83. Fractionation (i.e. halving) of the apparent contrast of edges revealed that apparent contrast is a linear function of the Michelson contrast, although the same method applied to sinewave gratings revealed exponents between 0.6 and 1.5 (Kulikowski, 1976) ...

On Luminance Contrast

In the foregoing, apparent or subjective contrast was related to brightness differences. Instead of this indirect relation $C_S = f(\Delta B) = g(\Delta L)$, a direct relation between apparent contrast and luminance contrast C is often looked for: $C_S = h(C)$. Unfortunately, this procedure has led to a variety of contrast formulas, applicable to different stimulus configurations. It has brought little insight, perhaps even confusion. Even with periodic gratings, for which the Michelson contrast is commonly used, no agreement has been reached on the question whether apparent grating contrast is a linear function of physical contrast (Cannon, 1980) or a Stevens power function with exponent 0.7 (Gottesman et al., 1981), while both used magnitude estimation. In a recently published paper (Burkhardt et al., 1984) it is reported that matching of apparent contrast yields stimuli with approximately

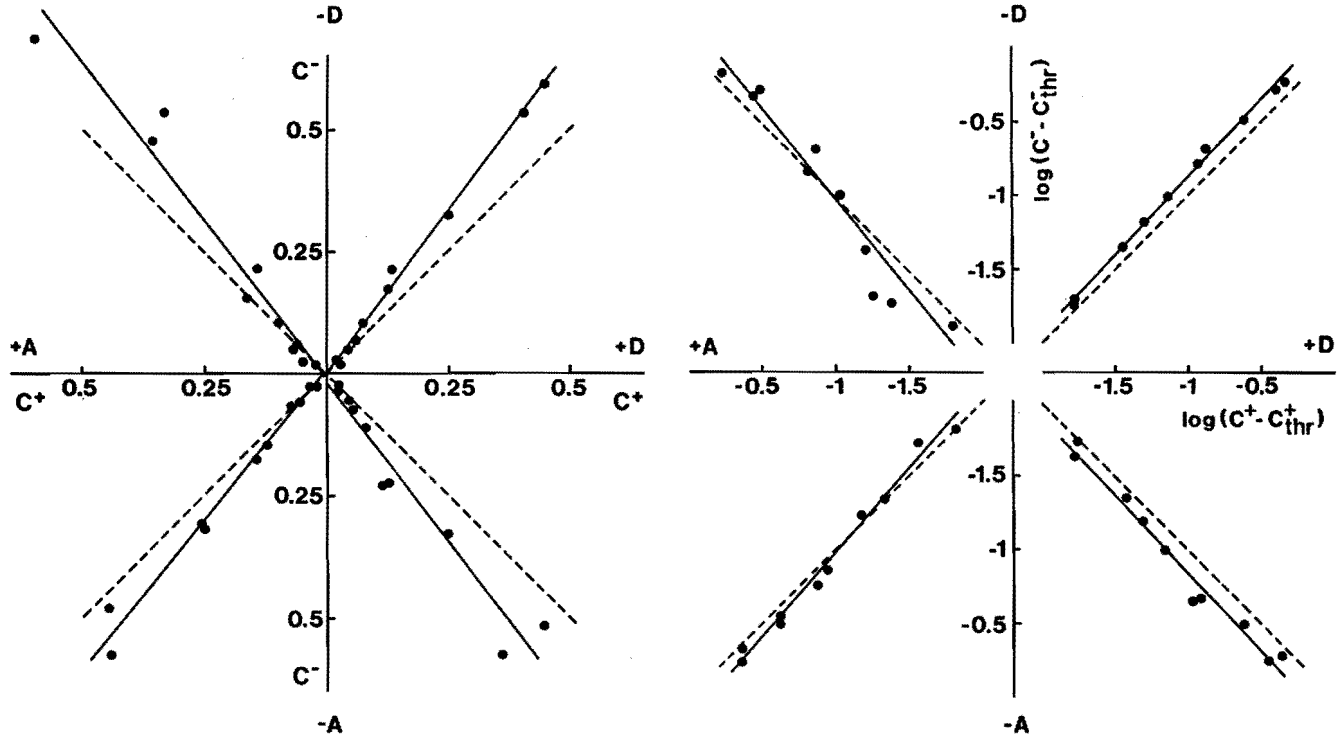


Figure 6: Apparent contrast matching results plotted in linear contrast coordinates (left panel) and in log threshold corrected contrast coordinates (right panel). In both graphs the Michelson contrast formula $C = (L_{max} - L_{min}) / (L_{max} + L_{min})$ has been applied. Dashed lines depict symmetry, drawn lines are least-squares approximations.

equal physical (Michelson) contrast: $C^+ = C^-$. In Burkhardt's study single 1.4° bars have been used, both as increments and decrements, on various backgrounds. Using the Michelson contrast formula, we are able to relate luminance increments with decrements for an equal apparent contrast. Substituting $L_{max} = L_b + \Delta L^+$ and $L_{min} = L_b$ for incremental stimuli on the one hand, and $L_{max} = L_b$ and $L_{min} = L_b - \Delta L^-$ for decremental stimuli on the other, we obtain

$$\Delta L^- = \frac{\Delta L^+ \cdot L_b}{\Delta L^+ + L_b} \quad (10)$$

where L_b , ΔL^+ and ΔL^- represent the background luminance, increments and decrements respectively. Obviously, Burkhardt's contrast symmetry leads to $\Delta L^+ = \Delta L^-$ for small contrasts. This is confirmed by our data, see Fig. 3: for luminance increments and decrements up to 100 cd.m^{-2} matching of apparent contrast yields approximately equal luminance differences. But what about larger values? In Fig. 6 our apparent contrast data are given in linear contrast coordinates as well as in log threshold corrected contrast coordinates. Contrary to Burkhardt's results, the linear plot shows a strong asymmetry: $C^- = 1.3C^+$. In log threshold corrected contrast coordinates however, symmetry is more pronounced. Using the empirical Stevens relation for apparent contrast, i.e. $C_s \propto (C - C_{thr})^\gamma$, it follows that the ratio of exponents $\gamma^+/\gamma^- = 1.1$ if γ^+ denotes the Stevens contrast-exponent for increments and γ^- that for decrements. In agreement with Burkhardt's results, we may conclude that the application of a luminance contrast formula produces a linearization of the matching results. Linear and logarithmic presentations appear to be appropriate, although neither renders exact symmetry.

Brightness versus Apparent Contrast

We noticed that matching of apparent contrast is a very easy task, suggesting the possibility that it is an independent perceptual attribute and, perhaps, as dominant as brightness. The same conclusion has been reached earlier by Burkhardt. Moreover, our results suggest that a distinction has to be made between the attributes of brightness and apparent contrast and that subjects should be instructed very carefully on their task. The question arises whether previous studies on brightness were influenced by ignoring this distinction between the perceptual attributes; i.e. whether in fact subjects judged the easy-to-handle (global) apparent contrast or the more difficult (local) brightness. Unfortunately there are very few studies on brightness available that allow for a quantitative comparison with our results. The only one we know of has been published by Bodmann et al. (1979). They performed bisection and ratio scaling experiments on the brightness of a 2° field having a 300 cd.m^{-2} surround. They also determined the absolute black level dependent on both visual angle and surround luminance. From these results they constructed the following brightness model:

$$B = C_T(\varphi) \cdot L_T^\beta - B_o(L_b, \varphi) \quad (11)$$

with

$$B_o(L_b, \varphi) = C_T(\varphi) \cdot [S_0(\varphi) + S_1(\varphi) \cdot L_b^\beta] \quad (12)$$

In these equations L_T and L_b are absolute luminances of the test field and surround respectively, B_o an absolute black level correction, β the brightness exponent, while C_T , S_0 and S_1 are constants dependent on the visual angle φ . Furthermore, the brightness was normalized: $\tilde{B} = B(L_T = L_b = 300 \text{ cd} \cdot \text{m}^{-2}) = 100$. Introducing luminance increments and decrements for equal brightness differences with respect to the surround leads to

$$\tilde{B} + \Delta B = C_T(L_b + \Delta L^+)^\beta - B_o \quad (13)$$

$$\tilde{B} - \Delta B = C_T(L_b - \Delta L^-)^\beta - B_o \quad (14)$$

These equations form an implicit relation between ΔL^+ and ΔL^- which we want to compute at given equal brightness differences ΔB . This procedure has been followed using Bodmann's brightness model, as mentioned above, as well as Burkhardt's contrast symmetry in accordance with eq. (10). The results are given in Fig. 7 along with our present data on the 1° field. Note that this graph, similar to Fig. 3, is given in log threshold corrected luminance increments and decrements. This means that a threshold correction has been applied to both Bodmann's and Burkhardt's model predictions. This threshold was symmetrical and equal to $5 \text{ cd} \cdot \text{m}^{-2}$, which corresponds to our threshold data, but had in fact no influence on all curves. It can be seen from Fig. 7 that the computed matching points based upon Burkhardt's contrast symmetry (solid squares) agree with our apparent-contrast data (open squares) quite well. However, the computed points according to Bodmann's brightness model (solid circles) also agree with our apparent-contrast results as well as Burkhardt's, but not with our results on brightness differences (open circles).

This finding, and the ascertained difference between brightness and apparent-contrast data in particular, leads to some interesting considerations. The first is whether matching of brightness differences is a valid paradigm and really reflects the asymmetry of brightness perception. There is evidence that judging brightness differences is a useful and reliable task indeed (Curtis, 1970; Curtis and Rule, 1972). This suggests at least the acceptability of the paradigm. The second is whether brightness and apparent contrast are indeed essentially different perceptual attributes. This conjecture is raised by the high degree of mutual consistency displayed by our results gathered for the various stimulus combinations. In chapter 4 additional evidence concerning this matter will be given.

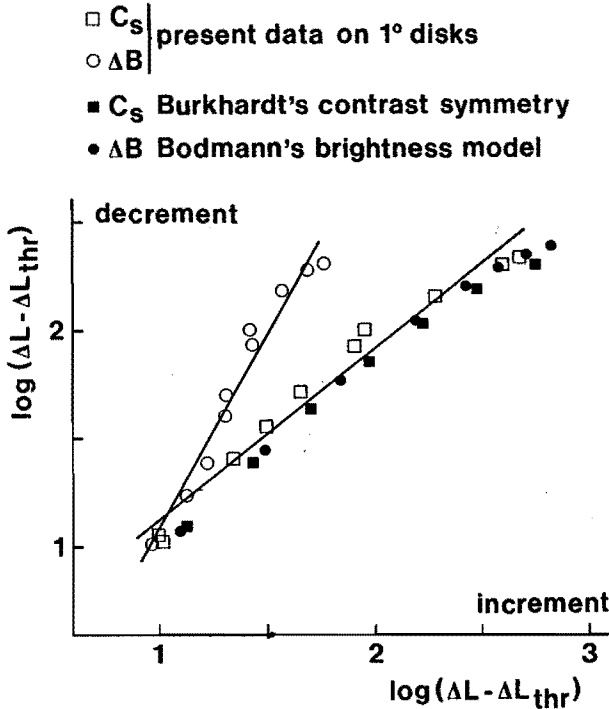


Figure 7: Our results on brightness differences (open circles) and apparent contrast (open squares) in comparison with predictions based upon Bodmann's absolute-brightness model (solid circles) and Burkhardt's contrast symmetry (solid squares). All graphs are given in log threshold corrected luminance increments and decrements. Our data correspond to the upper-right quadrant of Fig. 3.

Absolute Brightness and Absolute Luminance

The results discussed so far indicate that brightness and luminance should be considered relative to the steady background or adaptation level, i.e. in terms of luminance differences and consequently brightness differences with respect to the background, instead of in absolute magnitudes. The use of absolute luminances in comparable situations is often taken for granted, which hampers a direct comparison with our present data on brightness differences.

It is however possible to derive a graph of absolute brightness versus absolute luminance for the 1° disk surrounded by 300 $cd.m^{-2}$. Instead of using Stevens' relations for increments and decrements, we depart from a combination of our brightness-difference matching results with Stevens' relation applied to increments. Brightness-difference matching data can be rewritten as the explicit relation $\Delta L^- = f\{\Delta L^+ - \Delta L_{thr}^+\}$. In a first transformation step we derive the relation $\Delta L^- = g\{\Delta B^-\}$, by assuming $\Delta B^+ = (\Delta L^+ - \Delta L_{thr}^+)^{1/2}$ for increments

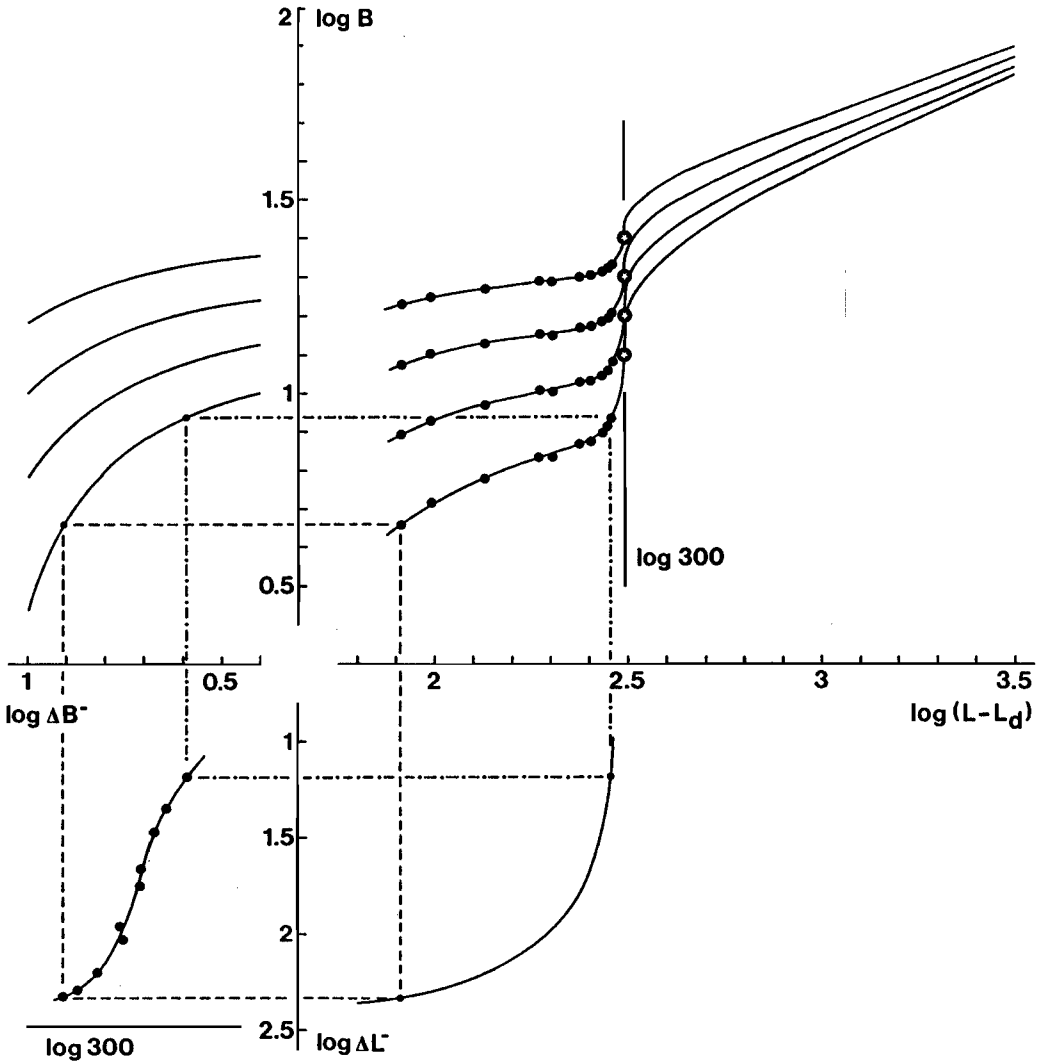


Figure 8: Illustration of the transform that yields a brightness versus luminance relationship for a 1° disk surrounded by 300 cd.m^{-2} . The result of the first step is shown in the lower-left quadrant. The final transformation result is shown in the upper-right quadrant. Graphs are supplemented for luminances above surround. Assumptions for the surround brightness B_b are indicated by inverted star symbols. For explanation see text.

and substituting the matching paradigm $\Delta B^+ = \Delta B^-$. Notice that in Stevens' relation for increments the proportionality constant has been taken as unity and that the exponent for large disks on a photopic background is assumed to be 0.5. The result of this first transformation step is presented in the lower-left panel of Fig. 8. If Stevens' relation applies also for decrements, linearity on the basis of log threshold corrected luminance decrements was to be expected. As shown, the converted data suggest a slight nonlinearity, even if threshold corrections are made. The same conclusion could be made on the basis of Fig. 3, although its significance is questionable because of the standard deviation of the matching results!

In a second transformation step absolute values are derived. Brightness B is given by $B = B_b - \Delta B^-$, where ΔB^- is the brightness decrement and B_b the brightness of the background/surround. An assumption has to be made for the value of B_b . Strictly speaking, the introduction of an explicit value for brightness, as for the proportionality constant in Stevens' relation, is meaningless, but it is required in order to construct curves of brightness versus luminance. The lower-left quadrant of Fig. 8 shows that the maximum brightness decrement ΔB_{max}^- , which depends on the assumptions made with respect to Stevens' relation for increments of course, occurs for $\log(\Delta B^-) \geq 1$. Once that the maximum brightness decrement is estimated, the numerical value of the background brightness is known, since $B_b = \Delta B_{max}^-$. In order to illustrate the influence of this estimation, we used four values for $\log(B_b)$: 1.1, 1.2, 1.3 and 1.4 respectively. Thus, ΔB^- can be converted into B . Similarly, the luminance decrement can be converted into absolute luminance, since $L = L_b - \Delta L^-$, with $L_b = 300 \text{ cd.m}^{-2}$. For low values of luminance a correction can be made for the absolute dark level, as suggested by Bodmann et al. (1979). From their results it can be assumed that this absolute dark level L_d approximates 6.5 cd.m^{-2} for a 1° disk surrounded by 300 cd.m^{-2} , although introduction of L_d is not crucial here. The final result of the conversion is given in the upper-right panel of Fig. 8. Graphs have been supplemented for luminances above 300 cd.m^{-2} , by using $B = B_b + (L - 300 - \Delta L_{thr}^+)^{1/2}$, in agreement with the assumed Stevens relation for increments. It may be concluded that a sigmoidal transition appears around surround luminance, and that it decreases if higher values for B_b are assumed. Finally, the constructed brightness versus luminance curves reveal a rough similarity with sigmoidal-shaped magnitude-estimation curves, obtained in comparable situations (Saunders, 1972; Onley, 1961). A closer similarity is demonstrated with the lightness curves as given by Semmelroth (1970). Our curves clearly disagree with the monotoneous curve from Bodmann et al. (1979) on the one hand, as well as the sharply kneed curves from Stevens (1961) and Horeman (1965) on the other.

In conclusion, it is possible to derive brightness versus luminance curves on the basis of brightness-difference data. These curves seem to agree with some published data, the occurrence of a sigmoidal transition around surround luminance

in particular. The significance of the resulting curves is questionable though, since they depend on rather arbitrary assumptions with respect to numerical values for the background brightness and the proportionality constant in Stevens' power law for increments.

4 Brightness and Apparent-Contrast Perception of Incremental and Decremental Disks with Varying Diameter

Abstract

This chapter concerns the matching of brightness and of apparent contrast of foveal disks, presented against a 300 cd.m^{-2} background. If the brightness in the centres of disks, with varying diameter, is matched with a constant reference brightness, the well-known spatial Broca-Sulzer phenomenon is found. However, this effect is not found if the apparent contrast is matched. All matching results and detection thresholds indicate that luminance increments and decrements are asymmetrically processed by the visual system. Two non-linear single-channel models are tested against the data.

4.1 Introduction

Varying the diameter of a disk with a constant luminance usually shows a specific diameter for which its brightness is larger if compared to smaller and larger disks. This spatial brightness-enhancement or Broca-Sulzer phenomenon is reported at dark backgrounds (Hanes, 1951; Glezer, 1965; Hay and Chesters, 1972) and at higher background levels (Higgins and Rinalducci, 1975; Björklund and Magnussen, 1979). The name of this effect is derived from the temporal Broca-Sulzer effect (Broca and Sulzer, 1902; Rinalducci and Higgins, 1971; Magnussen and Glad, 1975; Bowen and Markell, 1980; White et al., 1980). Spatio-temporal interaction with respect to this effect has also been studied (Arend, 1973; Higgins and Knoblauch, 1977; Bowen and Pokorny, 1978; Drum, 1984). The related Mach-band effect, often thought as a result of the band-pass behaviour of the visual system, also received considerable attention (McCollough, 1955; Matthews, 1966; von Békésy, 1968; Bergström, 1973).

Some experiments, dedicated to the temporal Broca-Sulzer effect, suggest that luminance increments and decrements are processed asymmetrically by the visual system. Data obtained with pulsed decrements (White et al., 1980) indicate that maximum darkness enhancement occurs for longer durations as compared with maximum brightness enhancement. This would imply that the impulse response for decrements is broader than that for increments. Such a shift has not been observed in the square-wave periodic situation (Magnussen and Glad, 1975). On the other hand, the latter authors conclude that the amplitude gain shows a strong asymmetry. However, there is some difficulty in interpreting their data. Graphs are presented in 'log relative luminance' (LRL) and amplitude gain is defined in terms of differences of the LRL. If expressed in log luminance increments and

decrements, their data show a much less pronounced asymmetry, and incremental gain even exceeds decremental gain!

In the only available study on the spatial Broca-Sulzer effect for decremental disks (Björklund and Magnussen, 1979), experimental data are given in absolute luminances and not in luminance differences with respect to the background as frequently used in case of increments. A curve with unit *slope* has been obtained for small disks, be it on the basis of log absolute luminance versus log diameter coordinates. This conflicts with the often confirmed Ricco's law, which implies a reciprocity between the luminance difference with the background and disk area, and therefore pure integration for very small stimuli. However, it can be verified easily that their data, if converted into log luminance decrement versus log area coordinates, yield an *asymptote* with unit slope for small disks. Their data on suprathreshold decremental disks do therefore agree with Ricco's law. Moreover, this conversion of the data renders a less pronounced spatial Broca-Sulzer effect, i.e. a smaller dip in the matching curve. It equals 0.2 log units, which is about half of its magnitude if expressed in log absolute luminance. As for the temporal Broca-Sulzer effect for aperiodic stimuli, a direct comparison of the spatial Broca-Sulzer effects, although measured by different subjects, suggests a strong asymmetry between incremental and decremental stimuli (Higgins and Rinalducci, 1975; Björklund and Magnussen, 1979).

Some of the studies mentioned above are, apart from spatial or temporal summation, also concerned with the question how the visual system deals with stimuli of opposite polarity. Physiology suggests that brightness and darkness perception is a consequence of processing by centre-on and centre-off retinal receptive fields. Significant differences are reported on receptive-field sizes as well as asymmetry in spike frequency (e.g. Krüger and Fischer, 1975). The increasing evidence that the visual system consists of two antagonistic neural B- and D-systems indeed invites for further psychophysical research on this subject (e.g. van Erning, 1984).

All studies on the spatial Broca-Sulzer effect are related to the perception of brightness (brightness-enhancement!). Recently published results, however, have shown that the apparent or subjective contrast can be judged directly, irrespective of the stimulus polarity (Burkhardt et al., 1984). This is confirmed by our own results on one-degree disk asymmetry (see chapter 3). These experimental results suggest that the perceptual attributes of brightness, being a strictly local phenomenon in the visual field, and apparent contrast as a more global property of a brightness pattern, are to be distinguished. In other words, matching either the brightness or the apparent contrast of disks with varying diameter might yield different experimental results. In addition, while most studies have been performed at relatively low background levels and moderate luminance increments, we now have the opportunity to use high background levels and yet high luminance increments.

In order to explore the spatial Broca-Sulzer effect for luminance increments and decrements, and its dependence on the perceptual attribute that is used as a matching criterion, we performed several experiments. In these experiments the subject matched either incremental or decremental disks, with varying diameter and with quasistatic temporal envelope, presented foveally and against a 300 cd.m^{-2} background. The only difference between the experiments was the perceptual attribute that the subject judged: the brightness in the centre of the disk or the apparent contrast with respect to the surround. Incremental disks were also matched with respect to the brightness maximum (for small disks in the centre, for large ones at the inner edge).

It should be emphasized that this study is part of a series in which other spatial patterns, such as blurred one-degree disks and radially symmetric cosine gratings are also considered. The aim of this series of experiments is to combine the various results by means of a spatial model that describes both brightness and apparent-contrast perception quantitatively. To this purpose the experimental conditions, including the same subject to perform all observations, have been kept constant as much as possible.

4.2 Methods

A special-purpose CRT to generate both background and stimuli was used. A detailed description of this display has been given in the foregoing chapter. The homogeneous and steady background of the radial screen, subtending 0.75 degrees of visual angle, was extended to 5x5 degrees. This extension had about the same hue and brightness. The background luminance was 300 cd.m^{-2} , and the hue white. The barely visible transition between screen and extension was used to fixate the centre of the screen.

The stimuli consisted of incremental and decremental luminous disks with varying diameter, always presented in the centre of the screen, and with quasistatic temporal envelope. This envelope had a duration of 900 msec. It consisted of a centre plateau of 300 msec that was flanked by errorfunction-shaped transitions of 300 msec.

All observations were performed by a well-trained subject (JDB). In all experiments he observed with the right eye, and made use of an artificial pupil, 2 mm in diameter, that was equipped with an entoptic guiding system.

On any trial, test and reference stimuli were presented sequentially, with an interstimulus interval of 500 msec. A delay of 300 msec was regarded between the control of a start-button and the release of the first stimulus. Sequences of both test-reference and reference-test stimuli were presented with an equal number of trials, showing no significant order effects. The method of constant stimuli has been applied throughout the experiments. For each determination a 50% point was

computed from two series of 10 trials, with observational probabilities between 10% and 90%. Both 'larger than the reference' and 'smaller than the reference' were used, with equal number of trials, in order to avoid systematic deviations due to just noticeable differences. This was done 8 times for every stimulus combination. The geometric mean of the 50% points was taken as the point of subjective equality. In addition, detection thresholds have been determined by following the same procedure.

In case of incremental disks, we performed three experiments in separated sessions. The only difference was the perceptual attribute that the subject used as a matching criterion: the brightness in the centre of the disk, the brightness maximum and apparent contrast. In order to exclude any absolute-brightness clue in the apparent-contrast experiment, we used a decremental reference there. This means that incremental test stimuli, with varying diameter, were compared with a fixed, decremental reference. The decremental reference was obtained by *mirroring* an incremental reference, such that both these references had an equal apparent contrast with the surround. The procedure to obtain this mirrored reference, in fact a matching experiment on its self, as well as the ease of the subject's task, has been described in chapter 3.

In case of decremental disks, we performed only two experiments: on centre-brightness and apparent contrast. To exclude any absolute-brightness clue in matching the apparent contrast, we provided an incremental reference.

4.3 Results

Centre-brightness of Incremental Disks

Fig. 1 shows the results of the experiment in which the brightness in the centre of the incremental disks was used as a matching criterion. The luminance increment that is required for detection decreases monotonously with the disk area, displaying Ricco's law for small disks. At suprathreshold levels the brightness-enhancement or spatial Broca-Sulzer phenomenon, the local minimum (dip) in the matching data, becomes evident.

In comparison with already published results (Higgins and Rinalducci, 1975) two observations can be made. First, the magnitude of the Broca-Sulzer effect but also the scattering of the measured data are much smaller in the present case. This may be a consequence of the different psychophysical methods applied. Higgins et al. used the method of adjustment, while we used the method of constant stimuli. Second, for small disks the slopes of the intermediate matching curves in Fig. 1 appear to be larger than 1. By way of comparison, thresholds for small disks do show a slope of value 1 and obey Ricco's law. The slope of value larger than 1 would

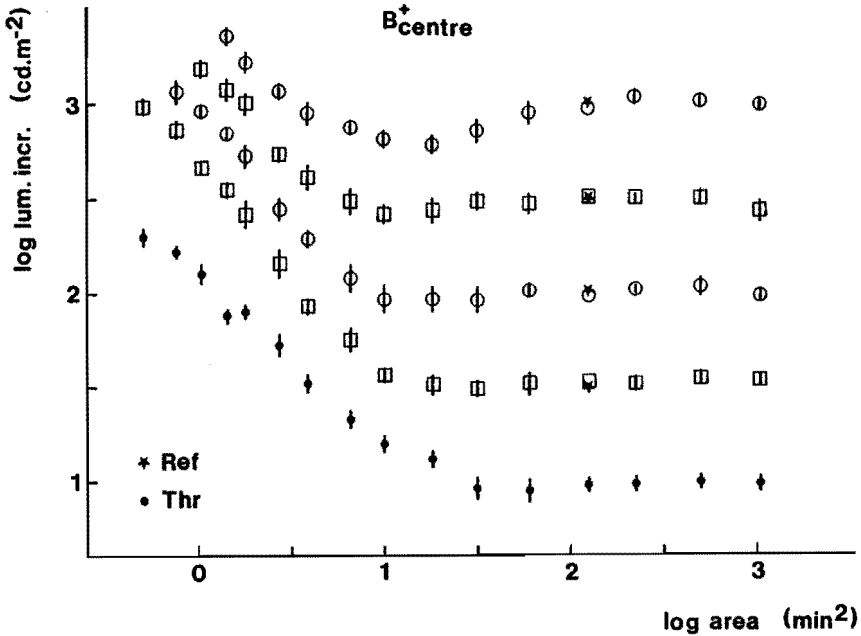


Figure 1: Centre-brightness matching results of incremental disks (open circles and squares). Solid stars represent suprathreshold references. Solid circles are detection thresholds. Vertical bars indicate standard deviations of individual measurements.

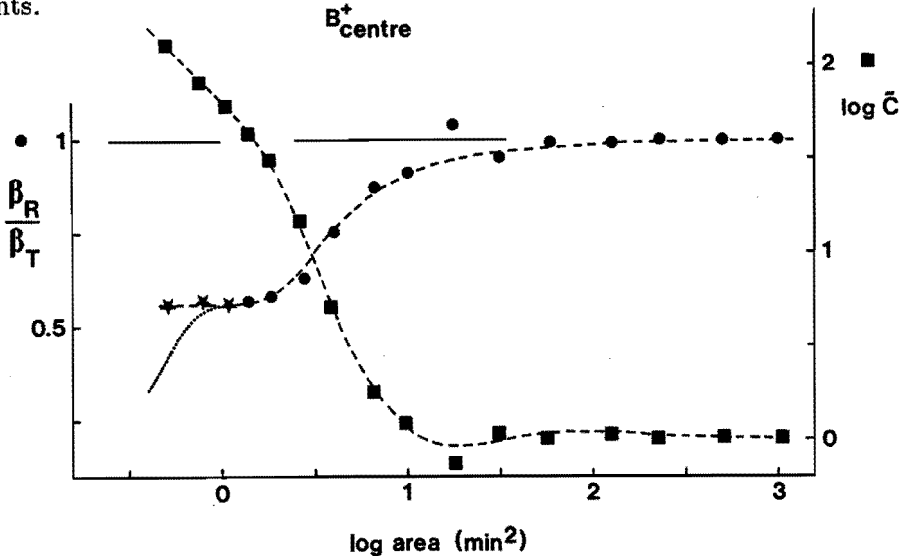


Figure 2: The exponent ratio and the intersection with the ordinate, derived from Fig. 1, as a function of disk area. The dashed curve through exponent-ratio data renders an analytical approximation. For log area smaller than 0 this approximation (the dotted curve) must be extrapolated to obtain a value of 0.56 (solid stars). The dashed curve through $\log \tilde{C}$ data equals a model A prediction. For explanation see text.

imply supersummation¹ (Glezer, 1965) and agrees with Higgins' results. They made use of a Maxwellian-view optical system and concluded that this *anomaly* was probably due to calibration error, i.e. a correction for the effect of diffraction at small apertures should be taken into account. Our experimental results suggest however that supersummation for iso-brightness is indeed significant, for we used a CRT and confirmed Ricco's law at threshold level.

Adopting Stevens' empirical relation for brightness and luminance increments against a photopic background,

$$\Delta B = C(\Delta L - \Delta L_{thr})^\beta \quad (1)$$

we are able to examine the influence of disk area on the proportionality constant C and the brightness exponent β . Matching of a test stimulus, with certain area, and a reference of for instance large area, can be written as $\Delta B_T = \Delta B_R$. With eq. (1) substituted it follows that

$$C_T(\Delta L_T - \Delta L_{T,thr})^{\beta_T} = C_R(\Delta L_R - \Delta L_{R,thr})^{\beta_R} \quad (2)$$

This can be rewritten as

$$\begin{aligned} \log(\Delta L_T - \Delta L_{T,thr}) &= \frac{1}{\beta_T} \log \frac{C_R}{C_T} + \frac{\beta_R}{\beta_T} \log(\Delta L_R - \Delta L_{R,thr}) \\ &= \log \tilde{C} + \frac{\beta_R}{\beta_T} \log(\Delta L_R - \Delta L_{R,thr}) \end{aligned} \quad (3)$$

In words, if log threshold-corrected luminance increments of a test and a reference stimulus are plotted on ordinate and abscissa respectively, the slope of the data points equals the exponent ratio β_R/β_T and the intersection with the ordinate equals $\log \tilde{C}$. The results of this procedure, if applied to the data of Fig. 1, are shown in Fig. 2. The function of $\log \tilde{C}$, dependent on stimulus area, can be regarded as the result of a fictitious matching experiment, obtained with a reference for which $\Delta L_R - \Delta L_{R,thr} = 1$. It can, in combination with the exponent ratio, also be interpreted as a summary of all matching data of Fig. 1. From Fig. 2 it is clear that the brightness exponent is monotonously related to stimulus area. Since the exponent for large, long-duration fields presented against a photopic background is reported to approximate 0.5 (Stevens and Stevens, 1960; Onley, 1961; Warren, 1976), see also chapter 2, it would follow that the exponent increases from 0.5 for large disks to about 0.9 for small ones.

We examined two simple nonlinear models to fit the centre-brightness matching results; see the Appendix. In order to avoid confusion, we will deal only with the first one (Model A) throughout the text. This means that all predictions to

¹Supersummation means more than pure integration of the luminance over the disk area by a low-pass filter.

be presented are based on model A. Model B is analyzed only in the Appendix, although both models appeared to render quantitatively similar results.

Model A consists of a linear operator, characterized by a fixed point spread function, followed by a compressive nonlinearity, being a powerfunction which depends on the disk diameter. The exponent ratio shown in Fig. 2, being derived from a comparison of input parameters, was used to describe the nonlinearity, and thus incorporated into the model. To this purpose, the exponent ratio has been fitted by the analytic expression

$$\frac{\beta_R}{\beta_T} = \begin{cases} \{ [1 + 7(\log A)^3]^{-1} + 1 \}^{-1} & ; \log A \geq 0 \\ 0.56 & ; \log A < 0 \end{cases} \quad (4)$$

in which $\log A$ denotes the log of the disk area in square min. of arc. The free parameters of the model, viz. being the amplitudes and 'standard deviations' of the point spread function (PSF), which is assumed to be shaped like the difference of two Gaussians (usually abbreviated DOG), have been determined to fit all centre-brightness data simultaneously. The resulting PSF for incremental disks is shown in Fig. 3 by solid circles. The excitatory region of this PSF is slightly wider than the optical PSF of the human eye for a 2 mm pupil (Vos et al., 1976). Furthermore, this suprathreshold PSF appears somewhat narrower than those measured at threshold level using the perturbation technique (Blommaert and Roufs, 1981). The latter are pure band-pass filters because of their much more pronounced inhibitory action, while the present suprathreshold PSF resembles a high-emphasis filter in the frequency domain, i.e. with a finite DC transfer. Finally, the model

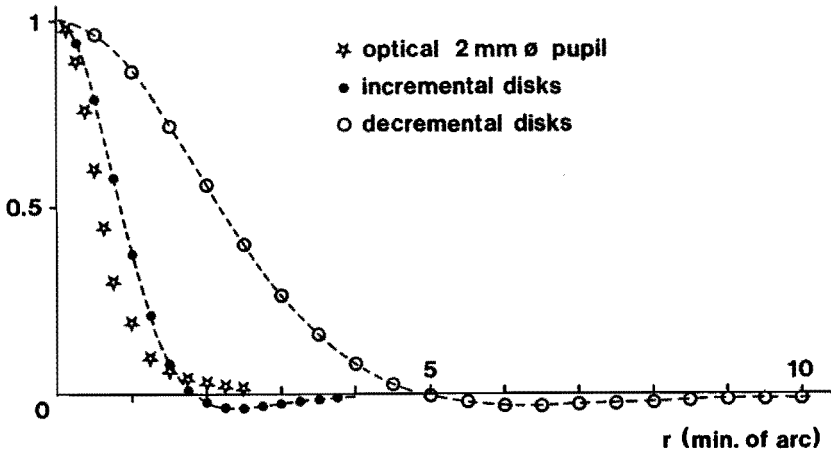


Figure 3: Normalized point spread functions of brightness Model A for increments (solid circles) and for decrements (open circles). The optical PSF for a 2 mm pupil is reproduced by open stars for comparison.

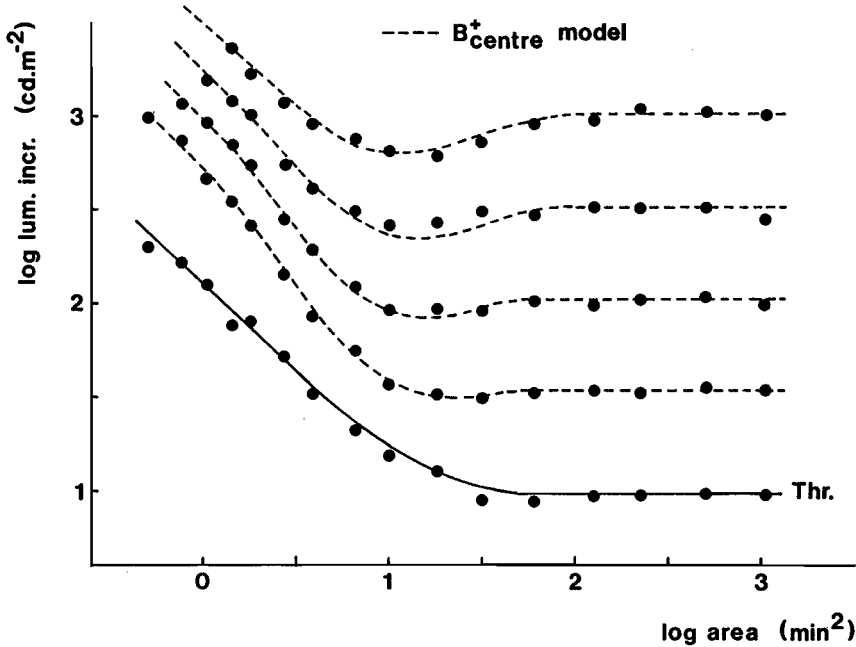


Figure 4: Measured data along with model A approximations for a centre iso-brightness of incremental disks (dashed curves). Detection thresholds have been fitted by means of a Gaussian low-pass PSF with $\sigma = 1.42$ min. of arc.

prediction for $\log \tilde{C}$, thought as an imaginary matching curve, is presented as the dashed curve in Fig. 2. In Fig. 4 our experimental results are shown in combination with the model A approximations. It is obvious that this model, although a bit peculiar at first sight, satisfies reasonably well. Moreover, the supersummation 'anomaly' is explained by the influence of the size-dependent nonlinearity in the model. This means that the suprathreshold PSF may be shaped rather normally, such as a DOG with a maximum in its centre. The alternative nonlinear model, which is based on a level dependent PSF as introduced by Furukawa and Hagiwara (1978), see model B in the Appendix, might also be considered. It can be shown, that this model renders point spread functions which display a local minimum in their centre. These point spread functions must therefore be shaped as the sum of at least three Gaussians in order to explain both the supersummation and the brightness-enhancement effects.

Centre-brightness of Decremental Disks

Disk thresholds and centre-brightness matching results are presented in Fig. 5. The detection threshold as a function of disk area varies in the same way as in case of increments. For small disks an asymptote with unit slope, in agreement with Ricco's law, is observed. Comparing Figs. 1 and 5, thresholds appear to

be exactly symmetrical for large disks. The main difference between detection-threshold curves of incremental and decremental disks is a shift of 0.6 log units along the abscissa (for a direct comparison see Fig. 14).

At suprathreshold levels the spatial Broca-Sulzer effect appears again. Its magnitude is about 0.1 log unit, which is smaller than in the incremental situation (0.2 log units). Maximum darkness enhancement is found for disks with larger diameters than maximum brightness enhancement. A direct comparison of results obtained with incremental and decremental disks, both at threshold and suprathreshold levels, therefore indicates that the spatial summation area changes by about a factor of 4 with polarity.

A high degree of similarity appears to exist between our decremental curves and that measured by Björklund and Magnussen (1979), provided that their data are converted into log luminance decrement versus log area coordinates. Moreover, the similarity between incremental and decremental curves shown in Figs. 1 and 5 (see also Fig. 14) suggests that, irrespective of the asymmetry, the visual system acts primarily on the basis of differences with respect to the homogeneous background.

Similar to the incremental situation, the relation between input parameters can be examined on the basis of the empirical Stevens relation. Adopting this relation also for decrements, we can apply eqs. (1) to (3). The result of this approach is presented in Fig. 6. The exponent ratio reaches a local maximum for disks subtending about 10 min. of arc. For incremental disks the exponent ratio was found to increase monotonously with area.

Both model A and model B have also been examined for decremental disks. The exponent of the compressive nonlinearity of model A, which depends on disk size, is derived from the exponent ratio as given in Fig. 6:

$$\frac{\beta_R}{\beta_T} = \sum_{i=0}^5 a_i (\log A)^i \quad (5)$$

with $a_0 = 0.209$, $a_1 = 1.032$, $a_2 = -0.448$, $a_3 = 0.173$, $a_4 = -0.070$, $a_5 = 0.011$ and $\log A$ the log of the disk area in square min. of arc. The resulting PSF for suprathreshold luminance decrements is reproduced in Fig. 3 by open circles. Obviously, the PSF for decrements is much broader than that for increments. The diameters of the excitatory centres appear to differ by about a factor of 2. If allowance is made for the optical PSF (Vos et al., 1976), it follows that the neural PSF strongly depends on stimulus polarity.

Curves of equal centre-brightness, as a consequence of the model A approximation, are presented in Fig. 7. The model prediction for $\log \tilde{C}$, to be considered as an imaginary matching result obtained with $\Delta L_R - \Delta L_{R,thr} = 1$, has already been given in Fig. 6. It can be concluded that an excellent fit is provided by Model A. The same conclusion can be made for model B: see Fig. 14.

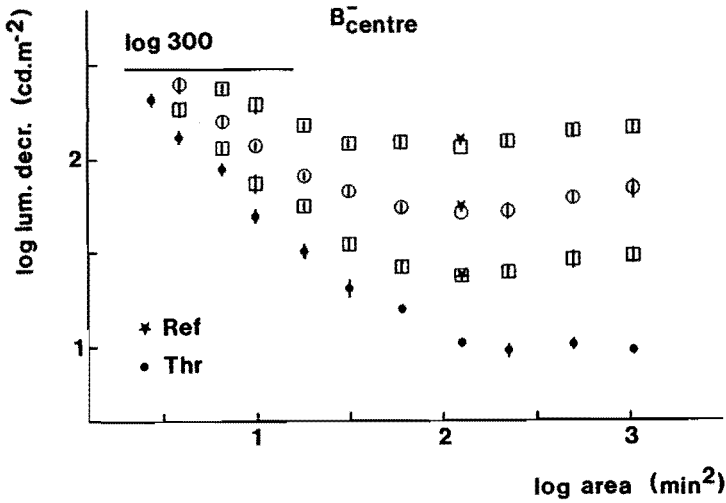


Figure 5: Detection thresholds (solid circles) and centre-brightness matching results (open circles and squares) for decremental disks. Solid stars represent suprathreshold references and vertical bars render the standard deviation of individual measurements.

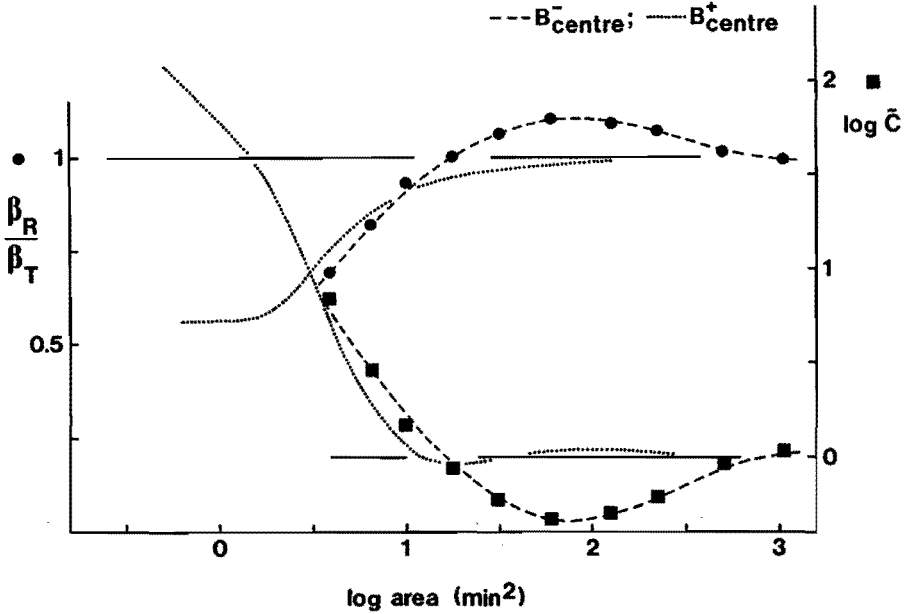


Figure 6: Exponent ratio and $\log \tilde{C}$ as a function of area for decremental disks, derived from Fig. 5. The dashed curve through exponent-ratio data represents a polynomial approximation, the dashed curve through $\log \tilde{C}$ data renders a model A prediction. Data for incremental disks are given by dotted curves for comparison.

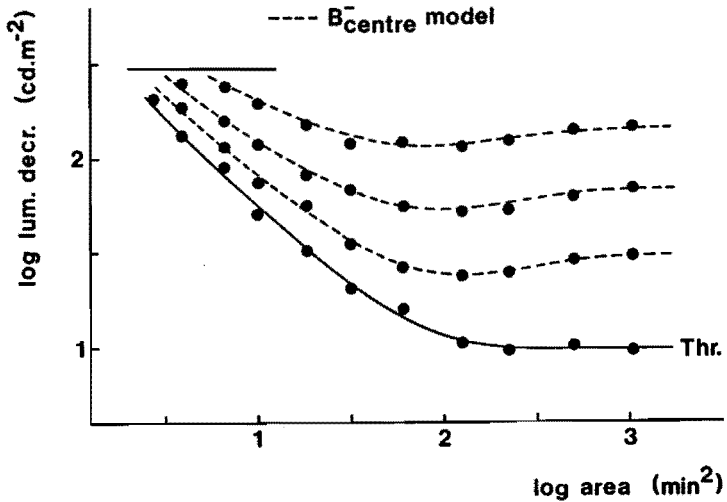


Figure 7: Centre-brightness matching data for decremental disks along with model A approximations (dashed curves). Detection thresholds have been fitted by means of a Gaussian low-pass point spread function with $\sigma = 2.9$ min. of arc.

Maximum Brightness of Incremental Disks

The results of this experiment are shown in Fig. 8. Compared with the centre-brightness matching data, which are reproduced by the dashed curves in Fig. 8, a somewhat larger luminance increment is required for small and intermediate disks, and the magnitude of the Broca-Sulzer effect has decreased. As indicated by the dash-dotted curves, the prediction of model A is quite accurate. It should be obvious that in this model prediction the convolution result of disk and PSF in the centre of the stimulus has been replaced by the convolution maximum, the maximum being transferred by the size-dependent nonlinearity. The position of this maximum depends on the disk diameter. For small disks it is found in the centre, while for larger ones it shifts towards the inner edge. Since the suprathreshold PSF is known, i.e. computed from the centre-brightness matching data, the maximum of the convolution result can be determined numerically for any disk size.

Apparent Contrast of Incremental Disks

The matching results on apparent contrast are presented in Fig. 9. As stated before, we used a decremental reference in this experiment to exclude any absolute-brightness clue. This means that the references given in Fig. 9 are indirect. For any level of the luminance increment we determined the luminance decrement such that the perceived apparent contrast was equal. The resulting luminance decrements provided fixed decremental references to be compared with the incremental test stimuli. From Fig. 9 we may conclude that the spatial Broca-Sulzer effect has

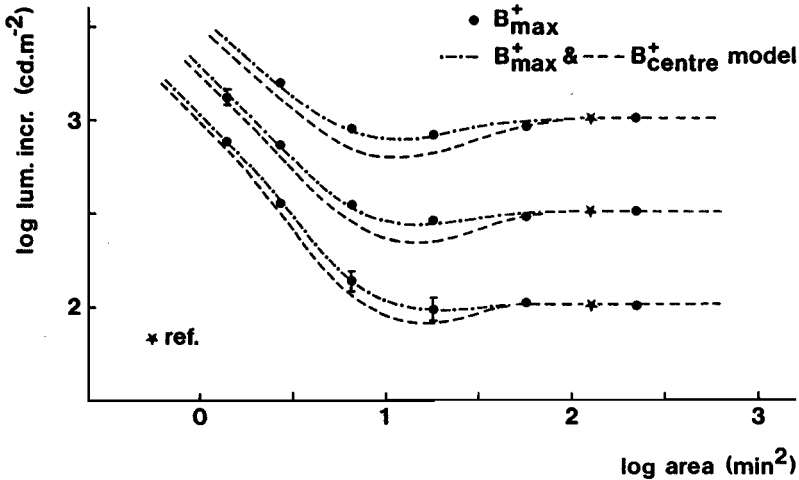


Figure 8: Maximum-brightness matching results of incremental disks, along with Model A predictions (dash-dotted curves). Centre-brightness results are indicated by dashed curves for comparison.

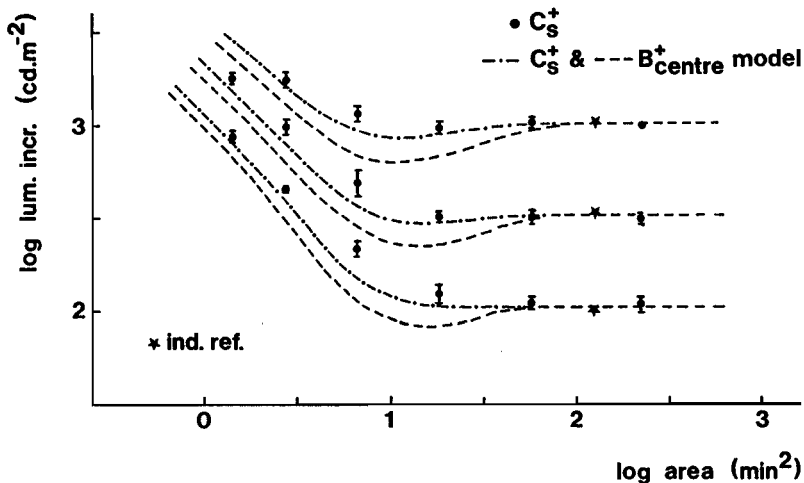


Figure 9: Apparent-contrast matching results for incremental disks. Dashed curves resemble an equal centre-brightness. Dash-dotted curves are model A predictions for an apparent iso-contrast, based on the difference between brightness extremes at the edge. Solid stars represent indirect, i.e. mirrored and therefore decremental, references.

vanished completely. Moreover, the supersummation effect has disappeared and curves of equal apparent contrast reflect a 'pure low-pass character' satisfying Ricco's law for small disks. These curves are therefore similar to the threshold detection curve, the only difference being a shift of the critical area. This critical area corresponds to the intersection of the respective asymptotes for small and large disks. It seems as if the critical area decreases for higher levels of stimulation.

Along with the experimental results, a model prediction is presented in Fig. 9 by the dash-dotted curves. In this prediction, in fact a first attempt to define the nature of apparent-contrast perception, apparent contrast is related to the difference between the local brightness extremes on either side of the disk edge. This difference was determined by convolving the disks with the suprathreshold PSF, as derived from the centre-brightness data, following the same procedure as was done for the maximum-brightness matching prediction. From Fig. 9 it follows that the prediction approaches experimental results for small disks, though does not quite satisfy for medium-sized ones. This could mean that apparent-contrast perception is not a function of the difference between the local brightness extremes at the edge (the Mach-band phenomenon), but should be related to some other function of the brightness pattern. For instance, the maximum brightness gradient at the edge might be considered. The consequences of these considerations will be discussed further on.

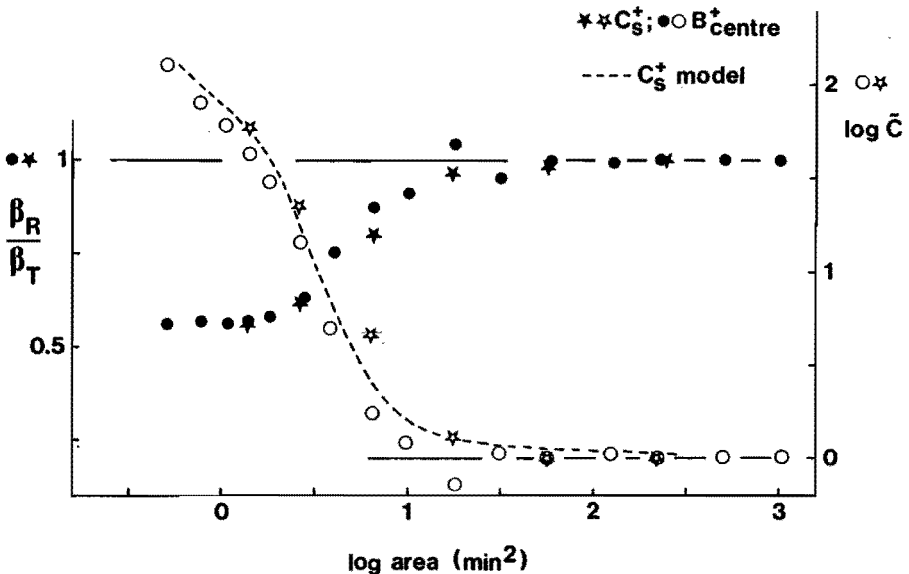


Figure 10: Summarized results for the apparent contrast of incremental disks (stars), similar to Fig. 2. The dashed curve is a model A prediction for an apparent iso-contrast, see text. The data on centre-brightness are reproduced for comparison (circles).

In the same way as was done for the centre-brightness results, the relation between input parameters can be studied for the apparent-contrast situation. The data on large-field asymmetry, see chapter 3, revealed the possibility that apparent-contrast perception can also be described by the empirical Stevens relation, i.e. a power function of threshold corrected luminance increments and decrements, similar as brightness though with different exponents. Applying this procedure (see also eq.(3) and Fig. 2) to the present data given in Fig. 9, we obtain Fig. 10. The exponent-ratio points for apparent contrast (solid stars) resemble those for centre-brightness (solid circles), but the intersection with the ordinate $\log \tilde{C}$ (open symbols) diverges for smaller disks. The dashed curve, being a model prediction for $\log \tilde{C}$ in case of apparent iso-contrast, approaches the data points for small, though deviates for medium-sized disks. As stated before, this is a clue that some other function of the brightness pattern or a better brightness model should be considered to deduce apparent-contrast perception.

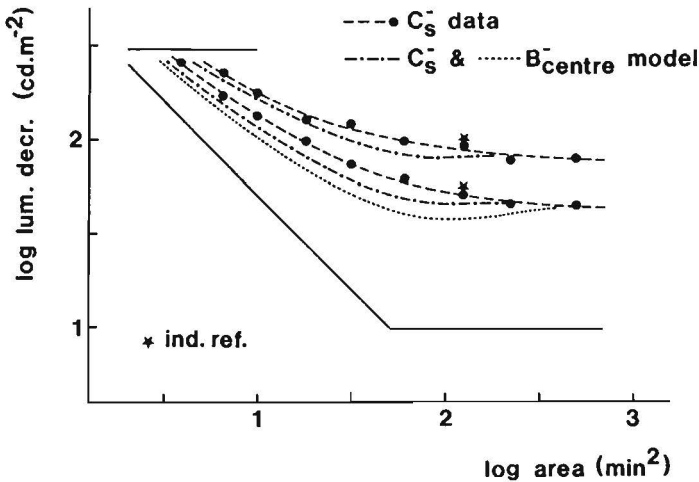


Figure 11: Apparent-contrast matching results for decremental disks. Dashed curves have been drawn freely. Dash-dotted curves correspond to model A predictions for an apparent iso-contrast, based on the difference between brightness extremes at the edge. The dotted curve corresponds to a centre iso-brightness. Detection-threshold asymptotes and the maximum luminance decrement are indicated by solid lines.

Apparent Contrast of Decremental Disks

Fig. 11 shows the results of this matching experiment. Note that indirect references have been used in order to exclude any absolute-brightness clue. This means that the apparent contrast of decremental test disks, with varying area, have been

compared with a fixed incremental reference. This procedure was already used in the incremental situation. From Fig. 11 we may conclude that curves of apparent iso-contrast decrease monotonously with disk area, showing no spatial Broca-Sulzer effect at all. A similar discrepancy between results on brightness on the one hand and apparent contrast on the other was displayed for incremental disks. Again, the model predictions for an apparent iso-contrast, based on the difference between the brightness extremes at the disk edge, do not quite agree with the data.

4.4 General Discussion

Summarizing all experimental results, we may conclude that different perceptual attributes render significantly diverging, though highly related matching curves. For incremental disks, the spatial Broca-Sulzer effect appears to be most pronounced in case of centre iso-brightness, somewhat less in case of maximum iso-brightness, and it vanishes completely in case of apparent iso-contrast. Similar results are found for decremental disks. The main difference between the incremental and decremental situations consists of a mutual shift of all curves, including detection thresholds, with respect to the log area coordinate. Both the Ricco interval and the maximum darkness enhancement effect for decremental disks are displayed for substantially larger disks if compared to incremental disks. Our experimental results can therefore be regarded as a further confirmation of the hypothesis that the visual system processes luminance increments and decrements rather asymmetrically, perhaps even by independent neuronal sub-systems such as centre-on and centre-off receptive fields.

Our present results, the discrepancy between brightness and apparent contrast in particular, link up with the problem that arises in judging suprathreshold sinewave gratings. Georgeson and Sullivan (1975) questioned the ambivalence between *contrast*, which would correspond to the modulation-depth in brightness, and *visibility* indicating apparent or subjective contrast. They suggested to expect different results from these two percepts. For sharp disks it has here been shown that a distinction should indeed be made between these perceptual attributes.

Rather than exploring possibilities to describe the apparent-contrast matching data directly, for instance by means of a spatial low-pass point spread function to be convolved with the disk-shaped luminance profile, our results suggest that apparent-contrast perception is (somehow) related to the brightness profile. Besides, an apparent-contrast model that consists of an initial pure low-pass filter would appear to be peculiar, since it conflicts with the Mach-band phenomenon as revealed in brightness perception. It therefore seems to be more sensible to think in terms of a cascaded model. Brightness is related to luminance in the first stage, while apparent contrast is deduced from the brightness profile in the second stage.

Another consequence of this approach is that direct apparent-versus-physical contrast relations, based upon physical contrast formulas, might become insignificant. The use of the brightness profile as an intermediate between luminance on the one hand and apparent contrast on the other might provide an advantageous alternative to evade the both numerous and confusing contrast formulas proposed in the past.

The suprathreshold disk models examined here are meant as a first attempt to achieve some insight into the mechanism that relates apparent contrast to brightness. Fitted to the centre-brightness data, they both accurately predict the maximum-brightness data. By using the same models, and substituting the absolute difference between the extremes of the convolution result, they fail in predicting the apparent-contrast matching data. We realize that a simple adjustment of the models, for instance by taking some other function of the brightness profile such as the maximum gradient at the edge of the disk, would have been an appropriate next step. The outcome of such attempts can be questioned in advance, however, if the present brightness models are applied. It is known that results obtained with preadaptation (e.g. Bagrash, 1973; Blakemore and Campbell, 1969) point towards multiple parallel channels that govern both disk and grating detection. For suprathreshold levels the same underlying mechanism is suggested (Blakemore et al., 1973). Furthermore, disk and grating results at both threshold and suprathreshold levels display rather 'antagonistic' properties of the visual system. Threshold curves of disks show a low-pass behaviour while iso-brightness curves imply a band-pass or high-emphasis characteristic. For gratings exactly opposite characteristics are found, i.e. band-pass at threshold and low-pass at suprathreshold levels (e.g. Georgeson and Sullivan, 1975; Blakemore et al., 1973). Both these arguments imply the necessity of a nonlinear multiple channel approach of the visual system.

It must therefore be emphasized that both brightness models examined here are to be considered preliminary. Despite their ability to cope with the centre and maximum brightness of disks, they are incapable to describe grating perception. Alternative models should be regarded similarly. The brightness model proposed by Furukawa and Hagiwara (1978), which consists of a level-dependent point spread function, is able to describe iso-brightness curves of disks presented against a dark background. It predicts sensitivity curves of sinewave gratings at different background levels, though fails for suprathreshold grating perception.

In spite of the foregoing, an important advantage of considering these models is that they provide an excellent fit to matching data, albeit with restricted validity. With only a few parameters the matching results can be interpolated using a simple software subroutine, thus allowing for a more profound multichannel model approximation afterwards.

4.5 Appendix

In this appendix we will derive two simple nonlinear models applicable to the brightness perception of disks. Both models contain a point spread function and a compressive nonlinearity. The difference between them consists of the choice of what stage is kept fixed: the PSF or the compressive nonlinearity. It may seem superfluous that we examine two models here. We would like, however, to emphasize the dual aim of this analysis.

Firstly, modelling of psychophysical data, and suprathreshold data in particular, is not a trivial problem. Suprathreshold models have already been explored (Furukawa and Hagiwara, 1978; Swanson et al., 1984). However, they seem to be of limited validity. The nonlinear single channel model derived by Furukawa describes the brightness perception of disks, if they are presented against a dark background. It should be adjusted to cope with brightness perception of disks presented against arbitrary backgrounds, see Model B further on, but it can not be made to agree with suprathreshold grating perception simultaneously. The multi-channel model derived by Swanson et al. is essentially dedicated to the perception of one-dimensional patterns, since it comprises line spread functions. By exploring two alternative models for the brightness perception of disks, we illustrate that the conception of models is no problem at all, provided that a limited stimulus set, such as disks of various diameters, is considered. The real problem is encountered in unifying different stimulus configurations, for instance disks and gratings.

Secondly, data on the perception of blurred disks and gratings, measured under comparable experimental conditions, will be presented subsequently. In order to facilitate further modelling, and the unification of disk and grating results in particular, it appears to be useful to obtain an accurate disk model. Such a model enables fast and smooth interpolation of the measured data, in stead of using the measured data themselves or polynomial approximations.

Model A

Model A consists of a fixed point spread function (PSF) and a nonlinear compression that is dependent on disk size, see Fig. 12. In the first linear stage the luminance pattern, a disk with radius ρ and luminance increment or decrement ΔL , is convolved with the PSF. The PSF is assumed to have a difference-of-Gaussians (DOG) profile

$$PSF(r) = g_1 \cdot \exp(-r^2/2\sigma_1^2) - g_2 \cdot \exp(-r^2/2\sigma_2^2) \quad (6)$$

In the centre of a disk, the convolution result $\Delta I(\rho, r)$ equals

$$\begin{aligned} \Delta I(\rho, 0) &= 2\pi\Delta L \int_0^\rho PSF(r)rdr \\ &= 2\pi\Delta L [g_1\sigma_1^2\{1 - \exp(-\rho^2/2\sigma_1^2)\} - g_2\sigma_2^2\{1 - \exp(-\rho^2/2\sigma_2^2)\}] \quad (7) \end{aligned}$$

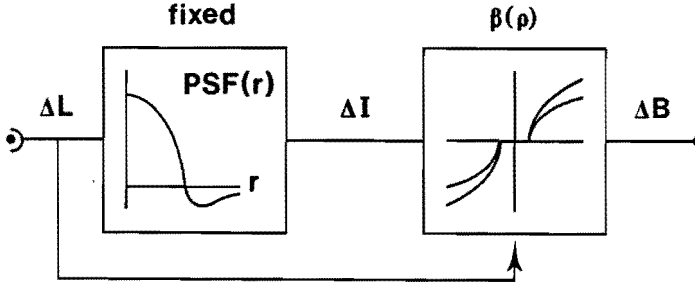


Figure 12: Brightness model A consists of a fixed point spread function, followed by a threshold mechanism and a compressive power function. The exponent β of the nonlinearity depends on the radius ρ of the disk.

For a reference stimulus, which is thought to be of large area, it follows that

$$\Delta I(\infty, 0) = 2\pi \Delta L (g_1 \sigma_1^2 - g_2 \sigma_2^2) \quad (8)$$

The second, nonlinear stage is modelled by means of a Stevens relation

$$\Delta B(\rho, 0) = k \{ \Delta I(\rho, 0) - \Delta I_{thr} \}^{\beta(\rho)} \quad (9)$$

in which ΔI_{thr} equals the unknown, internal signal threshold. For high luminance increments or decrements this threshold correction can be neglected. It has turned out that ΔI_{thr} can be approximated for low increments or decrements by using the suprathreshold PSF, which displays rather small inhibitory action, instead of using a pure low-pass PSF that is suggested by the monotoneous threshold curves of the disks. Doing this, we can approach the signal threshold by

$$\Delta I_{thr} \approx 2\pi \Delta L_{thr}(\rho) \left[g_1 \sigma_1^2 \{ 1 - \exp(-\rho^2/2\sigma_1^2) \} - g_2 \sigma_2^2 \{ 1 - \exp(-\rho^2/2\sigma_2^2) \} \right] \quad (10)$$

Giving subscripts R and T to the reference, with large area, and to the test stimulus, with varying area, respectively, and only regarding signal values in the centre of the disks, we obtain

$$\Delta B_R = k \left[2\pi (\Delta L_R - \Delta L_{R,thr}) \{ g_1 \sigma_1^2 - g_2 \sigma_2^2 \} \right]^{\beta_R} \quad (11)$$

$$\Delta B_T = k \left[2\pi (\Delta L_T - \Delta L_{T,thr}) \{ g_1 \sigma_1^2 (1 - \exp(-\rho^2/2\sigma_1^2)) - g_2 \sigma_2^2 (1 - \exp(-\rho^2/2\sigma_2^2)) \} \right]^{\beta_T} \quad (12)$$

Finally, in matching test and reference we yield

$$\begin{aligned} (\Delta L_T - \Delta L_{T,thr}) = & \\ & \frac{[2\pi (\Delta L_R - \Delta L_{R,thr}) \{ g_1 \sigma_1^2 - g_2 \sigma_2^2 \}]^{\beta_R / \beta_T}}{2\pi \{ g_1 \sigma_1^2 (1 - \exp(-\rho^2/2\sigma_1^2)) - g_2 \sigma_2^2 (1 - \exp(-\rho^2/2\sigma_2^2)) \}} \end{aligned} \quad (13)$$

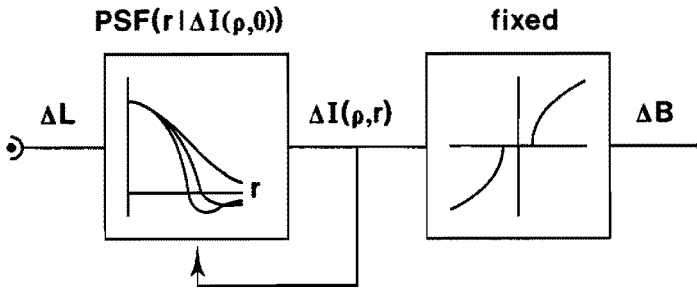


Figure 13: Brightness model B. A disk with radius ρ and luminance increment or decrement ΔL is convolved with a level-dependent point spread function. The compressive nonlinearity is kept fixed.

In this model the exponent ratio β_R/β_T is taken equal to the ratio of the exponents that follows from the empirical Stevens relation: Figs. 2 and 6 or eqs. (4) and (5). In other words, the exponent ratio obtained from a comparison of input parameters, i.e. the area and luminance increments or decrements of test and reference stimuli, has been incorporated into the model.

The parameters of the PSF's can be determined from the centre-brightness matching data. These resulting PSF's are shown in Fig. 3. The model prediction for $\log \tilde{C}$ (see eq. 3), as a result of an imaginary experiment on centre-brightness, can be obtained by substitution of $\Delta L_R - \Delta L_{R,thr} = 1$ in eq. (13). Since $\log \tilde{C}$ is valid for very low suprathreshold levels, the accurate predictions shown in Figs. 2 and 6 illustrate that the assumption for threshold correction in accordance with eq. (10) is not critical. In order to substitute an analytic expression for ΔL_{thr} in the matching equation, we approximated threshold data for convenience. The assumption of a pure low-pass Gaussian PSF that governs detection allows us to write threshold curves as

$$\Delta L_{thr}(\rho) = \frac{9.55}{1 - \exp(-\rho^2/2\sigma^2)} \quad (14)$$

in which ρ denotes the disk radius and $\sigma = 1.42'$ for incremental and $\sigma = 2.9'$ for decremental disks. These approximations are shown in Figs. 4 and 7.

Finally, the model predictions for maximum brightness and apparent contrast were obtained by replacing the convolution result in the centre. Instead of applying the analytic expressions given by eqs. (7) and (8), we substituted the maximum and the difference between maximum and minimum of the convolution result respectively in eq. (13). These values were computed by numerical convolution of course.

Model B

This second model also consists of a PSF and a compressive nonlinearity. Contrary to the first model, the nonlinearity is kept fixed now, while the PSF depends on

the internal signal level in the centre of the disk $\Delta I(\rho, 0)$, see Fig. 13. We assume that the PSF is shaped like a sum or difference of N Gaussians

$$PSF(r | \Delta I(\rho, 0)) = \sum_{j=1}^N g_j \cdot \exp(-r^2/2\sigma_j^2) \quad (15)$$

For the convolution result in the centre of a disk, with radius ρ and luminance increment or decrement $\Delta L(\rho)$, it follows that

$$\begin{aligned} \Delta I(\rho, 0) &= 2\pi\Delta L(\rho) \int_0^\rho PSF(r | \Delta I(\rho, 0)) r dr \\ &= 2\pi\Delta L(\rho) \sum_{j=1}^N g_j \sigma_j^2 \{1 - \exp(-\rho^2/2\sigma_j^2)\} \end{aligned} \quad (16)$$

and for large disks, ($\rho \gg \sigma_j$; $j = 1, \dots, N$)

$$\Delta I(\infty, 0) = 2\pi\Delta L(\infty) \sum_{j=1}^N g_j \sigma_j^2 \quad (17)$$

Matching the centre-brightness of a test stimulus with that of a large reference, i.e. $\Delta B(\rho, 0) = \Delta B(\infty, 0)$, the compressive nonlinearity can be omitted because it is kept fixed. We therefore yield the matching equation $\Delta I(\rho, 0) = \Delta I(\infty, 0)$. Substitution of eqs. (16) and (17) results in

$$\Delta L(\rho) \sum_{j=1}^N g_j \sigma_j^2 \{1 - \exp(-\rho^2/2\sigma_j^2)\} = \Delta L(\infty) \sum_{j=1}^N g_j \sigma_j^2 \quad (18)$$

Since $\Delta L(\rho)$ is measured and $\Delta L(\infty)$ approximates the luminance increment or decrement for large disks, the least-squares parameters of the PSF's can be computed for any brightness level, including detection thresholds. Threshold curves represent the most simple situation because the luminance difference with the background decreases monotonously with disk area. This implies that the PSF can be approximated by a single Gaussian. Detection-threshold curves can therefore be described by the equation

$$\Delta L_{thr}(\rho) = \frac{\Delta L_{thr}(\infty)}{1 - \exp(-\rho^2/2\sigma^2)} \quad (19)$$

This expression was already used to approximate the threshold data in Model A, see eq. (14). The procedure described has been applied to all centre-brightness and threshold data. It turned out that a maximum of $N=3$ satisfies for all levels. The left panel of Fig. 14 shows the least-squares fits to the data, while the corresponding level-dependent point spread functions are presented in the right panel. As can be seen, the second model can provide an excellent fit to the data also. The describing point spread functions for decremental disks are much broader than those for incremental disks. The supersummation effect, displayed by the steep slopes of incremental small disks, evokes PSF's with a local minimum in their centre.

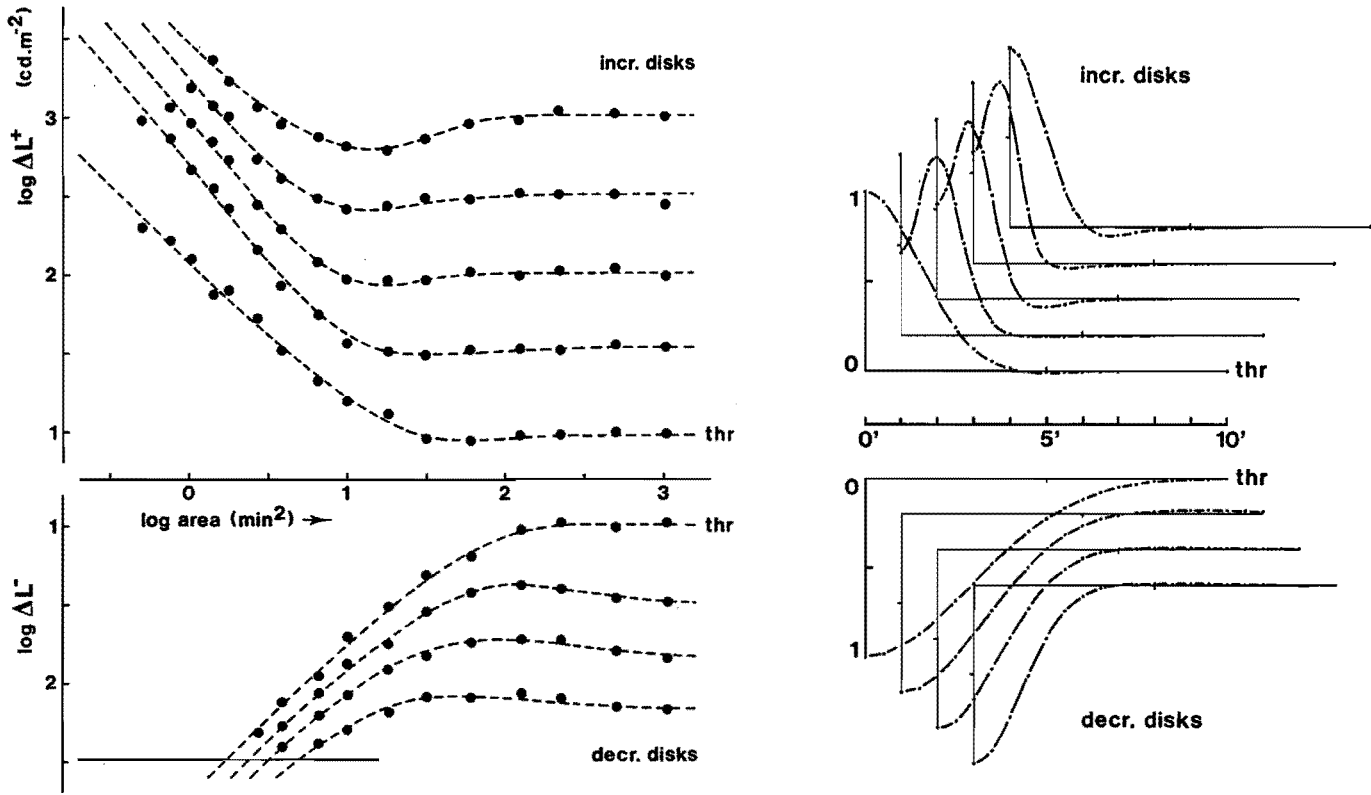


Figure 14: Left panel: Least-squares approximations by level-dependent PSF's (model B) of centre-brightness and detection-threshold (thr) data. Right panel: Normalized level-dependent PSF's for incremental disks and for decremental disks. Those describing detection thresholds are labelled 'thr'.

5 Brightness and Apparent-Contrast Perception of Blurred Disks and Circular Cosine Gratings

Abstract

As a further investigation of the (a)symmetry between brightness and darkness perception on the one hand, and the relation between brightness and apparent-contrast perception on the other, we performed matching experiments using blurred disks and radially symmetric cosine gratings.

Matching either the centre-brightness or the apparent contrast of incremental one-degree disks, with varying edge-sharpness, renders quite different results. These point towards the maximum brightness gradient as a determinant for apparent-contrast perception.

However, no significant differences are found in matching either the brightness maxima, the brightness minima, or the apparent contrast of radially symmetric cosine gratings with varying spatial frequency. This means that the spatial frequency influences both brightness extremes in the same way, and that apparent contrast is a function of the difference between the brightness extremes. The results for this configuration do therefore deviate from those obtained with all the other stimuli, i.e. sharp as well as blurred disks.

The contradictions found complicate the conception of a model which unifies disk and grating perception.

5.1 Introduction

It is known that iso-brightness curves of sharp disks display the spatial Broca-Sulzer phenomenon. This is true for incremental disks (Higgins and Rinalducci, 1975) and decremental disks (Björklund and Magnussen, 1979). Exploring the spatial Broca-Sulzer effect for incremental and decremental disks for a single subject, we found that maximum darkness enhancement occurs for larger disks than maximum brightness enhancement, see chapter 4.

We also found that the Broca-Sulzer effect disappeared if the apparent contrast of the disks is matched. This means that a distinction should be made with respect to the perceptual attributes of *local* brightness and *global* apparent contrast. It was argued that apparent-contrast perception can possibly be related to the perceived brightness profiles. The magnitude of the Mach-band effect, equal to the difference between the brightness extremes on either side of the disk edge, or the maximum brightness gradient are obvious possibilities that may be considered. The quantitative examination of both these alternatives depends on the availability of a spatial brightness model that accurately describes the perceived brightness profiles. For the moment no such model exists.

In view of the foregoing we performed additional experiments on brightness and apparent contrast. The aim of the experiments was twofold. First, we wanted to

gather brightness data by using other stimulus configurations, viz. being blurred one-degree disks and radially symmetric cosine gratings. In order for these data to be useful for brightness-modelling purposes, the experimental conditions, including the same subject to perform all observations, were kept unchanged. Second, apparent-contrast results obtained with blurred disks and gratings provide valuable information about the nature of apparent-contrast perception and its relation with brightness perception in particular.

The influence of edge-sharpness on the perceived brightness of one-degree bars has been studied by Thomas and Kovar (1965). They found that both for detection and for iso-brightness a larger luminance increment is required if the edge width is increased. The rate of increase was much too small for an explanation based upon the luminance gradient governing detection as well as brightness. Other investigations, however, do confirm the idea that the luminance gradient plays an important role in the detection of very broad one-dimensional stimuli (van den Brink and Keemink, 1976; Shapley, 1974).

Sinewave gratings are perhaps the most frequently used stimuli. Matching of the apparent contrast of gratings with varying spatial frequency results in curves that display a low-pass behaviour for high levels of physical contrast. Approaching the detection threshold a tendency towards a band-pass behaviour is observed. Several studies agree in this (Watanabe et al., 1968; Blakemore et al., 1973; Georgeson and Sullivan, 1975; Bowker, 1983), although one can question the subject's task in matching these patterns. Blakemore et al. referred to an *odd task* that is performed quite easily. Georgeson and Sullivan even questioned the duality between modulation-depth in brightness and the *visibility*, which would correspond to apparent contrast, perhaps expecting different results from both types of perceptual attributes. However, matching results on compound gratings, where the difference between local brightness extremes as well as the global apparent contrast was used as a matching criterion, were quite similar (Arend et al., 1981; Arend and Lange, 1980).

Bryngdahl (1966), who matched the brightness of a large field with the brightness extremes of gratings, obtained transfer functions that resemble the apparent iso-contrast functions mentioned above. It is, however, likely that his procedure has shortcomings, because he omitted the nonlinear brightness-luminance relation of the large field. It has often been assumed that this relation can be written as a Stevens power function with an exponent of $1/3$ (e.g. Mansfield, 1973). A similar conclusion holds for Springer (1978), who 'sampled' the brightness pattern of gratings by matching with a thin line.

Studying the empirical Stevens relation for apparent contrast of gratings, Kulikowski (1976) matched the apparent contrast of 1.67 and 15 cpd gratings to that of a 5 cpd grating. He found that his data are well described by linear functions of threshold corrected physical contrast. Cannon (1980), who reconsidered (only)

the high-frequency matching data from Georgeson and Sullivan (1975), seems to have confirmed this linear relation.

However, applying magnitude estimation, i.e. the most direct method to examine the apparent to physical contrast relationship, quite different results have been obtained. Linear Stevens relations are found to be independent of the spatial frequency (Cannon, 1979 and 1980) and to depend on spatial frequency (Biondini and Mattiello, 1985). Nonlinear relations that are independent of the spatial frequency are reported with Stevens exponents of 0.7 (Gottesman et al., 1981) and of 0.5 (Cannon, 1985). An intermodal technique even rendered nonlinear relations with Stevens exponents that depend on spatial frequency (Franzén and Berkley, 1975). This was recently confirmed (Quinn, 1985).

There seems to be something weird about sinewave gratings. Even Weber's law, often validated for other patterns, does not seem to be obeyed. If Weber's law is generalized by a power function, i.e. $\Delta m \propto m^\alpha$, contrast discrimination data are described by α values of 0.6 and 0.7 (Legge, 1981). We must therefore conclude that we are still far from a general consensus, and that additional data on this issue are useful.

5.2 Methods

We used a CRT, with radial screen and white phosphor, throughout our experiments. The screen subtended 3.3 degrees of visual angle. The background luminance of the screen was 300 cd.m^{-2} . It was extended to about 5×5 degrees, with about the same brightness and hue. The barely visible transition between screen and extension was used to fixate the centre of the screen. All stimuli were generated centralized with respect to the centre of the screen.

Two sets of spatial stimuli were used. The first set consisted of incremental luminous disks, with a diameter of one degree and with varying blur. The edge profiles of the luminance increment were error-function shaped, using the standard deviation σ as a parameter:

$$L(r, \varphi) = L_b + 0.5\Delta L \left\{ 1 \pm \operatorname{erf} \left(0.6 \frac{|r - r_o|}{\sigma} \right) \right\} \quad (1)$$

with L_b the background luminance, ΔL the luminance increment in the centre and $r_o = 30 \text{ min. of arc}$. The profiles are shown in Fig. 1. At a distance of $\pm \sigma \text{ min. of arc}$ from the edge, the value of the luminance increment equals 0.8 or 0.2 times ΔL . The maximum luminance gradient at the edge equals $\Delta L/3\sigma$. The value of σ was varied between 0 (unblurred disk) and 8 min. of arc, in 1' steps:

$$\sigma = n' ; n = 1, \dots, 8 \quad (2)$$

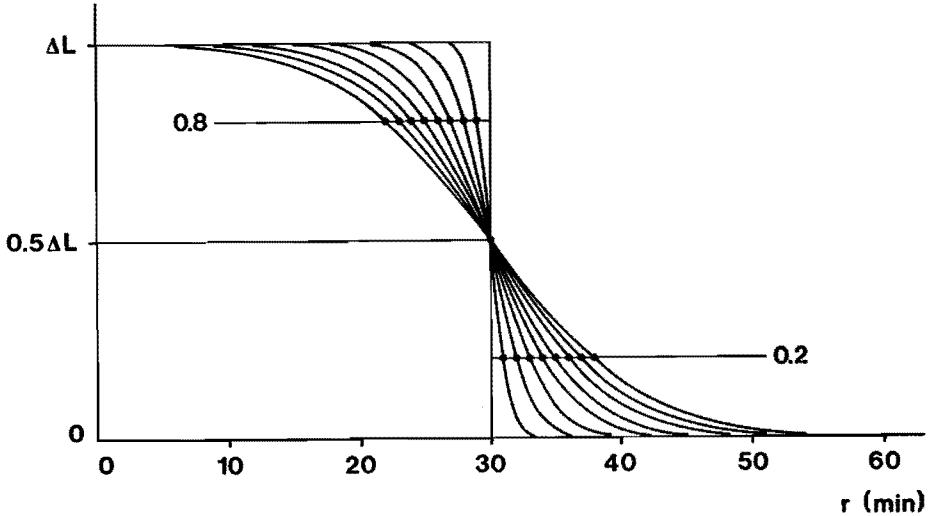


Figure 1: Schematic cross-section of the blurred one-degree disks. The σ parameter, describing the errorfunction-shaped edge profile, was varied between $0'$ (sharp disk) and $8'$, in $1'$ steps. At a distance of $\pm \sigma$ min. of arc from the $30'$ edge, the luminance increment equals either $0.2\Delta L$ or $0.8\Delta L$, if ΔL equals the luminance increment in the centre.

The second set of stimuli consisted of radially symmetric cosine gratings. This means that a luminance maximum was always positioned in the centre. The spatial frequency, defined as one divided by the radial period, was varied between 0.61 and 19.91 cycles per degree (cpd). At the lowest frequency one period corresponded to the screen radius. The modulation depth of gratings is defined by the Michelson formula

$$m = \frac{L_{max} - L_{min}}{L_{max} + L_{min}} \quad (3)$$

Since

$$L(r, \varphi) = L_b + \hat{\ell} \cos(2\pi f_s r) \quad (4)$$

with L_b and $\hat{\ell}$ equal to the background luminance and the modulation amplitude, the Michelson contrast corresponds to $m = \hat{\ell}/L_b$.

All patterns were presented with quasistatic temporal envelopes. These envelopes, of 900 msec duration, consisted of three contiguous time-functions. A centre plateau of 300 msec was flanked by error functions truncated at 1% of their asymptotic tails. Stimulus combinations of test and reference were presented sequentially, with an interstimulus interval of 500 msec. A delay of 300 msec was regarded between the control of a start-button and the release of the first stimulus.

All experiments were performed by a well-trained subject (JDB). He observed with the right eye, and made use of an artificial pupil, 2 mm in diameter, that was equipped with an entoptic guiding system to check the centering of the pupils.

For the blurred disks we used two perceptual attributes as a matching criterion: the brightness in the centre and the apparent or subjective contrast with respect to the surround. In both cases a fixed, unblurred disk provided the reference. In order to exclude any absolute-brightness clue in the apparent-contrast matchings, we presented the unblurred reference as a luminance decrement. Decremental references were, prior to the experiment, obtained by mirroring incremental disks. This procedure, in fact a matching experiment on its own, renders therefore unblurred disks with different luminance increments and decrements, though with an equal apparent contrast (see foregoing chapters).

The gratings were matched by three perceptual attributes: the brightness maxima, the brightness minima and the global apparent contrast. In all cases a 4.2 cpd grating provided the reference.

The method of constant stimuli has been applied throughout the experiments. A 50% point was computed from two series of 10 trials, with observational probabilities between 10% and 90%. This was done 8 times for every stimulus combination. Both 'larger than the reference' and 'smaller than the reference' were used as criteria, with equal number of trials, in order to avoid systematic deviations due to just noticeable differences. The geometric mean of the 50% points was taken as the point of subjective equality. Detection thresholds were determined following the same procedure. Different stimulus patterns and different matching criteria were considered in separated sessions.

5.3 Results

Blurred Disks

Detection thresholds and curves of centre iso-brightness are presented in the left panel of Fig. 2, while curves of apparent iso-contrast are given in the right panel. Obviously, there is a distinct difference between the brightness and apparent-contrast data. Detection thresholds and iso-brightness curves for small increments increase with the blur. The centre-brightness appears to be almost independent from the degree of blur for luminance increments of about 200 cd.m^{-2} . For higher levels the effect is reversed: an equal brightness requires a smaller luminance increment of the disk if it is blurred. This tendency is not displayed by the apparent-contrast data: increasing the blur requires a larger luminance increment at all levels.

As was done for sharp disks with varying diameter, see the foregoing chapter, the brightness data may be analyzed by applying Stevens' empirical relation. The

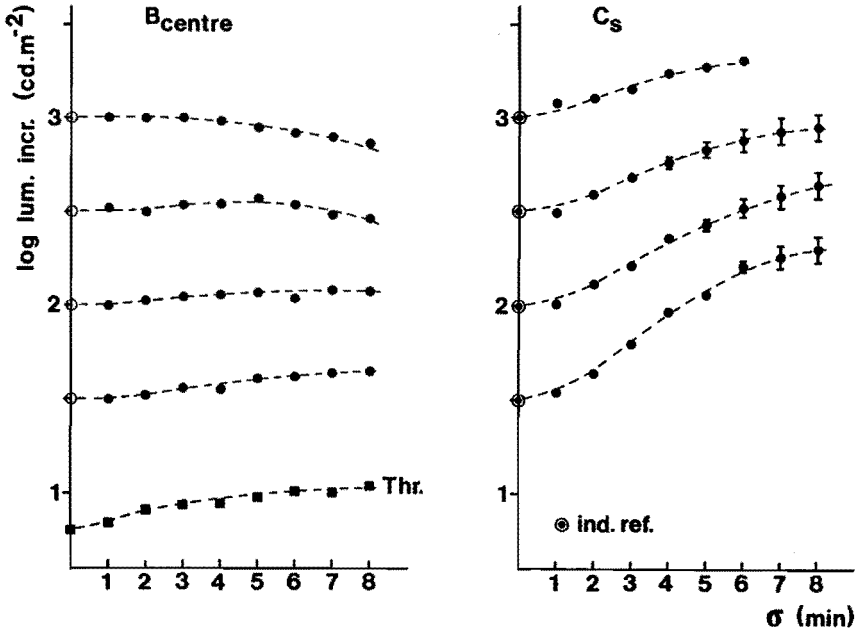


Figure 2: Matching results obtained with blurred one-degree disks. Curves of centre iso-brightness (solid circles) and detection thresholds (solid squares) are shown in the left panel, curves of apparent iso-contrast in the right panel. In both cases an unblurred ($\sigma = 0$) disk was used as a reference. Vertical bars indicate standard deviations of individual measurements; if omitted these amounted to less than 0.05 log units typically.

brightness increment on a steady background is expressed in terms of a power function of the threshold corrected luminance increment, i.e.

$$\Delta B = C(\Delta L - \Delta L_{thr})^\beta \quad (5)$$

From the matching equation for a (blurred) test and an (unblurred) reference stimulus, viz. $\Delta B_T = \Delta B_R$, it can be derived that

$$\begin{aligned} \log(\Delta L_T - \Delta L_{T,thr}) &= \frac{1}{\beta_T} \log \frac{C_R}{C_T} + \frac{\beta_R}{\beta_T} \log(\Delta L_R - \Delta L_{R,thr}) \\ &= \log \tilde{C} + \frac{\beta_R}{\beta_T} \log(\Delta L_R - \Delta L_{R,thr}) \end{aligned} \quad (6)$$

This means that, if the log threshold-corrected luminance increments of a test and reference stimulus are plotted on ordinate and abscissa respectively, a straight line is expected. The slope of the data points equals the exponent ratio β_R/β_T and the intersection with the ordinate equals $\log \tilde{C}$. This analysis applied to the data of Fig. 2 appeared to render linear curves indeed, not only for the brightness data but also for apparent contrast, and the results are presented in Fig. 3.

The Stevens brightness exponent increases monotonously with the blur, since the exponent ratio (solid circles) decreases. For a test disk with $\sigma = 8'$ it follows that $\beta_R/\beta_T = 0.81$ and $\log \tilde{C} = 0.42$. Assuming a Stevens brightness exponent for an unblurred 1 degree disk to be 0.5 (Stevens and Stevens, 1960; Onley, 1961; Warren, 1976), the brightness exponent of the mostly blurred disk equals $\beta_T = 0.5/0.81 = 0.62$. Since $\log \tilde{C} = (1/\beta_T) \log(C_R/C_T) = 0.42$, it follows that $C_T = 0.55 C_R$. Hence, increasing the blur implies that the Stevens brightness exponent β increases, while the proportionality constant C decreases. Similar results are found if the procedure explained above is applied to the apparent-contrast data, see the open and solid stars in Fig. 3. This means that the apparent contrast of blurred disks can also be described by a power function of the threshold-corrected luminance increment, similar to brightness, though with a different exponent β and proportionality constant C . The consistency of this consideration is an indication for the significance of Stevens' power law for blurred disks.

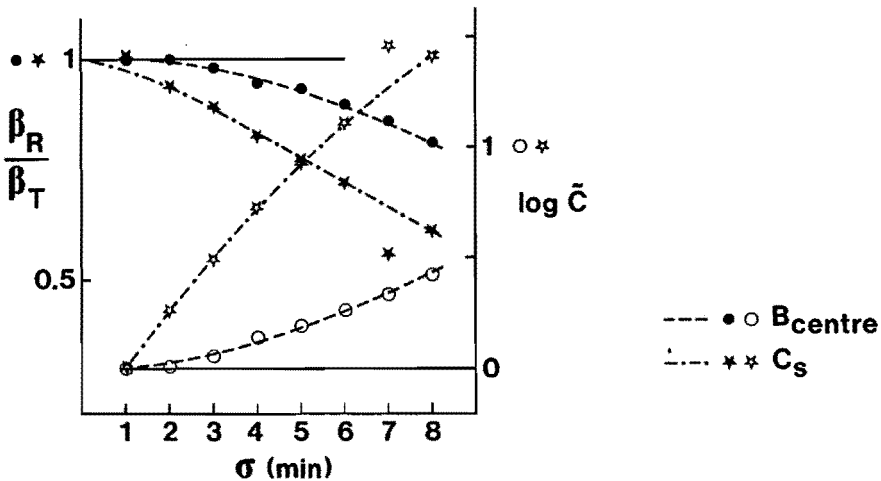


Figure 3: The exponent ratio and $\log \tilde{C}$, which follow from Stevens' power law applied to the data of Fig. 2, as a function of the blur.

In order to compare our present brightness data with results on the brightness of 1 degree bars with extended edges (Thomas and Kovar, 1965), we must use linear luminance coordinates. Our brightness data are reproduced in the left panel of Fig. 4. Obviously, there is only a scanty agreement between our results and those of Thomas and Kovar: their data, measured at lower background levels and lower reference increments, approximate our open-star curve in the left panel of Fig. 4 (labelled 1.5). Perhaps the most important conclusion is that no direct proportionality exists between the brightness increment and the luminance gradient. A similar conclusion can be made for our apparent-contrast data, see the right panel of Fig. 4. The slope of only one of the curves appears to approximate a prediction on the basis of luminance-gradient constancy.

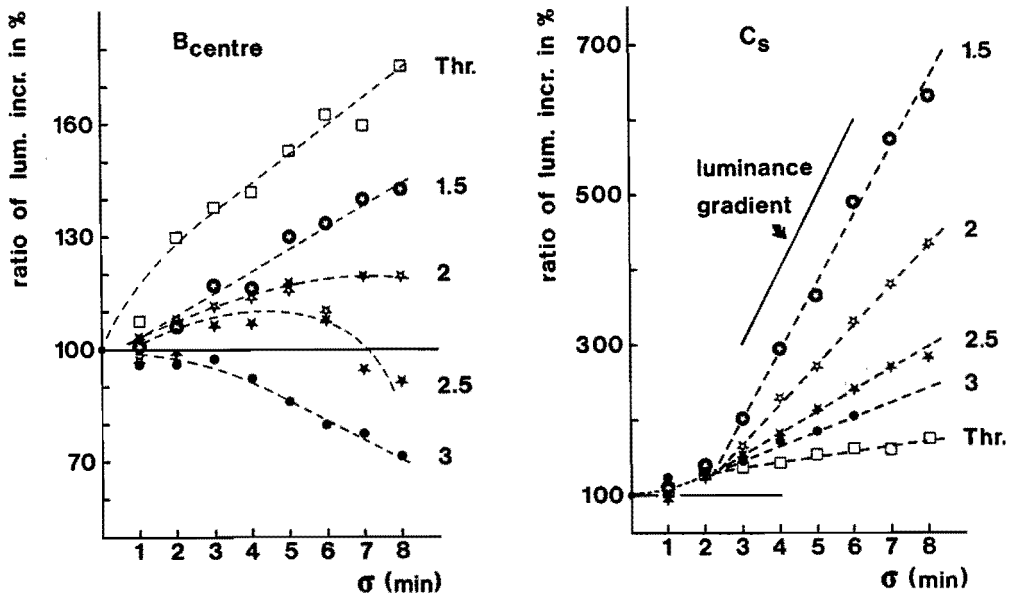


Figure 4: Left panel: Detection thresholds and iso-brightness curves in linear coordinates, relative to the unblurred reference luminance increments. Parameters given next to the curves correspond to the log of used reference luminance increments. Right panel: Detection thresholds and curves of apparent iso-contrast in linear and relative coordinates. A prediction based on constancy of the maximum luminance gradient at the edge is indicated by the slope of the drawn line. Note the difference between the ordinate scales in the left and right panels.

Circular Cosine Gratings

The results for this stimulus configuration are summarized in Fig. 5. Modulation thresholds seem to reflect a band-pass behaviour of the visual system. This agrees with well-known data on one-dimensional sinewave gratings, as well as circular gratings (Kelly, 1984). The band-pass filter characteristic changes into a low-pass behaviour if the modulation depth is increased. However, there is no significant difference between the results measured by applying different perceptual attributes as a matching criterion. This means that neither the asymmetry in the brightness perception of disks, nor the difference between brightness and apparent contrast, is confirmed here. The implications for the modelling of brightness as well as apparent-contrast perception is one of the main issues in the General Discussion of this chapter.

Anyhow, the duality between modulation depth in brightness and apparent contrast, as questioned by Georgeson and Sullivan (1975), has not been confirmed.

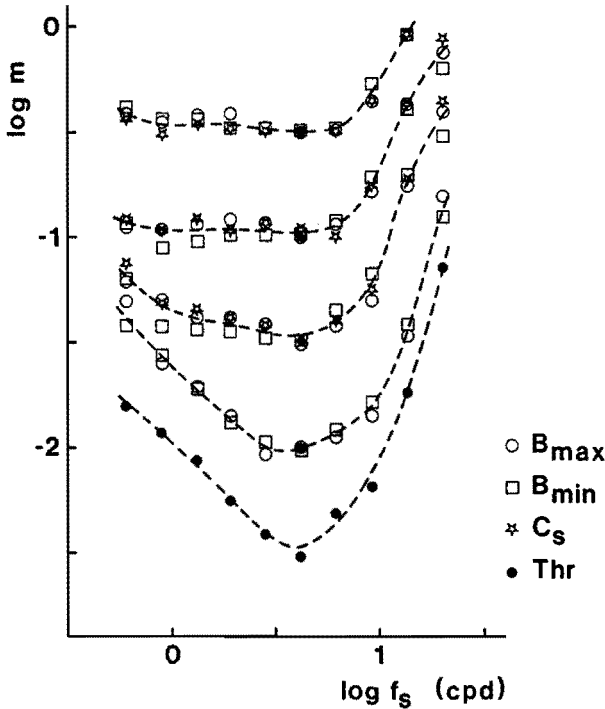


Figure 5: Detection thresholds (solid circles) and matching results obtained with radially symmetric cosine gratings. Different perceptual attributes are indicated by different symbols. Dashed curves approximate the geometric means of all individual data. The standard deviation of individual measurements was about 0.05 log unit typically.

This may be the reason for the high degree of correspondence between the results of similar matching experiments performed in the past (Watanabe et al., 1968; Blakemore et al., 1973; Bowker, 1983). Furthermore, there is hardly any difference between our results on circular gratings and the one-dimensional case. The only difference between our data and those referred to is the pronounced cut-off at a frequency of about 7.5 cpd for the highest levels of modulation depth. Note that the detection-threshold curve of dynamic (briefly presented) gratings displays the same low-pass shape with a same cut-off frequency of about 7.5 cpd (see chapter 6).

As in the case of disk-shaped stimuli, we can examine the empirical Stevens relation for gratings. Since no significant difference was measured between the brightness extremes, nor between brightness and apparent contrast, it seems obvious to assume an identical Stevens function for each perceptual attribute and to take the geometric mean of the data (the smooth dashed curves in Fig. 5 approach these geometric means). Suppose that the magnitude M_{PA} of any perceptual attribute PA , with $PA \in \{B_{max}, B_{min}, C_S\}$, is a power function of threshold-corrected modulation depth m , i.e.

$$M_{PA} = C(m - m_{thr})^\beta \quad (7)$$

If this relation holds for grating perception, eq.(6) is applicable and linearity on the basis of log threshold-corrected modulation depth is expected. Fig. 6 shows that this concept fails for the low-frequency low-level data¹. It seems as if Stevens' relation with simple threshold correction is only correct for low-frequency high-level gratings and for high-frequency gratings. The linearity with about unit slope suggests that the exponent β in these cases does not depend on spatial frequency, although nothing can be said about its value of course. The parallel shift of the high-frequency curves implies that the proportionality constant C in eq.(7) decreases with the frequency. This consideration, especially the use of graphs in log units, emphasizes the idea of a nonlinear Stevens relation with an exponent $\beta \neq 1$. Perhaps an examination on the basis of a linear Stevens relation, with $\beta = 1$ substituted in eq.(7), and consequently graphs in linear units, is a better starting point. Fig. 7 shows that a linearization of the low-frequency data is indeed obtained, but this is merely a consequence of the reduced resolution at low levels, and the high-frequency data display some nonlinear tendency now.

The grating 'enigma' seems to be still unsolved. Neither linear nor nonlinear approximations appear to make sense. The choice between one of these may depend on the coordinates that one usually applies. This would partly explain the large disagreement between magnitude-estimation results (see Introduction). A related problem is the inaccuracy of magnitude estimation as a psychophysical method. It is known that magnitude estimation, in which subjects are asked to generate numbers proportional to the strength of a perceived attribute, is obscured by the nonlinear way of number-handling (Bartleson and Breneman, 1973; Saunders, 1972; Curtis and Rule, 1972). We must therefore not exclude the possibility that we are chasing a chimera here. The *empirical* Stevens relation, which is often found to be a correct reflection of the brightness perception of disk-shaped stimuli, may turn out inappropriate for describing grating perception. If this is true, the nonlinear transfer characteristics as demonstrated in Fig. 5 may still be used for further modelling.

5.4 General Discussion

Rather than recalling the experimental results that we discussed in the foregoing, we would like to emphasize their implications for the modelling of brightness and apparent contrast. Moreover, it is of interest to compare or combine the present results with those obtained by matching sharp disks. It should be stressed that all results, both previous and present, were gathered under identical experimental

¹Note that Cannon (1980) considered only the high-frequency data from Georgeson and Sullivan (1975) to demonstrate linearity, but omitted (dropped?) their low-frequency data.

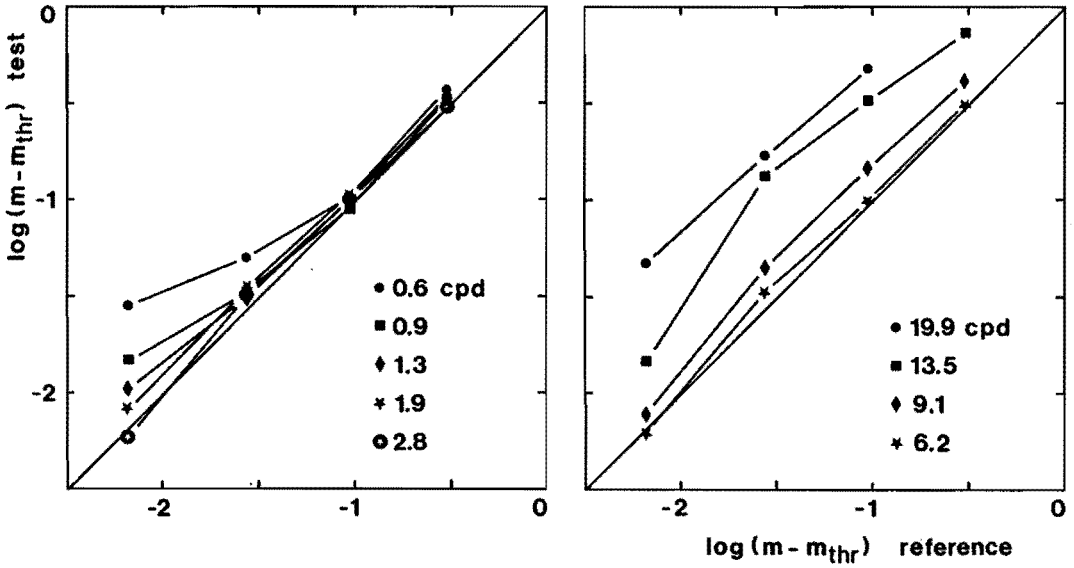


Figure 6: Analysis of the grating results in log threshold-corrected modulation depth. Reference values of the 4.2 cpd grating are plotted on the abscissa. Different symbols reflect test gratings with lower (left panel) and higher (right panel) spatial frequencies.

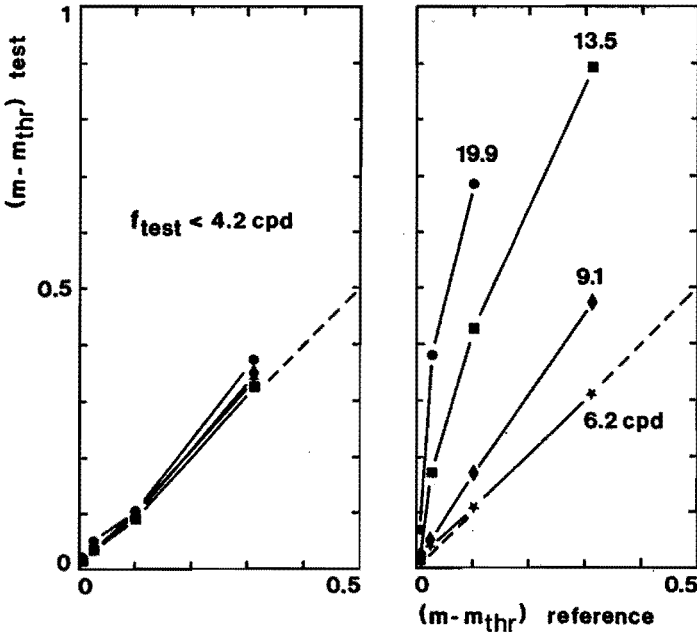


Figure 7: Same as Fig. 6, but now in linear threshold-corrected coordinates.

conditions. We used the same apparatus, background level, temporal envelopes of the spatial patterns, sequential presentation with fixation in the centre, as well as the same subject throughout all experiments, allowing a quantitative analysis of the various results. Brightness will be dealt with first, and apparent contrast there after.

Brightness

Previous results on the brightness perception of incremental and decremental sharp disks, with varying diameter, indicated that the spatial Broca-Sulzer phenomenon depends on the polarity. Maximum darkness enhancement was found to occur for larger disks in comparison with maximum brightness enhancement. Moreover, the Ricco-domain, which implies pure integration for small stimuli, was found to be larger in case of decremental disks. This asymmetry in the processing of disk-shaped luminance increments and decrements would lead one to expect a difference between the brightness extremes of (high-frequency) gratings. This is not confirmed here, because we measured no significant differences by matching either brightness maxima or minima. It seems as if the discrepancy between aperiodic spatial stimuli (disks) and periodic ones (gratings) resembles the same discrepancy as was found in the temporal situation: maximum darkness enhancement of pulsed decrements occurs for longer durations with respect to maximum brightness enhancement (White et al., 1980). In the square-wave periodic situation no shift in temporal frequency is observed (Magnussen and Glad, 1975).

It is known that contemporary models of the visual system should contain multiple parallel channels. These underlying mechanisms were indicated by a threshold elevation that is evoked by preadaptation. This was demonstrated for the case of disks (Bagrash, 1973) as well as gratings (Blakemore and Campbell, 1969). A frequency-selective reduction in the apparent contrast of suprathreshold gratings was also demonstrated (Blakemore et al., 1973).

The incorporation of such multiple parallel channels into a model appeared to be able to unify threshold and suprathreshold perception of Gabor-sine-like patterns (Swanson et al., 1984). Despite the fact that both the spatial properties, i.e. the line spread functions, and the nonlinear amplitude transfer functions of the channels were determined by independent experiments, the model satisfied reasonably well.

Applying such a nonlinear multiple channel configuration, we can now examine our present brightness results by assuming:

- Radially symmetric channels, and thus point spread functions, each of pure band-pass character with a DOG-shaped profile. The luminance pattern is convolved with any of the point spread functions.

- All channels contain a nonlinear amplitude transfer function. This function can be asymmetrical for some channels in order to explain for instance the asymmetry in detection thresholds of small incremental and decremental disks.
- The outputs of all channels are summed (non)linearly at any location in the visual field. For instance by applying a fourth-power summation rule (e.g. Quick, 1974), which is an intermediate condition between the extreme cases of linear summation on the one hand and determination of the response of the channel that maximally responds (inclusive-OR) on the other.
- Instead of deriving the amplitude transfer functions from just noticeable differences (Swanson et al., 1984), they can be determined on the basis of matching data. This involves the use of a nonlinear least-squares algorithm.

Convolving a DOG-shaped, pure band-pass point spread function with disks of various diameters renders a spatial response profile that varies with the disk diameter. Increasing the diameter, the log amplitude versus log area graph displays a unit slope for small disks, and a local maximum for disks with a diameter that corresponds to the width of the excitatory centre of the point spread function (see Fig. 8 in chapter 8). A further increase in diameter means that the convolution result in the centre decreases until it approximates zero, while the maximum shifts towards the edge. For very large disks the maximum response at the edge will be smaller than the response in the centre of 'optimal' disks. The iso-brightness data of blurred one-degree disks, see Figs. 2 and 3, can be explained. Only the responses of the channels in the centre of the disk have to be considered, because we matched the brightness in the centre, and the responses of different channels are assumed to be summed at that location. The channel that maximally responds to the unblurred disk has a point spread function of which the excitatory-centre diameter equals one degree. Increasing the blur implies that the response in the centre is governed by successively broader channels. The dashed curves presented in Fig. 3 can therefore be seen to reflect the variation of the nonlinear amplitude transfer functions of very broad channels. If these amplitude transfer functions are characterized by a proportionality constant and a power function, it follows that the constant decreases while the exponent increases for the successively broader channels.

Note that this conclusion for the properties of very broad channels is an extension to that for narrow channels, which is evaluated from the matching results obtained with sharp incremental disks with varying diameter. Figure 2 from chapter 4 shows that the exponent ratio decreases for smaller diameters, which means that the exponent itself increases for successive narrower channels. This tendency changes for disks subtending about 1.5 min. of arc. For smaller disks the expo-

ment ratio becomes independent from the diameter, which would mean that the most narrow channel is reached. The largest disk that was used in the matching experiment subtended about 40 min. of arc. Combining the results of sharp and blurred disks, in particular the present Fig. 3 and Fig. 2 from chapter 4, it appears that the exponent of the narrowest channel approximates $0.5/0.56 = 0.9$. The exponents of broader channels decrease rapidly to 0.5, and become constant for channels with an excitatory-centre diameter between 10 and 60 min. of arc. For successive broader channels the exponent increases again, but less abruptly.

So far no problems, but how about unifying disk and grating results? Figure 14 from chapter 4 shows quite a difference between the iso-brightness curves of incremental and decremental sharp disks. The present data on the brightness extremes of gratings, see Fig. 5, do not reflect any asymmetry at all. Furthermore, suprathreshold curves of disks display a Broca-Sulzer phenomenon, while detection thresholds do not. For gratings a low-pass character is suggested at suprathreshold levels, in contrast to the band-pass characteristic at threshold. These apparent contradictions imply that linear and single channel models are out of question. All curves are merely to be considered as a consequence of the envelope of the responses of various spatial channels. Preliminary attempts in fitting these data simultaneously, by adopting the multichannel model configuration as explained above, failed however. There appeared to be two crucial problems:

- 1) If the nonlinear amplitude transfer functions of the channels, i.e. the proportionality constants and exponents, are determined such that the model fits the grating curves, the model predicts a Broca-Sulzer effect for the detection thresholds of disks. For suprathreshold disks, on the other hand, it predicts no Broca-Sulzer effect.

- 2) Fitting the model to the symmetric grating results evokes symmetry for small incremental and decremental disks. The reversed procedure, by fitting asymmetric amplitude transfer functions to the disk results, renders an asymmetry for the brightness extremes of high-frequency gratings.

These problems appeared to be similar in case of linear summation of channel outputs as well as in case of inclusive-OR response evaluation. This means that the intermediate condition, i.e. nonlinear summation of channel outputs with summation exponents between 1 and ∞ , is unlikely to provide a solution in unifying the present disk and grating data. Whether the inclusion of spatial probability summation within channels may yield better simultaneous approximations is not yet certain.

Apparent Contrast

Similar problems are encountered in explaining apparent-contrast perception, in particular if we try to link apparent contrast to the perceived brightness pattern.

The results on sharp disks with varying diameter (chapter 4) raised the conjecture that apparent contrast is essentially a function of the perceived brightness profile, for instance the maximum brightness gradient or the magnitude of the Mach-band effect, which equals the difference between the brightness extremes at the edge. Our present results on blurred disks and gratings were expected to allow for a distinction between these two alternatives. The data obtained with blurred disks, see Fig. 2, indicate that the maximum brightness gradient is to be preferred. For a luminance increment of about 200 cd.m^{-2} the centre brightness is almost independent of the degree of blur, although the luminance gradient, and consequently the brightness gradient, vary strongly with the blur. This influence is reflected by the apparent-contrast data indeed.

On the other hand, the apparent-contrast data obtained with gratings, see Fig. 5, agree with the brightness data. This means that the difference between the brightness extremes could be acceptable as a definition for apparent-contrast perception. On the basis of brightness-gradient evaluation quite different matching curves were to be expected, because the brightness gradient strongly varies with the spatial frequency if the perceived brightness extremes are kept constant. Hence, blurred disks and gratings suggest rather opposite explanations for the nature of apparent-contrast perception. It should be emphasized that this visual percept, as reported by the subject, does not depend on the stimulus configuration. Judgment of its magnitude can be made almost instantaneously, and seems to be easier than judging the magnitude of the brightness at a specified location in the visual field. A well-trained subject might even match the apparent contrast of a disk to that of a grating for instance.

For the moment we must conclude that the unification of the experimental data obtained with disks and gratings is a serious problem. There are two alternatives: First, the structure of the multichannel brightness model could, perhaps even should, be chosen quite different from the one examined here. Second, the difficulty in unifying the various experimental results might be an indication that the visual system processes disks and gratings, perhaps all different spatial patterns, in different ways or by different subsystems, for instance by matched filters as advocated by Hauske et al. (1976). This would imply stimulus specificity, ignoring the significance of profound modelling on the basis of abstract stimuli for normal visual perception in advance, which we do not prefer to accept.

6 Detection Symmetry and Asymmetry

Abstract

Until now no consensus has been reached on the question whether incremental and decremental detection thresholds of disks, as a function of diameter and duration, are equal or not. It will be shown that thresholds of dynamic (briefly presented) foveal disks at a 300 cd.m^{-2} background are symmetrical for all diameters, and that thresholds of quasistatic disks are symmetrical for large diameters only. Threshold curves of quasistatic incremental and decremental disks are mutually shifted along the log area axis.

Threshold curves obtained with disks are somehow related to thresholds of spatial sinewave gratings. In order to obtain a better insight into the underlying detection mechanism, experiments have been performed with halfwave rectified radially symmetric cosine gratings, i.e. with either incremental or decremental phases. Threshold curves of these gratings proved to be identical, independent of polarity, and of the same shape as those obtained with full cosine gratings, though 0.3 log units shifted in amplitude. The discrepancy between threshold curves of quasistatic disks (asymmetry) and single-phase gratings (symmetry) is discussed in terms of a multiple channel theory.

6.1 Introduction

A considerable amount of research has been done on detection thresholds of disks as a function of both diameter and duration. It is not fully understood, however, whether or not disk thresholds for luminance increments and decrements are symmetrical, as appears from reported discrepancies (e.g. Cohn, 1974; Roufs, 1974). For one-dimensional sinewave gratings with varying spatial frequency, consisting of simultaneous incremental and decremental phases, a high degree of consistency has been found in the shape of threshold curves: band-pass in case of quasistatic and low-pass in case of dynamic presentation against a photopic background (e.g. Olzak and Thomas, 1986). In addition, threshold curves for radially symmetric gratings look quite alike (Kelly, 1984). Physiological evidence suggests that luminance increments and decrements are processed by separate neural networks, which differ in amplitude response as well as in spatial extent (Krüger and Fischer, 1975). The question therefore arises whether psychophysically determined disk thresholds for increments and decrements do reflect this asymmetry. Furthermore, it is of interest to study its implications for the thresholds of gratings.

To this purpose we introduced single-phase gratings, which are a result of halfwave rectification of fullwave radially symmetric cosine gratings. These single-phase gratings contain periodic patterns of either luminance increments or decrements, and thus provide an intermediate condition between disks on the one hand and fullwave gratings on the other. By studying quasistatic and dynamic thresh-

olds of disks, single-phase and fullwave gratings under comparable conditions, we hope to gain a better insight into the (a)symmetry problem mentioned.

6.2 Apparatus and Methods

Stimuli were presented on a special-purpose CRT that generates approximately white light. This device has a spiral scan of 256 turns, with a refreshing rate of 150 Hz. The homogeneous and steady background luminance of the circular image, subtending 3.3 degrees, was 300 cd.m^{-2} . The radial screen was extended to 6×6 degrees with an external source of about the same brightness and hue. The barely visible transition between screen and extension was used as an aid in fixating the centre of the screen. The experiments were performed by a well-trained subject (JDB). In all experiments he observed with the right eye, made use of an artificial pupil, 2 mm in diameter, and an entoptic guiding system to check the centering of the pupils.

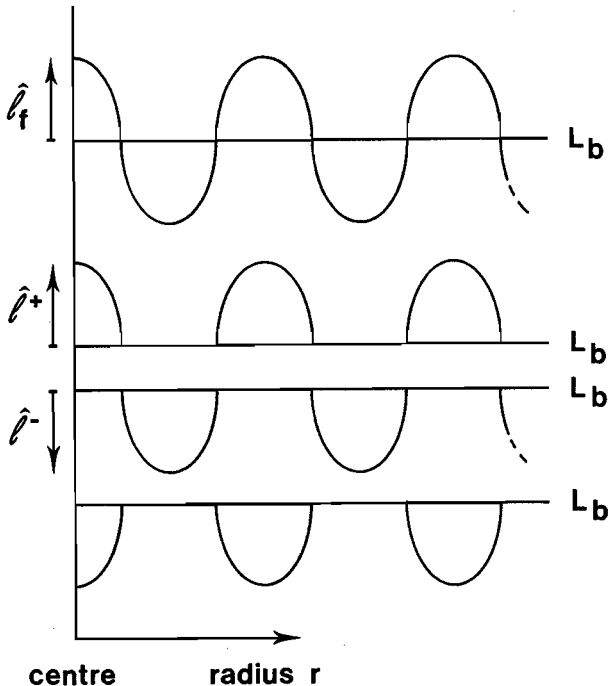


Figure 1: Cross-section of circular grating patterns superimposed on the background with luminance L_b . From top to bottom: full cosine gratings, positive single-phase gratings, negative single-phase gratings, and negative single-phase gratings with shifted spatial phase. The latter are mirrored with respect to the positive single-phase gratings.

Two sets of spatial stimuli were used in this study. The first set consisted of homogeneous disks varying in diameter and presented either as a luminance increment or as a decrement. The second set consisted of radially symmetric cosine gratings with a luminance maximum in the centre of the screen, and single-phase gratings, either incremental or decremental. The latter are to be considered as a result of halfwave rectification of the chosen fullwave cosine gratings, see Fig. 1. To explore the possible influence of the inhomogeneous retinal sensitivity, the negative single-phase gratings were also used with 180 degrees phase shift, such that a luminance minimum was positioned in the centre of the screen. At the lowest spatial frequency (0.61 cpd) one period of the grating corresponded to the radius of the CRT screen. Note that spatial frequency is defined as the inverse of the radial period of the pattern.

Both grating and disk thresholds were determined with two temporal envelopes. Dynamic thresholds were measured by displaying only one frame of 6.7 msec. For quasistatic thresholds an envelope was used that comprised a 300 msec gradual rise, a 300 msec plateau, and a 300 msec decay. Transitions were shaped as error functions truncated at 1% of their asymptotic tails.

Detection thresholds were measured in a one-interval paradigm by the method of constant stimuli. For each threshold determination, a 50% point was computed from two series of ten trials with resulting detection probabilities between 10% and 90%. This was done 8 times for all stimuli; the geometric mean of these was taken as the detection threshold.

It should be emphasized that detection thresholds for disks are given in (log) luminance increments and decrements and not in absolute luminances. For the radially symmetric cosine gratings, where $L(r, \varphi) = L_b + \hat{\ell} \cos(2\pi f_s r)$, modulation depth is defined as $m = \hat{\ell}/L_b$, with $\hat{\ell}$ equal to the peak amplitude of the luminance modulation and L_b equal to the steady background luminance. Modulation depth of single-phase gratings is defined by the same formula for convenience.

6.3 Results

Disks

All threshold curves obtained with disks are presented in Fig. 2. For large diameters all thresholds are symmetrical and dynamic thresholds are higher than quasistatic ones. However, quasistatic threshold curves are shifted horizontally with respect to each other while dynamic ones are exactly symmetrical. All curves show an asymptote of unit slope for small diameters. This is consistent with Ricco's law. Since the optical point spread function (PSF) of the eye was kept constant on account of the artificial pupil used in the observations, the shift of the Ricco domain reflects a difference in the neural processing of the stimuli.

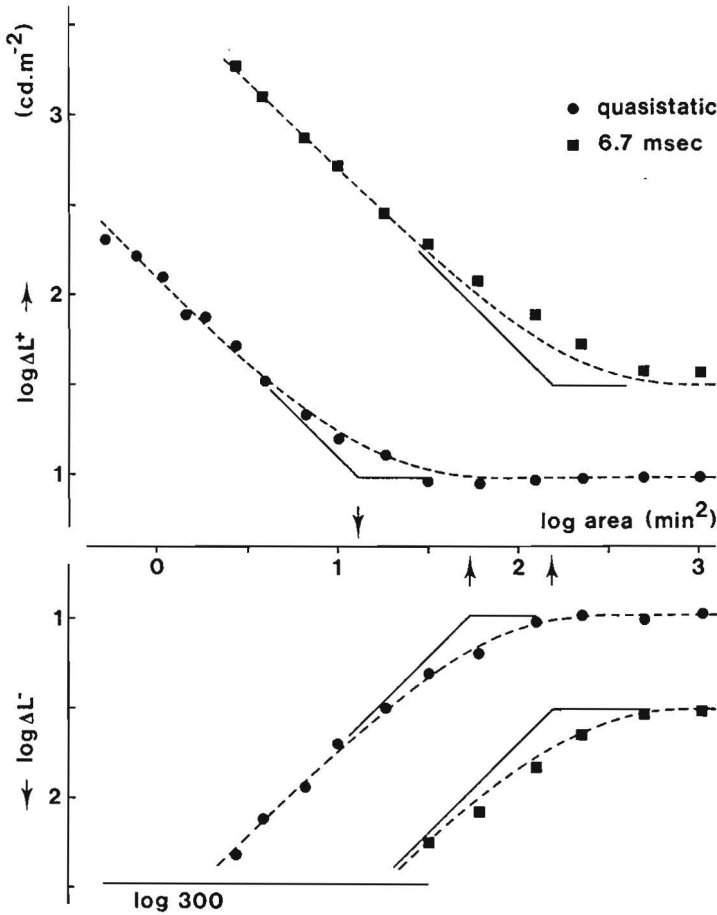


Figure 2: Disk thresholds in log luminance increment and decrement versus log area coordinates. Dashed curves reflect approximations by Gaussian low-pass point spread functions, while drawn lines reflect asymptotes.

Let us, in a first approximation, fit these threshold data by convolving a disk-shaped function with a low-pass PSF, with Gaussian shape and therefore characterized by means of the standard deviation parameter. Given a Gaussian point spread function

$$PSF(r) = g \cdot \exp(-r^2/2\sigma^2) \quad (1)$$

the convolution result $R(r)$ in the centre of a disk, with luminance increment or decrement $\Delta L(\rho)$ and radius ρ , equals

$$R(0) = 2\pi\sigma^2 g \Delta L(\rho) [1 - \exp(-\rho^2/2\sigma^2)] \quad (2)$$

Note that we consider stimuli and responses in terms of increments and decrements against a fixed background. The concept of using a PSF, according to Fourier

optics, implies that the convolution result will be identical though mirrored in these cases. For a large disk, i.e. $\rho \gg \sigma$, the response will be

$$R(0) = 2\pi\sigma^2 g \Delta L(\infty) \tag{3}$$

If a fixed -internal- signal threshold is assumed, the equalization of eqs. (2) and (3) provides a *descriptive* relation between thresholds of arbitrary disks and that of a large one:

$$\Delta L(\rho) = \frac{\Delta L(\infty)}{1 - \exp(-\rho^2/2\sigma^2)} \tag{4}$$

The measured data show that $\log \Delta L(\infty)$ equals 1.52 for dynamic and 0.99 for quasistatic curves, and the parameter σ can be solved. The dashed curves in Fig. 2 show the predictions. The shift of the intersection of the asymptotes implies that the standard deviation parameter is smallest for incremental quasistatic disks, larger for decremental quasistatic ones, and is largest for dynamic disks ($\sigma=1.45, 2.9$ and 5.0 min. of arc respectively).

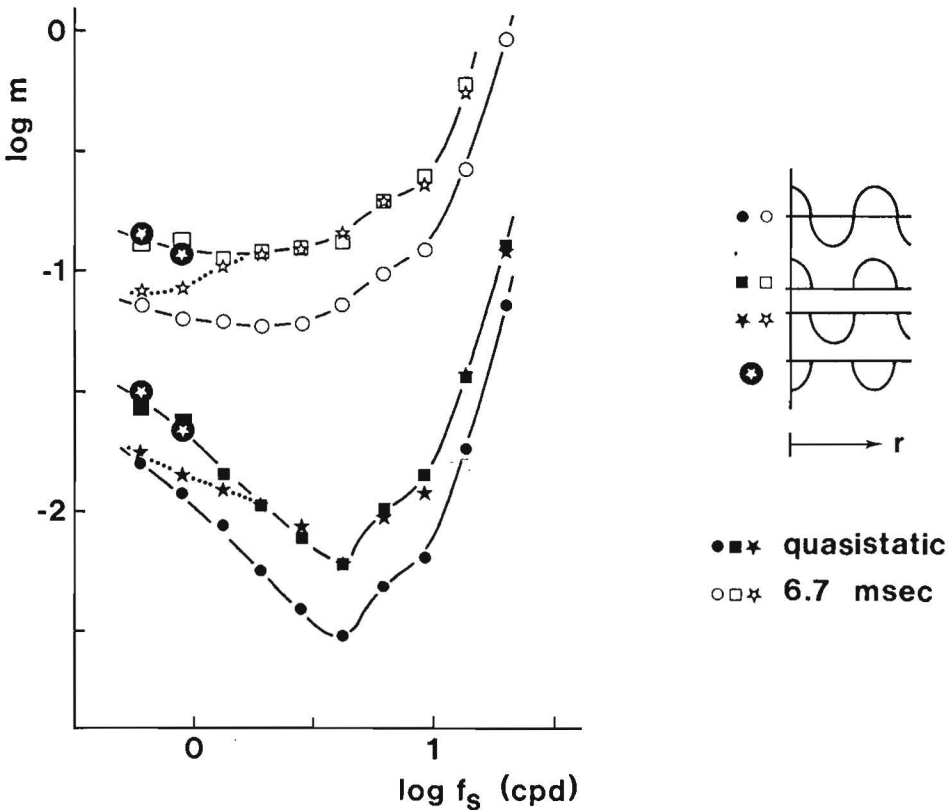


Figure 3: Threshold curves obtained with full cosine gratings (circles) and with single-phase gratings (squares for positive, stars for negative polarity gratings). Dashed curves were drawn by eye.

Circular Gratings

In Fig. 3 all threshold curves obtained with circular gratings are presented. For the full-wave grating threshold curves (open and solid circle symbols) there appears to be a high degree of correspondence to results already published; on both radially symmetric gratings (Kelly, 1984) and one-dimensional gratings (e.g. Campbell and Robson, 1968; Arend, 1976). From Fig. 3 it follows that an asymptotic slope of value -1 for quasistatic gratings is found at low spatial frequencies and that peak sensitivity occurs at 4.2 cpd. The curious local irregularity at $\log f_s = 0.8$ has also been reported by Patel (1966) and many others.

The quasistatic curves reflect a band-pass characteristic while the dynamic ones suggest a more or less low-pass characteristic. From Fig. 3 it also follows that threshold curves obtained with single-phase cosine gratings have the same shape as those obtained with fullwave cosine gratings. This is true even for the lower spatial frequencies, since thresholds for negative single-phase gratings have also been measured with 180 degrees shifted spatial phase (inverted-star symbols). In these last measurements, the spatial phase was shifted in such a way that a peak luminance decrement was positioned in the centre, i.e. patterns were exactly mirrored in luminance with respect to the positive single-phase gratings (squares). This indicates that the deviation found for low-frequency negative-phase gratings (stars) is due to the retinal position, and thus is a consequence of the inhomogeneous retinal sensitivity.

The slope of value -1 for quasistatic single-phase gratings at low spatial frequencies appears to agree with a multiple channel model prediction based on peak detection (Jaschinski-Kruza and Cavonius, 1984). This model prediction was carried out for a low-frequency single cosine-shaped bar. The inclusion of spatial probability summation would result in a slope of -0.8 (Jaschinski-Kruza, private communication). This might mean that probability summation in multichannel modelling may not be required to predict detection thresholds of single-phase gratings.

In conclusion, the single-phase threshold curves of the mirrored patterns are identical and have the same shape as the full-wave grating threshold curves, though are 0.3 log units (a factor of two) shifted in modulation depth. It should again be emphasized that modulation depth of single-phase gratings is defined by using the same magnitudes of $\hat{\ell}$ and L_b that were used for the full-wave gratings. If, in the case of a full-wave grating, the maximum modulation amplitude is designated by $\hat{\ell}_f$, and if, with the rectified wave, the maximum difference with L_b is designated by $\hat{\ell}^+$ or by $\hat{\ell}^-$, the shift of 0.3 log units in Fig. 3 implies that $\hat{\ell}^+ = \hat{\ell}^- = 2\hat{\ell}_f$ at threshold.

Combining disk and single-phase grating results, we must conclude that dynamic thresholds are symmetrical, and thus independent of polarity, provided that

incremental and decremental patterns are presented with the same spatial phase. In contrast to this, quasistatic threshold curves of disks are shifted with respect to each other, while those of single-phase gratings are not.

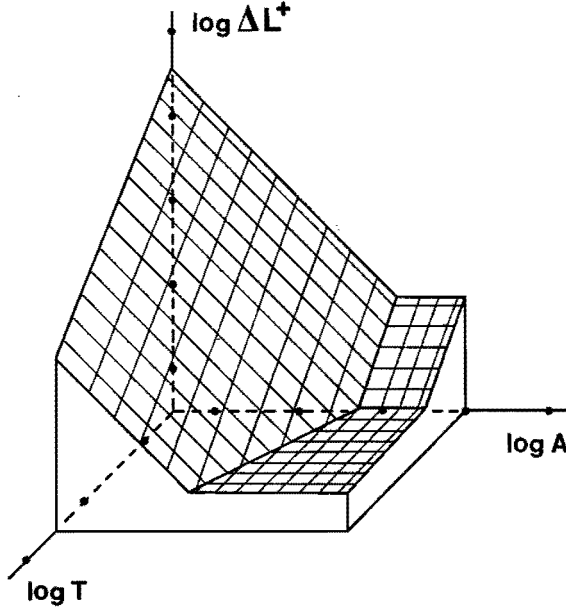


Figure 4: Threshold surface of incremental disks as a function of area A and duration T . This surface demonstrates spatiotemporal inseparability.

6.4 Discussion

From Fig. 2 it is evident that an asymmetry in the detection of incremental and decremental disks can be found only if a) the diameter is small enough and b) the duration is long enough or the temporal envelope is quasistatic. It is therefore not surprising that different authors came to different conclusions in the past (e.g. Roufs, 1974; Toet, 1987).

Threshold curves of disks may be described by overall spatial low-pass processing in view of the monotonic decrease of threshold with area. Since these curves are translated over both axes, it seems obvious that vision at threshold level reflects spatiotemporal inseparability. This means that the processing of the visual system can not be described by a simple (temporal) impulse response followed by a (spatial) point spread function. For the temporal analogue, i.e. threshold curves of small and large disks dependent on duration, approximately similar results are found (de Ridder, 1987). Combining spatial with temporal threshold curves, all being understood as intersections of a three-dimensional space, a threshold surface can be constructed as a function of disk duration and area. In Fig. 4 this

has been done by combining the asymptotic approximations of all curves, thus displaying Ricco's law for small area's and Bloch's law for short durations. This surface illustrates the reciprocity between the luminance increment and the product of disk duration and area. The same procedure can be applied to decremental disks and will result in an asymmetrical threshold surface of course. Now the problem arises that the two threshold surfaces for disks cannot be directly related to the single threshold surface for spatiotemporal sinewave gratings (Kelly, 1984; Bowker, 1983). Neither do isolated point spread functions and impulse responses (Blommaert and Roufs, 1981; Roufs and Blommaert, 1981) constitute the missing link between both types of threshold surfaces. If these are considered to reflect the spatial or temporal behaviour of single channels, additional channels and some asymmetrical mechanism ought to be introduced.

Experimental results obtained with squarewave gratings (Campbell and Robson, 1968; Ginsburg and Cannon, 1980) suggested that the visual system might operate in such a way that Fourier analysis is applicable. In other words, that detection is determined by the amplitude of the fundamental Fourier component in case of high-frequency gratings or by the amplitudes of higher Fourier components in case of low-frequency gratings. For a frequency f_0 , the Fourier series of a positive single-phase rectified cosine grating equals

$$L(r, \varphi) = L_b + \hat{\ell}^+ \left\{ \frac{1}{\pi} + \frac{1}{2} \cos(2\pi f_0 r) + \frac{2}{3\pi} \cos(4\pi f_0 r) + \dots \right\} \quad (5)$$

The amplitude of the fundamental or first harmonic is $0.5 \hat{\ell}^+$. The factor of 0.5 is confirmed by our experimental data: modulation depth of single-phase gratings is twice (0.3 log units above) that of full-wave gratings, or in luminance amplitudes $\hat{\ell}^\pm = 2\hat{\ell}_f$. The second harmonic at $2f_0$ is $4/3\pi = 0.42$ times the fundamental. Fig. 3 shows that below 2 cpd the detection curves of single-phase and full-wave gratings remain similar. This finding would lead one to assume that detection is governed by the fundamental and not by higher harmonics. Our observation thus agrees with experimental data on triangular gratings and trapezoid-wave gratings with ramps that occupy 50% of a cycle, which also suggest that detection is governed by the fundamental (Campbell et al., 1981; Jaschinski-Kruza, 1984). However, detection thresholds of low-frequency squarewave gratings as well as trapezoids with steep slopes (Campbell and Robson, 1968; Campbell et al., 1981), which seem to contradict the unique role of the fundamental, can be accurately predicted by means of a multiple channel model (Jaschinski-Kruza and Cavonius, 1984). Results obtained with preadaptation to higher harmonics confirm the role of low-frequency channels mediating detection of such low-frequency gratings (Greenlee and Magnussen, 1985). Despite the fact that simple Fourier analysis would perfectly explain our present grating data, this means that model predictions should involve multiple channels.

In view of the asymmetry problem, it is of interest to confront our data with existing multichannel models. We then make the following observations:

- Publications on multiple channel models deal with the one-dimensional case. The correspondence between our disk results and receptive field properties from physiology would favour treatment in terms of radially symmetric channels, thus point spread functions. Even if physiology would explain psychophysics, it cannot provide a decisive answer here: retinal ganglion cells respond according to (approximately) circular receptive field profiles, but the visual cortex is organized in elongated field profiles that resemble Gabor functions. Besides, models based on channels which represent underlying information transmitting mechanisms, either radially symmetric or one-dimensional, are to be considered abstractions of a much more complicated neural system. Actually, the only requirement of a model is to provide correct fitting of and predictions for psychophysical experimental data.
- Existing multichannel models ignore stimulus polarity and assume peak detection (Jaschinski-Kruza and Cavonius, 1984) or detection in combination with spatial probability summation and nonlinear response pooling (Wilson and Bergen, 1979). Physiological and psychophysical evidence for asymmetry in the processing of visual stimuli should be incorporated in the model. This can be achieved by assigning a polarity-dependent gain to the transfer functions of some channels or an asymmetrical threshold-detection mechanism.
- Multichannel models should be able to account for results obtained with periodic as well as aperiodic patterns. Moreover, model parameters should be fitted simultaneously to three-dimensional (spatiotemporal) threshold surfaces, instead of to some intersections.

Let us assume a static model that consists of a limited number of channels which may represent a continuous ensemble:

1. The spatial response profiles or point spread functions of the channels can be selected more or less arbitrarily, for instance as circular difference-of-Gaussians (DOG) functions. In the frequency domain they may be pure band-pass filters (Blommaert and Roufs, 1981) but such that the transfer function of the narrowest channel corresponds to the high-frequency cutoff as measured for sinewave gratings. The properties of such a channel are demonstrated in the Appendix of this chapter. For frequencies not too low it appears that a) the amplitude response to a single-phase grating is half that to a full cosine grating and b) the maximum and (negative) minimum of the response to a single-phase grating are equal.

2. Different channels are assumed to have the same bandwidth in octaves and to be distributed equidistantly in the log frequency domain. Quasistatic threshold curves of disks are shifted over 0.6 log units (Fig. 2). This corresponds to point spread functions that differ by a factor of two in spatial extent and thus with a shift of one octave. Note that a one-octave shift of channels also agrees with frequency-discrimination data presented by Hirsch and Hylton (1982).
3. Furthermore, a symmetrical or asymmetrical nonlinear amplitude transfer function is assigned to each channel and some form of summation of the channel outputs has to be considered. In view of the high degree of symmetry reflected by our threshold data, a symmetrical detection mechanism, i.e. peaks with equal though opposite threshold values, is most likely. For the broad channels this implies also symmetrical amplitude transfer functions.

Within this concept, the shift of the quasistatic threshold curves of disks can be explained by assigning an asymmetrical amplitude transfer function to the narrowest channel(s). This asymmetrical mechanism means that positive gain is larger than negative gain, and that detection of small incremental disks is governed by the positive peak, while that of negative small disks is determined by the negative peak. In the case of single-phase gratings, convolution with a point spread function which resembles a pure band-pass filter in the frequency domain yields approximately the same fundamental Fourier component for positive and negative phases, i.e. for spatial frequencies not too low (see Appendix). In combination with the asymmetrical gain, it therefore follows that thresholds of positive and negative single-phase gratings are both mediated by detection of the positive peaks. Thus, the introduction of an asymmetrical amplitude transfer function for the narrowest channel(s) can possibly provide a satisfactory explanation for the discrepancy between quasistatic thresholds of disks and single-phase gratings.

6.5 Appendix

In this appendix we will derive the response of pure band-pass channels to the radially symmetric periodic patterns that we used in our experiments. Consider for any channel a difference-of-Gaussians (DOG) spatial response profile

$$PSF(r) = g_1 \cdot \exp(-r^2/2\sigma_1^2) - g_2 \cdot \exp(-r^2/2\sigma_2^2) \quad (6)$$

In order to normalize the profile and to exploit possible benefits of recursion (Hartmann, 1982), the constants a and b are introduced. The amplitude constant a is chosen such that $g_2 = ag_1$. If $g_1 - g_2 = 1$ it follows that $g_1 = 1/(1 - a)$ and $g_2 = a/(1 - a)$. The width constant b is chosen such that $\sigma_2 = b\sigma_1$. If subsequent broader channels are tuned in octaves, it follows that the excitative Gaussian of a

broader channel corresponds to the inhibitive Gaussian of the narrower if $b = 2$. However, the choice of b is not crucial for the conclusions which follow. Alternative values, implying other bandwidths or shifts of the channel responses can be considered. For a pure band-pass character, the surface integral

$$\int_0^{2\pi} \int_0^\infty PSF(r) r dr d\varphi = \frac{2\pi\sigma_1^2}{1-a} \{1 - ab^2\} \quad (7)$$

has to be zero. If $b = 2$, it therefore follows that $a = 1/4$, and thus $g_1 = 4/3$ and $g_2 = 1/3$.

Convolving a radially symmetric cosine grating, different response values are obtained in the centre of the pattern and at some distance of the centre (where the local pattern approaches a one-dimensional grating), see Fig. 5. The off-centre response is symmetrical and cosine shaped. Since no dominant role of the centre-response has been observed, at both threshold and suprathreshold levels of modulation, an overall approximation of the convolution result by the regular off-centre response is suggested. Furthermore, the amplitude of the off-centre response proved to be identical to the amplitude of the convolution result in the one-dimensional case. For this, the line spread function of any channel is determined by integration:

$$\begin{aligned} LSF(x) &= \int_{-\infty}^{\infty} PSF(x, y) dy \\ &= \sqrt{2\pi} \{g_1\sigma_1 \exp(-x^2/2\sigma_1^2) - g_2\sigma_2 \exp(-x^2/2\sigma_2^2)\} \end{aligned} \quad (8)$$

Its convolution with a one-dimensional grating $mL_b \cos(2\pi fx)$ gives a response $R(x) = mL_b G(f) \cos(2\pi fx)$ with a gain

$$G(f) = \frac{8}{3} \pi \sigma_1^2 [\exp\{-2(\pi f \sigma_1)^2\} - \exp\{-8(\pi f \sigma_1)^2\}] \quad (9)$$

if the constants a and b , as derived above, are substituted. We are now able to determine the σ_1 parameter of the narrowest channel. For high spatial frequencies the influence of the inhibitive Gaussian can be neglected, and the amplitude of the response equals

$$G(f) \approx \frac{8}{3} \pi \sigma_1^2 mL_b \exp\{-2(\pi f \sigma_1)^2\} \quad (10)$$

Substitution of two measured data points (m_1, f_1) and (m_2, f_2) , both from the high-frequency cutoff region of the threshold curve, and equalization of eq. (10) leads to

$$m_1 \exp\{-2(\pi f_1 \sigma_1)^2\} = m_2 \exp\{-2(\pi f_2 \sigma_1)^2\} \quad (11)$$

From this the σ_1 parameter can be solved:

$$\sigma_1^2 = \frac{\log m_1 - \log m_2}{2\pi^2(f_1^2 - f_2^2) \log e} \quad (12)$$

This procedure provides us with a value of 1.08 min. of arc for σ_1 . The zero crossing of the PSF thus obtained occurs for a radius of 2.07 min. of arc. The PSF of the narrowest channel agrees therefore quite well with those directly measured by means of the perturbation technique, i.e. foveal and against a 1200Td background (Blommaert, 1987).

As mentioned above, the amplitude gain in the one-dimensional case equals the off-centre response. The gain given by eq. (9), with the parameters of the narrowest channel substituted, agrees with the solid-circle curve presented in Fig. 5. In order to derive the response to a normalized (positive) single-phase grating, we depart from its Fourier series:

$$F(x) = \frac{1}{\pi} + \frac{1}{2} \cos(2\pi fx) + \frac{2}{\pi} \sum_{i=1}^N \frac{(-1)^{i+1}}{(2i)^2 - 1} \cos(4i\pi fx) \quad (13)$$

Substitution of the gain for each component, in accordance with eq. (9), leads to the spatial response

$$R(x) = mL_b \left\{ \frac{1}{2} G(f) \cos(2\pi fx) + \frac{2}{\pi} \sum_{i=1}^N \frac{(-1)^{i+1}}{(2i)^2 - 1} G(2if) \cos(4i\pi fx) \right\} \quad (14)$$

Instead of solving the convolution integral numerically, as was done to achieve the data presented in Fig. 5, the evaluation of eq. (14) provides a correct response that allows for easy determination of for instance maximum and minimum peak values at different spatial frequencies. This is illustrated in Fig. 6. For spatial frequencies above 10 cpd the output of the narrowest channel will approximate the fundamental Fourier component, the amplitude being reduced by a factor of two with respect to the amplitude of the response to a fullwave cosine grating. Below 10 cpd the maxima and (negative) minima will diverge, the minimum even exceeding the maximum for frequencies below 2.3 cpd.

Finally, it can be argued from Fig. 6 that the introduction of broader channels allows for a correct prediction of threshold curves obtained with single-phase gratings. All channels are assumed to be equidistantly distributed in the log frequency domain. A shift of one octave implies a multiplication of the spatial extent of the point (line) spread functions by a factor of two. The gain curves of successive broader channels are therefore 0.3 log units shifted towards lower frequencies. To each channel a weighting factor is assigned, such that the envelope of the responses of all channels predicts the threshold curve as measured with fullwave cosine gratings. From Fig. 6 it therefore follows that the envelope of the maxima of the

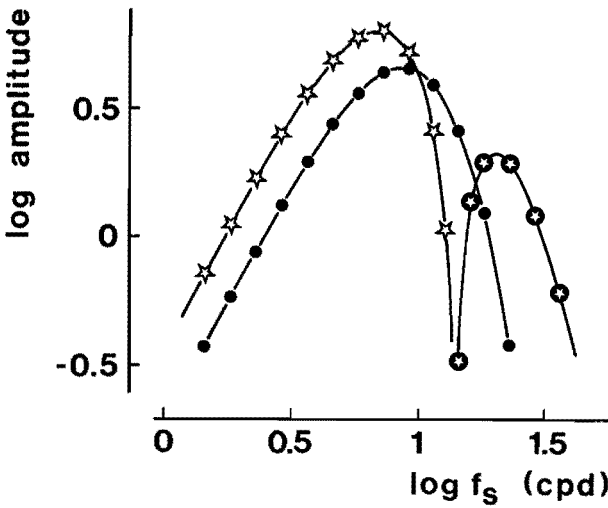


Figure 5: Amplitude of a normalized radially symmetric cosine grating which is convolved with the normalized DOG-shaped point spread function of the narrowest channel ($\sigma_1 = 1.08'$, $a = 1/4$ and $b = 2$). The response in the centre of the grating is positive for spatial frequencies below 14 cpd (open stars) and negative for frequencies above 14 cpd (inverted stars). The off-centre response resembles a symmetrical cosine pattern (solid circles).

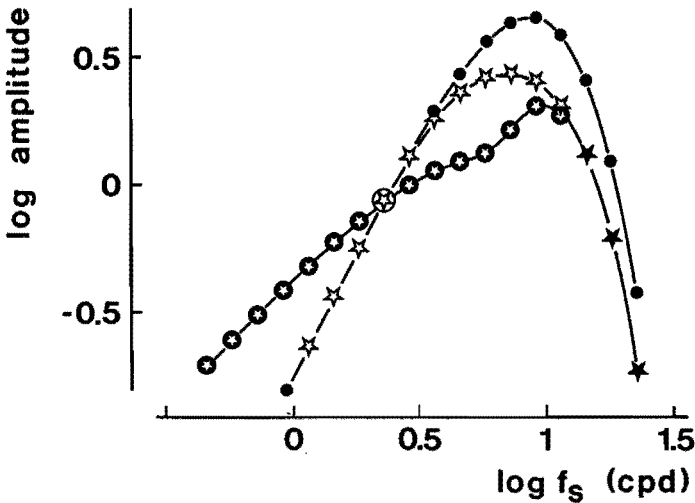


Figure 6: The amplitude response of the narrowest channel to a full cosine grating (solid circles). For spatial frequencies above 10 cpd the response to a positive single-phase grating will equal that of a full grating, though with halved amplitude (solid stars). Below 10 cpd the non-cosine response shows a deviation between maxima (open stars) and negative minima (inverted stars).

channel responses to single-phase gratings will approximate the threshold curve as measured.

7 Apparent Contrast of Noise Gratings

Abstract

The apparent-contrast perception of radially symmetric noise gratings has been studied. These patterns are defined in the frequency domain by a central frequency and a bandwidth. They provide a stimulus type that represents an intermediate condition between isotropic textures and abstract, deterministic stimuli, such as disks and pure-cosine gratings.

At a fixed central frequency of 4.2 cpd, the maximum luminance difference with the background as well as the root-mean-square (RMS) value required for detection increases with the bandwidth, while apparent contrast is independent of the bandwidth.

Both detection threshold and apparent iso-contrast curves, as a function of the central frequency, appear to flatten with increasing bandwidth and reference level if compared to the frequency characteristics of pure-cosine gratings.

Results suggest that stochastic patterns are perceived with an equal apparent contrast, irrespective of their frequency distribution, if their RMS value is equal and sufficiently high.

7.1 Introduction

Spatial visual processing is commonly investigated by exploring threshold and suprathreshold perception of deterministic, rather abstract stimuli. Most frequently used are periodic stimuli, such as sinewave gratings with varying spatial frequency, and aperiodic stimuli, such as disks with varying diameter. The main goal is to obtain a better insight into the behaviour of the visual system. The conception of models of visual processing, and their generalized value for everyday perception of complex scenes, is of eminent interest. Real scenes only occasionally contain the abstract patterns mentioned. Although modern environment increasingly involves the presence of artificially shaped and therefore more and more abstract objects to be perceived, there still are quite some patterns that are best described in stochastic terms. Apart from theoretical modelling, the study of the perception of (deterministic and) stochastic patterns may therefore be of some practical importance. Besides, certain developments in contemporary technology explicitly emphasize the importance of visual perception of stochastic patterns: for instance textural image patterns in remote sensing and medical diagnostics.

A complication involved in the perception of complex or stochastic patterns is the question of what exactly is being perceived. A stochastic (physical) luminance pattern causes also a stochastic (subjective) brightness pattern. This means that one can speak of a distinct and therefore *local* magnitude of perceived brightness at any location of a pattern. However, irrespective of the complexity of a luminance

pattern, and consequently brightness pattern, there appears to exist an unambiguous impression of the *global* apparent contrast, i.e. of the pattern as a whole. The pronounced role or even dominance of this visual percept has been demonstrated in literature, both in case of one-dimensional sinewave gratings (e.g. Blakemore et al., 1973) and in case of stochastic patterns (Quick et al., 1976; Hamerly et al., 1977; Mayhew and Frisby, 1978).

As a consequence of the experimental results in the foregoing chapters, one can question the significance of data, obtained by using abstract stimuli such as disks and sinewave gratings, for the perception of complex scenes. It was shown that threshold and suprathreshold data of incremental and decremental disks (chapter 4) and circular cosine gratings (chapter 5) imply *seemingly* contradicting spatial characteristics for the visual system. The different explanations given there for the nature of apparent-contrast perception, its relation with brightness perception in particular, suggest that a unification of disk and grating results, by means of a single spatial model, is quite a problem. The difficulties met, which point towards a stimulus-specific processing, would therefore suggest that visual perception should also be studied by using complex patterns, such as normal scenes, photographs, diagnostic images in medicine, and so on.

The more pragmatic approach of using normal scenes in studying brightness perception is not new. Previous investigations concerned with photographic gray-tone reproduction are available (Simonds, 1961; Bartleson and Breneman, 1967a,b; Bartleson, 1968). However, a drawback of some of these studies is the application of scaling techniques, and magnitude estimation in particular. It is now known that magnitude-estimation results can be seriously obscured by the nonlinear number handling of subjects (Curtis and Rule, 1972; Saunders, 1972; Bartleson and Breneman, 1973) and that different subjects may use different number scales.

In view of the foregoing, we wanted to study the perception of complex, stochastic patterns by performing matching experiments, without shifting too abruptly from the abstract stimuli commonly used to complex scenes. Since our previous experiments were all performed under equal conditions, including the same background level, quasistatic temporal envelope of the spatial patterns etcetera, we maintained these conditions and considered patterns that may bridge the gap between deterministic stimuli on the one hand and real scenes on the other. In order to link up with available results on radially symmetric cosine gratings, and to enable further apparent-contrast modelling, we used radially symmetric noise gratings. These circular patterns are defined by their Gaussian spectra, i.e. a central frequency and a bandwidth, assuming a random phase of the frequency components. Since they are radially symmetric as well as stochastic, they can be regarded as an intermediate condition between two-dimensional isotropic textures

and one-dimensional sinewave gratings¹.

A further advantage of considering these patterns is that data on similar patterns are available. Mostafavi and Sakrison (1976) measured detection thresholds of various noise patterns, and derived some properties of a single spatial channel. Their results will be discussed in detail further on. Mayhew and Frisby (1978) matched suprathreshold two-dimensional textures with different spectral distributions, and found that the apparent contrast is constant if the root-mean-square (RMS) value of the patterns is constant. The same conclusion was established by Quick, Hamerly and Reichert (1976). They matched noise gratings with different bandwidths, but corrected the noise spectra for the contrast sensitivity function (CSF) of pure sinewave gratings. The slight difference between their matching curves is perhaps a clue for the limited validity of CSF correction of suprathreshold patterns: curves measured at a reference level of 5% are flatter than those measured at 20%². CSF-correction of noise gratings was also applied by Jamar and Koenderink (1985). Their detection-threshold data do not depend on the bandwidth. In agreement with the foregoing studies, they concluded that detection requires a fixed RMS value. Finally, the role of the RMS value as a determinant for apparent-contrast perception was partly rejected by Hamerly, Quick and Reichert (1977). They found that linear summation of the modulation depths of the components in complex gratings, consisting of two sinewave gratings with different frequency and phase, can also govern global apparent-contrast perception. They argued that the difference between established summation rules (linear in case of modulation depth, quadratic in case of RMS value) is merely a reflection of the nonlinear amplitude transfer characteristic, the so called transducer function, of the visual system.

7.2 Methods

We used a CRT, with radial screen and white phosphor. A detailed description of the device is given in chapter 3. The screen subtended 3.3 degrees of visual angle; the background luminance was 300 cd.m^{-2} . The screen was extended to 5x5 degrees by an external source, and the extension had about the same hue and brightness as the screen. The barely visible transition between screen and extension was utilized to fixate the centre of the screen. Radially symmetric cosine gratings were always presented with a luminance maximum in the centre. At the

¹An example of a circular cosine grating is given by Kelly and Magnusky (1975), and the appearance of a one-dimensional noise grating is demonstrated by Stromeyer and Julesz (1972).

²The left panel of Fig. 3, for instance, shows that the frequency characteristic for sinewave gratings varies with the reference level, the lowest curve being the CSF. Modulation depths of 5% and 20% correspond to log modulation depths of -1.3 and -0.7 respectively. This implies that CSF-correction is only correct for low suprathreshold patterns, but evokes an overcompensation for frequencies around 4 cpd at higher levels.

lowest spatial frequency, which was 0.61 cpd, one period corresponded to the screen radius. Note that modulation depth of pure cosine gratings is defined by the Michelson formula $m = (L_{max} - L_{min}) / (L_{max} + L_{min})$ and that the spatial frequency equals one divided by the radial period.

All patterns were presented with a quasistatic temporal envelope of 900 msec duration. This envelope consisted of a constant centre plateau of 300 msec, flanked by errorfunction-shaped transitions of 300 msec. Stimulus combinations of test and reference were presented sequentially, with an interstimulus interval of 500 msec. A delay of 300 msec was regarded between the control of a start-button and the release of the first stimulus.

Observations were performed by a well-trained subject (JDB). In all experiments he observed with the right eye, and made use of an artificial pupil, 2 mm in diameter, that was equipped with an entoptic guiding system. The subject was instructed to judge the global apparent contrast of the patterns, both in case of fixed references (circular cosine gratings with a frequency of 4.2 cpd) and in case of noise gratings, and to pay less attention to local brightness extremes or the difference between these.

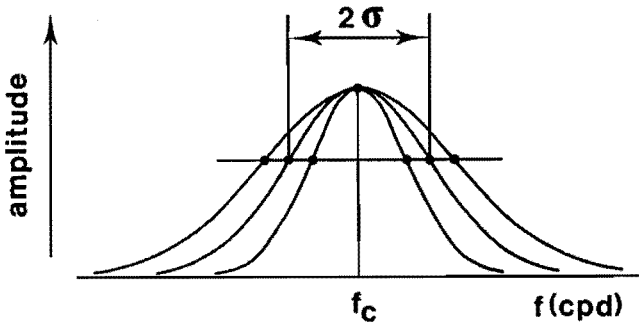


Figure 1: Noise gratings are here defined in the frequency domain. The Gaussian amplitude distribution is specified by the central frequency f_c and the standard deviation σ . The bandwidth corresponds to the interval $[f_c - \sigma, f_c + \sigma]$.

The radially symmetric noise gratings were achieved by summation of many (25) cosine gratings, with random phase and Gaussian amplitude distribution, approximating:

$$\tilde{L}(r, \varphi) = L_b + \hat{\ell} \cdot c \cdot \int_0^\infty \exp \left[\frac{-(f - f_c)^2}{2\sigma^2} \right] \cdot \cos(2\pi fr + \tilde{\vartheta}_{random}) df \quad (1)$$

if L_b represents the background luminance. At a given central frequency f_c , the bandwidth corresponds to the frequency interval $[f_c \pm \sigma]$; see Fig. 1. If the bandwidth is expressed in octaves BW , i.e. $BW = \log_2(f_c + \sigma) / (f_c - \sigma)$, it therefore follows that

$$\sigma = f_c \cdot \frac{2^{BW} - 1}{2^{BW} + 1} \quad (2)$$

The constant c in eq. (1) was determined such that the maximum amplitudes of the stochastic patterns were normalized. This was done to achieve a same amplitude resolution for all patterns, including pure cosine gratings: all patterns were thus computed and stored with an amplitude resolution of 8 bits. At a given attenuation, the maximum luminance difference $\hat{\ell}$ with respect to the 300 cd.m^{-2} background was therefore equal for all stimuli, but situated at different places on the screen. In the experiments, we determined the amplitude attenuation required for detection or an apparent iso-contrast with a pure cosine grating. This is one way to look at the data. It is essentially based on (local) maximum amplitudes $\hat{\ell}$ in cd.m^{-2} which are related to (local) maximum modulation depths \hat{m} by $\hat{\ell} = L_b \cdot \hat{m}$ with $L_b = 300 \text{ cd.m}^{-2}$.

Another way of considering measured data involves the root-mean-square (RMS) value of the noise gratings. To this purpose, the spatial patterns were integrated over the screen with radius R ,

$$RMS = \left[(1/\pi R^2) \int_0^{2\pi} \int_0^R \ell^2(r, \varphi) r dr d\varphi \right]^{1/2} \quad (3)$$

if $\ell(r, \varphi)$ equals the luminance amplitude of the pattern superimposed on the background. For a pure-cosine grating it follows that

$$RMS = \frac{\hat{\ell}}{\sqrt{2}} = \frac{mL_b}{\sqrt{2}} \quad (4)$$

This definition therefore corresponds to the effective value which is expressed in cd.m^{-2} .

For any central frequency and bandwidth, we used 16 uncorrelated patterns. This was done, because we expected to find rather large differences between different spatial patterns with an equal spectral distribution. Since the performance will vary from pattern to pattern, the method of constant stimuli, which was shown to be very precise for deterministic stimuli, is less suitable for stochastic patterns. For this reason we applied the balanced method of adjustment. This means that the attenuation of a test stimulus was adjusted to match the apparent contrast of a reference by starting at both larger and dimmer apparent contrasts with respect to the point of subjective equality with equal numbers of trials. Accordingly, detection thresholds and points of subjective equality were determined 8 times for each of the 16 independent patterns. This was done for all central frequencies, bandwidths and reference levels. The geometric means of the 128 individual measurements were computed, both in terms of maximum luminance amplitudes and in terms of pattern-specific RMS values.

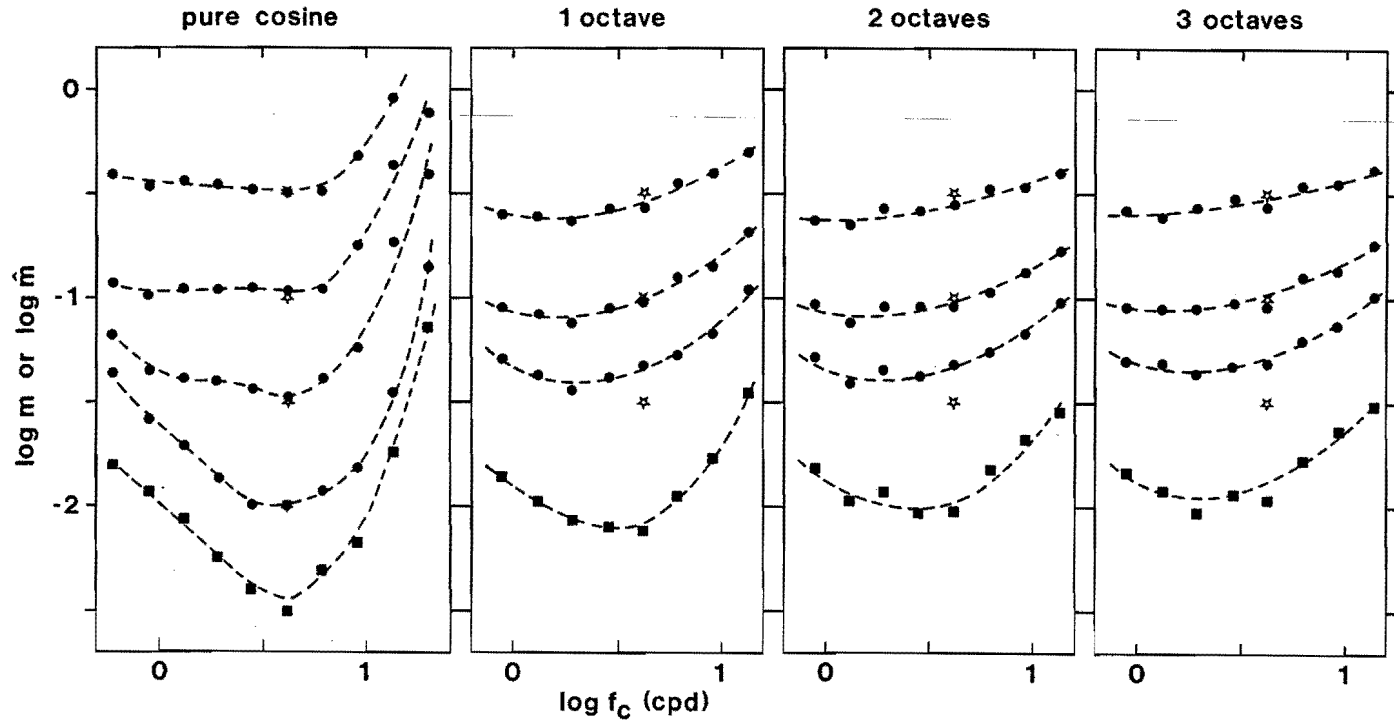


Figure 3: Detection thresholds (solid squares) and apparent iso-contrast curves (solid circles), for different bandwidths and reference levels, as a function of the central frequency. Open stars render pure-cosine references; dashed curves were drawn freely. The left panel shows previous data on pure-cosine gratings for comparison. Standard deviations are comparable with those displayed in Fig. 2.

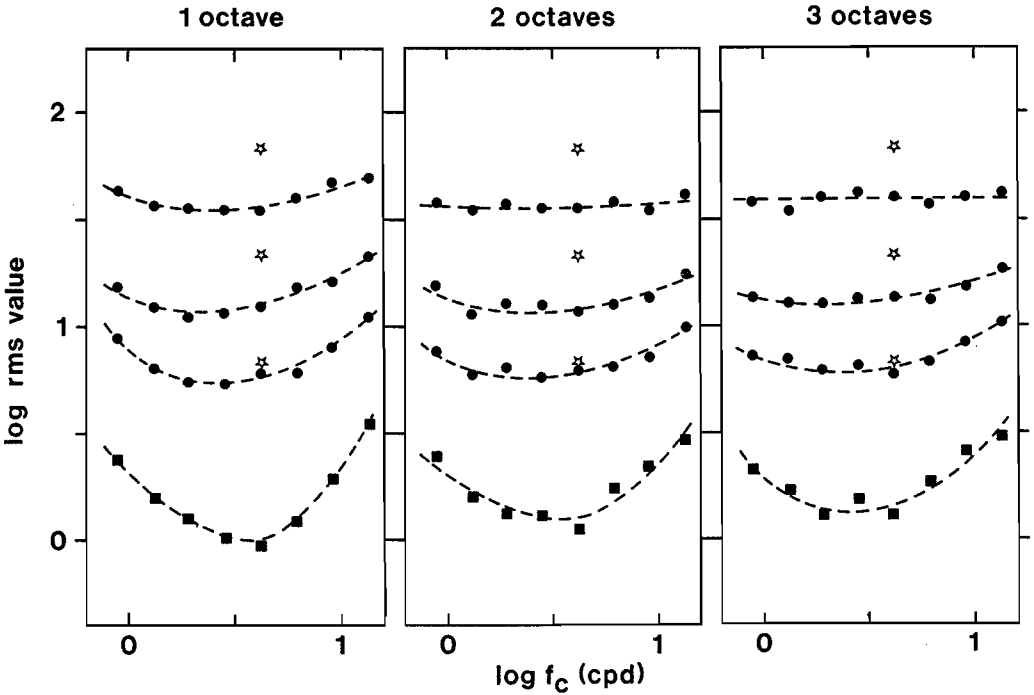


Figure 4: Same as Fig. 3, but now in pattern-specific RMS-value units.

'frequency characteristic' approximates the contrast sensitivity function indeed. A comparison with the detection-threshold data of Jamar et al. (1985) is not possible, because they corrected the spectral distributions of their patterns for the CSF.

7.4 Discussion

Summarizing our results, we found that detection threshold increases with the bandwidth if a central frequency of 4.2 cpd is used, while apparent contrast is constant. Varying both the central frequency and the bandwidth, we yielded detection-threshold and apparent iso-contrast curves that flattened increasingly with the bandwidth. For 2 and 3 octave gratings apparent contrast appeared even independent from the central frequency for RMS values that are large and constant.

With respect to the perceptual phenomena involved in performing threshold experiments, it should be mentioned that detection occurs if some patch of the radial pattern becomes visible, i.e. an angularly and radially limited part of the pattern at a certain distance from the centre, without showing any predominant role of the centre itself. Consequently, detection is related to strictly *local* luminance amplitudes. In view of the reduced curvature of the circular grating pattern

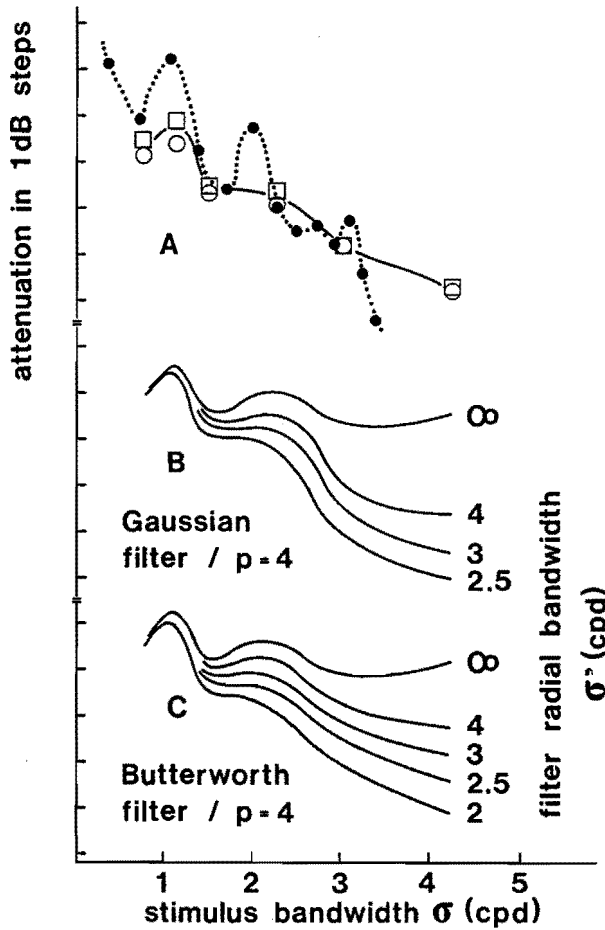


Figure 5: (A) Comparison between detection thresholds of both angularly and radially band-limited noise (open symbols connected by solid curve; angular bandwidth $\pm 10^\circ$, central frequency 4.5 cpd; Mostafavi et al. (1976)) and circular noise gratings (solid circles connected by dotted curve; central frequency 4.2 cpd; duplicated from left panel Fig. 2). (B) Single channel model predictions assuming an inhomogeneous retinal sensitivity, a Gaussian filter with angular bandwidth $\pm 10^\circ$, and nonlinear integration ($p=4$) over a 2×2 degree window; taken from Mostafavi et al. The curve with a filter radial bandwidth $\sigma' = \infty$ corresponds to the unfiltered situation. (C) Same as (B) though with assuming a Butterworth filter. The $\sigma' = 2.5$ cpd curve provides a good prediction for Mostafavi et al.'s data (the solid curve in panel A).

off-centre, a provisional one-dimensional approximation in modelling would be quite acceptable. Furthermore, the resemblance between the perceived patches of radial noise gratings used here and a limited part of both angularly and radially band-limited noise patterns, as used by Mostafavi et al. (1976), suggest that detection data for these two types of patterns should be comparable.

For suprathreshold levels the stochastic luminance patterns evoke also a stochastic *local* brightness pattern of course, but the apparent contrast is judged on the basis of a more *global* though unambiguous percept. This means that apparent-contrast matching involves judgment of some unknown property of the entire pattern. Although the subject was instructed to pay less attention to local brightness extremes or the difference between these, the modelling of apparent-contrast perception might nevertheless be based on some function of the (subjective) brightness pattern, for instance by taking into account the difference between local brightness extremes in some dominant part of the pattern (see also chapter 5). In agreement with the experiences reported by Quick et al. (1976), Mayhew et al. (1978) and Blakemore et al. (1973), contrast matches, even in case of stochastic patterns, are relatively easy for subjects to perform. The fact that a univocal magnitude of the apparent contrast can be attached to these stochastic brightness patterns confirms the importance of this global perceptual attribute.

Our results agree, where comparable, with data presented by Mostafavi et al. (1976), Quick et al. (1976) and Mayhew et al. (1978). These studies are, as far as we know, the only ones that allow for a direct comparison. Other studies, in which for instance the masking effect on the detection of sinewave gratings was determined, deal with different perceptual tasks (Stromeyer and Julesz, 1972; Pollehn and Roehrig, 1970; Henning et al., 1981; Jamar and Koenderink, 1985; Van Meeteren and Valetton, 1985). The apparent correspondence between our threshold curves and for instance the masking data from Pollehn and Roehrig (1970), the flattening and shift of maximum sensitivity towards lower frequencies and higher modulation depths for larger bandwidths in particular, can not be explained intuitively. Model predictions must be calculated by using a nonlinear multichannel configuration, at threshold level (Wilson and Bergen, 1979) as well as suprathreshold levels (Swanson et al., 1984). Besides, the large spread of our data, being a consequence of repeated measurements with uncorrelated spatial patterns, which was quite large for detection thresholds, is an indication that Monte-Carlo simulations should be used. This means that predictions must be determined also by repeated calculations with different, uncorrelated patterns.

Mostafavi and Sakrison (1976) tried to derive some properties of a single spatial channel from detection thresholds of two-dimensional noise patterns, i.e. isotropic as well as both angularly and radially band-limited noise. Their results obtained

with narrow-band stimuli of fixed angular bandwidth ($\pm 10^\circ$)³ as a function of the radial bandwidth, measured at a fixed central frequency of 4.5 cpd, are replotted in Fig. 5A (open symbols) along with our present results on radially symmetric patterns (solid circles); see also Fig. 9 from Mostafavi et al. (1976). Although the spatial patterns used differ and the spread of the data has been neglected, the direct comparison between their and our data illustrates that the increasing maximum luminance amplitude with the bandwidth (the decreasing attenuation of amplitude-normalized patterns) required for detection roughly corresponds, be it that our results suggest a more oscillatory behaviour. Moreover, Mostafavi et al.'s predictions, computed on the basis of a single Gaussian (Fig. 5B) or Butterworth (Fig. 5C) filter demonstrate the same effect, with only a small oscillatory behaviour. These predictions were computed by assuming an inhomogeneous retinal sensitivity, nonlinear integration with an exponent $p=4$ over a 2×2 degree window, which means 4th-power summation of response samples taken at closely spaced points, and an angular filter bandwidth of $\pm 10^\circ$. As shown by the solid curve in Fig. 5A, a Butterworth filter with a radial bandwidth (σ') of 2.5 cpd provides a good prediction for their data and for the global behaviour of our present data. Whether such a single-channel approach, with other parameters describing the spatial probability summation, would explain a more pronounced oscillatory behaviour, is not yet certain (apart from the question how significant the oscillatory behaviour is with respect to the spread of our data, see Fig. 2).

Figure 6 demonstrates the influence of the pattern bandwidth on the output of a pure band-pass narrow-bandwidth filter, as a function of the central frequency. No presumptions with respect to the inhomogeneous retinal sensitivity and probability summation as made by Mostafavi et al. were incorporated. The data were achieved by convolving 25 normalized patterns, each with the same central frequency and bandwidth, with a normalized DOG-shaped point spread function. This point spread function corresponds to that of the narrowest channel, as derived in the appendix of chapter 6. The ensemble means of the maxima of 25 responses were computed. Figure 6 shows it follows that the 'frequency response' of a single spatial channel becomes flatter if the bandwidth of the pattern is increased. Note that the visual system is assumed to contain a number of such channels, and that they are distributed in the frequency domain. The sensitivities of all channels can be determined on the basis of the CSF for pure cosine gratings, i.e. such that the envelope of all channel responses to these patterns agrees with the CSF. Detection thresholds of noise gratings with different bandwidths can be predicted by using the response curves as shown in Fig. 6 for each channel. As a flattening of the 'frequency characteristic' with the bandwidth is already demonstrated for

³Mostafavi et al. (1976) defined the modulation transfer function of a frequency and orientation selective channel as the product of a Gaussian radial filter and a Gaussian angular filter. Hence, the radial bandwidth is expressed in cycles per degree and the angular bandwidth in degrees.

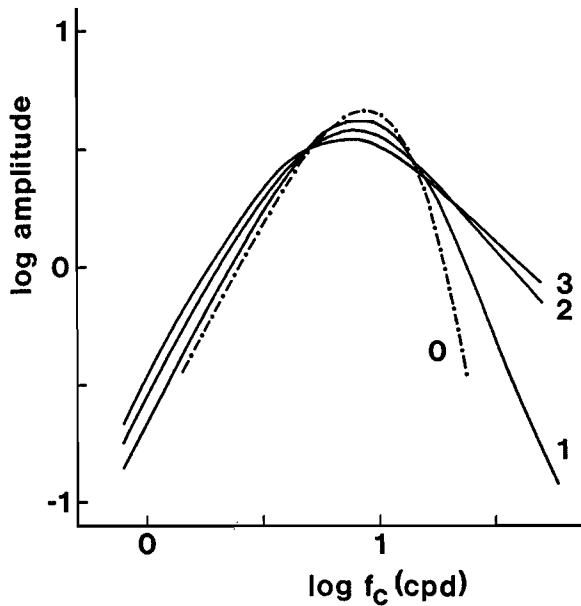


Figure 6: The maximum of the output of the narrowest channel. The normalized pure band-pass DOG-shaped point spread function was convolved with normalized pure-cosine gratings (dash-dotted curve) and with normalized noise gratings of 1, 2 and 3 octave bandwidths (solid curves). Solid curves represent the ensemble means of 25 computations; each determination was performed by using uncorrelated input patterns with similar spectral distributions.

one channel (Fig. 6), it may be expected that a multichannel model can predict the flattening threshold curves shown in Fig. 3. A similar observation holds for the increasing detection threshold with the bandwidth, which is found in case of a fixed central frequency f_c (Fig. 2). Because of the decreased maximum amplitude observed in Fig. 6, it follows that a larger bandwidth of the pattern requires a larger input amplitude $\hat{\ell}$ in order to evoke a constant amplitude at the output. In the next chapter we shall deal with multichannel model predictions more extensively.

Apart from theoretical modelling, one can discuss the implications of our present data for normal, everyday, visual perception. Georgeson and Sullivan (1975) introduced the idea of 'contrast-constancy', which means that the apparent contrast of suprathreshold sinewave gratings does not depend on the spatial frequency. Real scenes contain, as a rule, few or no areas with pure, one-dimensional, sinewave gratings. Taking circular gratings instead of the one-dimensional ones commonly used, no significant differences between apparent iso-contrast curves were found. It should be noted that the contrast constancy demonstrated by Georgeson et al., even up to spatial frequencies of 25 cpd, is not fully confirmed by other one-dimensional studies (Watanabe et al., 1968; Blakemore et al., 1973;

Bowker, 1983). The typical high-frequency attenuation is demonstrated in the left panel of Fig. 3. The second step, from circular pure-cosine gratings to circular band-limited noise gratings, showed a flattening in the high-frequency region. This means that the constancy of apparent contrast is maintained better, even for higher central frequencies, if the bandwidth of the stimuli is increased. It may therefore be expected that high-contrast isotropic patterns, for instance two-dimensional textures, are perceived with an equal apparent contrast, perhaps almost irrespective of their frequency distribution. This was also found by Mayhew and Frisby (1978) and may be of some practical importance.

This conclusion would imply a justification of the perceptual consequences of homomorphic filtering, which is a special technique in digital image enhancement (see for instance Oppenheim et al., 1968). A high-frequency textural pattern frequently shows a multiplicative low-frequency spatial envelope. This envelope is often referred to in case of natural scenes, where illumination and reflectance of objects are combined by multiplication in image formation (e.g. remote sensing). Homomorphic filtering is a method for the removal of these envelopes. By taking the logarithm of an image, the multiplicative envelope becomes additive, contributing to the low-frequency part of the spectrum, and can be reduced by high-pass filtering. Subsequent exponentiation of the filtered image thus results in an amplitude normalization of the local, high-frequency pattern.

Returning to vision, our results suggest that homomorphic filtering evokes also a constant perceived local contrast, in particular if the 'local' RMS value of the textures is normalized in stead of the local modulation depth. The images thus generated might provide a better starting-point for visual texture discrimination, because global apparent-contrast gradients in the original image have been removed. Previous reports on visual discrimination of stochastic gray-level textures demonstrated that one cannot discriminate between pairs of texture fields with differing third-order statistics⁴ when their lower order statistics are equal (see for instance Julesz, 1962; Pratt et al., 1978). This finding would mean that visual discrimination is only possible on the basis of first and second order statistics, i.e. the mean, standard deviation and second-order Markovian densities of pixel values (or luminances). A constant RMS value means that the standard deviations of the luminance patterns are equal. In this case visual discrimination would only involve the local mean, viz. being the average background level which may also be normalized, and the second order statistics.

In conclusion, our experiments show that in case of stochastic luminance patterns, and consequently stochastic brightness patterns, an unambiguous impression of the global apparent contrast exists. Results confirm the importance of

⁴The conditional probability density of a pixel x_0 conditioned on the state of its J neighbouring pixels x_1, \dots, x_J is given by $p(x_0 | x_1, \dots, x_J)$. The second-order density $p(x_0 | x_1)$ implies $J = 1$. The third-order density implies $J = 2$, etc. See Pratt et al. (1978).

this perceptual attribute for the perception of complex patterns or scenes. For circular noise gratings apparent contrast is even independent from the spectral distribution for bandwidths larger than one octave if the RMS value is sufficiently high. If this result is generalized, it may be of practical importance for the contrast perception of isotropic textures, and would imply a perceptual justification of the consequences of homomorphic filtering in digital image enhancement or visual texture discrimination.

8 On Modelling Spatial Vision at Threshold Level

Abstract

A concise review of available spatial models is presented, with a more detailed description of multiple channel ones.

Without using the explicit assumption of spatial probability summation, multichannel models are shown to provide good simultaneous predictions of threshold curves of sinewave gratings and other gratings. They fail in predicting thresholds of disk-shaped stimuli.

If it is assumed that spatial probability summation within channels takes place over a circularly bounded region of the responses, correctly shaped threshold curves of disks can be predicted. However, the predicted curves appear about a factor of 5 too low if compared to measured curves.

Possible extensions of the models, viz. being based on more local summation of channel responses and/or models consisting of initial radially symmetric channels (retina) followed by more orientation-selective channels (cortex) are discussed.

8.1 Introduction

An important objective of vision research is to generalize predictions of the processing of the visual system by modelling on the basis of available experimental data. It is therefore not surprising that quite a variety of models has been attempted in the past. We will review some familiar single and multiple channel approaches to spatial vision. These also illustrate the evolution of threshold and suprathreshold modelling as well as the different points of view which have emerged over the years. Available multichannel models will be analyzed in detail¹ and some alternatives will be studied in subsequent sections.

History

The application of linear system theory and Fourier analysis to spatial vision is not a recent development. Ernst Mach, in 1866, proposed the use of different periodic patterns with related Fourier-series expansions (see Ratliff, 1965). The real break-through came not before 1948 though, when Schade and Selwyn applied recently established methods (by Burger and van Cittert in 1932 and Duffieux in 1946; see van Nes (1968)) of characterizing diffraction limited optical systems to human vision. The modulation depth of sinewave gratings required for detection, as a function of the spatial frequency, demonstrated a band-pass characteristic. The reciprocal curve, known as the contrast sensitivity function (CSF), was thus

¹For a recent and more extensive review of multichannel models see for instance Olzak and Thomas (1986).

considered to reflect the modulation transfer function of the visual system. Modulation transfer functions of the (passive) dioptric mechanism of the eye and the (active) visual nervous system have been independently determined since (Campbell and Green, 1965; Campbell and Gubisch, 1966). Lowry and DePalma (1961) used slit photometry to scan the perceived brightness profiles of Mach bands. By dividing the Fourier transform of the luminance edge by the Fourier transform of the matching results, they obtained a modulation transfer function which agreed with a directly measured contrast sensitivity function of sinewave gratings. The dual approach, convolution of a luminance edge with the line spread function (LSF), being the Fourier transform of the CSF, was shown to generate Mach bands. In a subsequent paper (DePalma and Lowry, 1962) they tried to apply the same method in predicting detection thresholds of squarewave gratings. However, their results did not allow for a quantitative comparison between threshold curves of sinewave and squarewave gratings, may be because they did not use an artificial pupil. Campbell and Robson (1968) managed to obtain more reliable experimental results on detection thresholds of various patterns: sinewave, squarewave, sawtooth-wave and rectangular-wave gratings with varying duty cycle. Using harmonic analysis and assuming a simple peak detector mechanism, they demonstrated that the fundamental harmonic plays an important role for medium and high spatial frequencies. The deviations found for low frequencies, i.e. below 1 cpd in case of squarewave gratings and below 6 cpd in case of rectangular-wave gratings with a duty cycle of 0.1, led them to the conclusion that a number of independent and narrow-bandwidth filters (channels) governs visual perception, in stead of a single broad-bandwidth filter. This conclusion was also supported by physiologically obtained data on cat retinal ganglion cells, which became available at that time, and psychophysically confirmed by a frequency-selective threshold elevation evoked by preadaptation later on; see for instance Georgeson and Harris (1984). Campbell et al. (1969) showed that the single-channel approach was able to account for some aperiodic high-frequency patterns, thereby improving the performance of the model by introducing a peak-to-trough detection mechanism.

About the same time Davidson (1968) matched briefly flashed exponential sinewave gratings with varying spatial frequency. If extrapolated to zero contrast, these data were shown to agree with directly measured detection thresholds. His results caused Hall and Hall (1977) to propose a model that consists of a low-pass filter, cascaded by a logarithmic compression and a high-pass filter. This model provided a good approximation to Davidson's data. A similar approach was propagated by Stockham (1972), who argued the plausibility of modelling early steps in the visual processing by a logarithmic compression, followed by a high-pass filter and a saturation mechanism. This structure was supported by three observations: a logarithmic sensitivity function derived from just noticeable differences, linear filtering by neural interaction which is demonstrated by simultaneous contrast ef-

fects and the Mach-band phenomenon, and the physical limitation of saturation at high intensity levels. Applying Oppenheim's theory of homomorphic filtering to digital image processing, Stockham argued that if an image is preprocessed by logarithmic compression, low-pass filtering and exponential expansion, the overall transfer function might become very simple. Obviously, the exponential expansion of the homomorphic filter is compensated by the logarithmic compression of the visual system, and the high-pass filter of the visual system can be compensated by accurately tuning the low-pass filter. The overall transfer is thus thought to be reduceable to a logarithmic compression followed by saturation for high levels. Stockham convincingly demonstrated the useful properties of this approach by supplying some (pre)processed images.

Budrikis (1973) made an attempt in fitting Robson's and Kelly's experimental data on detection thresholds of spatiotemporal sinewave gratings. He introduced a spatiotemporal inseparable system, that consists of the difference of an excitatory and an inhibitory term, each term being separable into a product of a spatial and a temporal function. Despite all effort, he had to conclude that his best approximation of the data must be regarded as fairly qualitative.

Furukawa and Hagiwara (1978) constructed a nonlinear parametric brightness model. Assuming a Stevens' power function with an exponent of 0.5 for point targets and 0.33 for large targets, and proposing a model structure that consists of a luminance dependent point spread function (PSF) followed by a 0.5-power compression, they managed to predict data on the brightness perception of disks presented against a dark background (Hanes, 1951; Glezer, 1965; Hay and Chesters, 1972). The PSF, with a difference-of-Gaussians (DOG) profile, becomes narrower, with increasing inhibitive action, for higher luminance levels. Unfortunately, they had to conclude themselves that this model can not be made to simultaneously agree with data on suprathreshold contrast perception of gratings (Watanabe et al., 1968). Hamada (1984) changed Furukawa's model. Investigating the one dimensional analogue, and assuming also response-gradient extraction and edge determination, he managed to describe some border contrast phenomena which follow from Bergström's (e.g. 1973) research on Mach bands.

As a late example of single channel modelling, Cornsweet and Yellott (1985) introduced a new spatial summation mechanism, in which the area of a strictly positive and local, for instance Gaussian, spread function becomes narrower with increasing local luminance while its volume remains constant. This approach appears to possess some useful qualities, such as its capability to create Mach bands at edges and sombrero-shaped responses to very small stimuli. However, its predicted CSF's at different background levels and its incapability to render constant and different amplitudes within the plateaus of large stimuli (it only predicts transient phenomena at edges) are not quite satisfactory yet.

MacLeod and Rosenfeld (1974) on the one hand and Legédy (1975) on the

other made attempts of explaining the difference between the sinewave and square-wave data of Campbell and Robson without refraining to Fourier or harmonic analysis. They assumed that the visual system contains numerous DOG-shaped receptive fields of different spatial extent. The sensitivities of these fields are determined from the sinewave CSF, and a pattern is detected if any output exceeds a fixed signal level. These models approximate a continuum of channels, each with a pure band-pass PSF or LSF to be convolved with the luminance pattern, and with inclusive-OR detection between the channels. The difference between the two models consists in the way in which the channel responses are determined: MacLeod uses simple peak detection, while Legédy uses averaging over different local extremes of the convolution result. The latter author justifies this averaging process by remarking that it has been consciously considered in order to yield better predictions; without this process the fits seem to be totally unsatisfactory. This conclusion appears to be rather odd, since Jaschinski-Kruza and Cavonius (1984), who explored the performance of MacLeod's model also for low-frequency trapezoid-wave gratings, conclude that simple peak detection within channels and inclusive-OR detection between channels is sufficient. Besides, comparing Legédy's with Jaschinski's model predictions, it can not be denied that the latter are much better.

Wilson and Bergen (1979) examined a model that consists of only four channels. Two channels are represented by measured LSF's, using either sustained (quasistatic) or transient (dynamic) temporal modulation. The other two were assumed to have narrower and broader LSF's in order to account for high and low spatial frequencies. In addition, they assumed that spatial probability summation occurs within each channel and that the responses of the channels are nonlinearly summed. This means that each LSF is convolved with the luminance profile first. The response of each channel is determined by sampling its spatial response at 2.0 min. of arc intervals and nonlinear summation of the sampled values over a 8° interval by using a fourth-power summation rule. The overall response is computed by also applying a 4th-power summation rule to the individual channel responses. This model appears to predict sustained and transient CSF's of sinewave gratings. Moreover, it was shown to predict detection thresholds of other stimulus patterns, amongst others squarewave gratings (Bergen et al., 1979). By assigning a nonlinear amplitude transfer function, derived from contrast increment thresholds, to each channel, the model was even shown to provide reasonable predictions for the suprathreshold contrast perception of Gabor-sinewave patterns (Swanson et al., 1984).

Review and Scope

The multichannel models discussed above have a similar structure. In the first linear step, the luminance profile of a stimulus is convolved with the LSF's of all channels. The second step consists of determining the channel outputs from the spatial response patterns. This can be done by using a simple peak detection mechanism² (MacLeod, Jaschinski), averaging over different extremes (Legédy) or by probability summation (Wilson). In a final step the overall output is computed by assuming either inclusive-OR detection between channel outputs (MacLeod, Legédy, Jaschinski), or nonlinear response pooling (Wilson).

Nonlinear response pooling between channel outputs, for instance by applying Quick's (1974) 4th-power summation rule or 'pythagorean' summation as used by Koenderink and van Doorn (1978, 1982), provides an intermediate condition between linear summation on the one hand and inclusive-OR detection on the other. Its influence on the performance of a model can be studied by regarding the extreme cases. Modelling by curve fitting, i.e. by adjusting model parameters to fit one curve and to predict other ones, is a method of examining the necessity of nonlinear summation. A related problem is the choice of the number of required channels. Multichannel models are commonly assumed to contain LSF's with relatively narrow-bandwidth amplitude transfer functions to sinewave gratings. In order to obtain a smooth fit to a broad-bandwidth CSF, it follows that inclusive-OR detection requires many channels which are slightly shifted in the frequency domain. As a consequence, the amplitude transfer functions of these channels must have a considerable overlap. Linear summation on the other hand requires fewer channels with less overlap. It should be emphasized that linear summation at the output does not necessarily mean a linear model. A model that consists of linear channels, linear summation of the local responses followed by peak detection is, at least for sinewave gratings, completely equivalent to a model consisting of linear convolution, peak detection within channels and linear summation of the peak values. The first one is linear and can be replaced by a linear single channel model. A comparison between the detection threshold curves of sinewave gratings and disks shows that the channels must contain some nonlinearity, such as the peak detection mechanism in the second model. Other nonlinearities can be considered, not only in case of linear summation at the output but also in case of inclusive-OR detection. Simple alternatives are the difference between the maximum and minimum (peak-to-trough) value of the spatial responses of each channel, such as applied in the single-channel approach of Campbell et al. (1969), or averaging over different extremes (Legédy). Spatial probability summation is, in view of the

²More precise: probability summation is not explicitly but implicitly included in these models. Predictions remain valid if probability summation affects channel responses to sinewave gratings and other gratings in the same way.

additional free parameters, more complicated. However, these parameters might provide a means of adjusting the model to fit data on quite different stimulus types simultaneously. Besides, the importance of probability summation as a simulation of the internal noise in the visual system, which is thought to cause the gradual shape of psychometric functions and for this reason propagated by Wilson among others, can not be denied.

The objective of the subsequent sections is to achieve insight in the potentials of a few alternative multiple channel models, meanwhile keeping them as simple as possible. A straightforward approach is regarding the visual system as a nonlinear optical system, which maps luminance patterns into some two-dimensional perceived plane. This might for instance lead to a model consisting of point spread functions which resemble pure band-pass filters in the frequency domain, in combination with nonlinear amplitude transfer functions and (non)linear summation of the spatial responses at the output. Such a structure, which is based on 'sampling' the retinal image by receptive fields and backprojection by summation of the nonlinearly amplified receptive field profiles, can not satisfy the brightness perception of disks and gratings simultaneously (see chapter 5). This means that suprathreshold perception requires a more complicated model structure. Vision at threshold level is perhaps easier, since it only requests the exceeding of some fixed output level, somewhere in the visual field, and the familiar multichannel model structure as mentioned above can be studied. The incorporation of amplitude asymmetry (see chapter 6) in high-frequency channels and the modelling of suprathreshold perception (chapter 5) are complications that have been laid aside for the moment.

8.2 Simple Nonlinear Multichannel Detection Models

In order to handle one- and two-dimensional stimulus patterns simultaneously, it is convenient to assume radially symmetric point spread functions (PSF's). Disks can be easily convolved with these profiles. Application of the Abel transform to the PSF's (e.g. Bracewell, 1978) renders the corresponding line spread functions (LSF's) and enables one-dimensional convolution with gratings. Convolution of radially symmetric gratings with DOG-shaped PSF's shows a deviant behaviour in the centre. For the sake of simplicity the response in the centre is neglected and the one-dimensional approximation is applied; see chapters 6 and 7. The channel characteristics proposed and the narrowest or highest-frequency channel derived in the appendix of chapter 6 will be applied throughout the subsequent study.

The most simple model structures are shown in Fig. 1. Inclusive-OR detection means that a pattern is detected whenever at least one of the channel responses exceeds a fixed threshold level. This can be realized by assuming fixed channel sensitivities and adjusting threshold levels, or by assuming fixed threshold levels

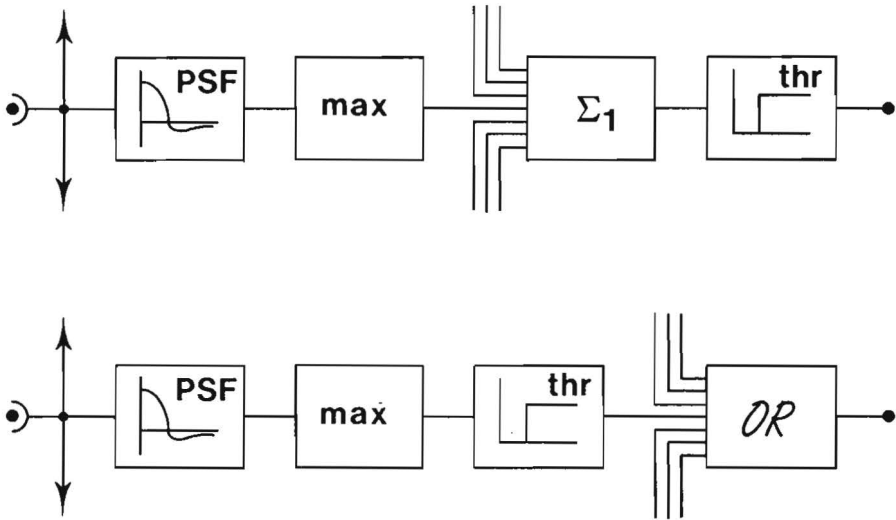


Figure 1: Two simple multichannel model structures based on maximum detection within channels. Linear summation of channel responses (top) and inclusive-OR detection (bottom) can be assumed.

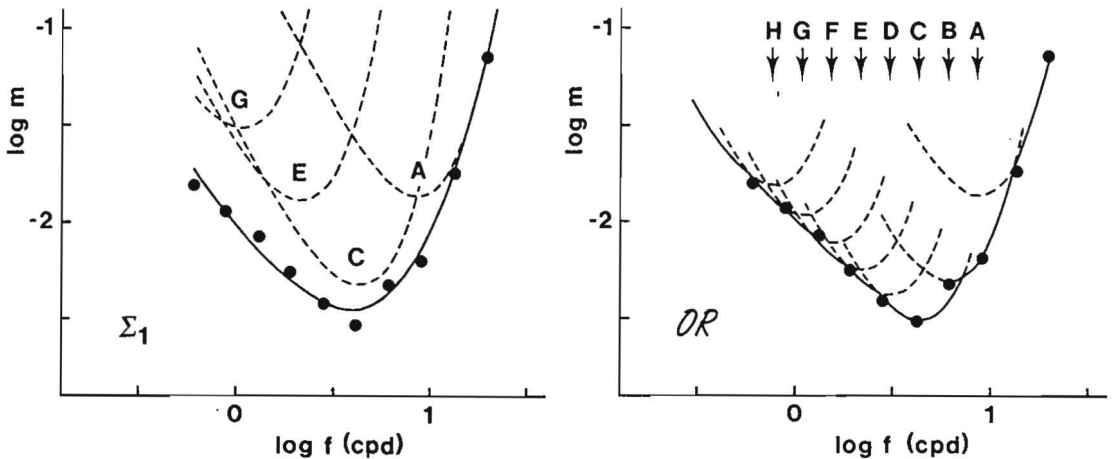


Figure 2: Measured modulation thresholds of radially symmetric cosine gratings (solid circles) approximated by the models (solid curves) shown in Fig. 1. Linear summation was applied by using 4 channels (left panel), while inclusive-OR detection was approximated by using 8 channels (right panel). This was accomplished by assuming additional channels B, D, F and H. Predictions of the individual channels, by neglecting contributions of other channels, have been drawn dashed in order to illustrate the approximation process.

and different channel sensitivities. Linear summation, abbreviated by Σ_1 , means that the sum of all individual channel outputs has to exceed a fixed value. Maximum (peak) response evaluation is referred to in Fig. 1, but the difference between maximum and minimum (peak-to-trough) will be considered also. This makes no difference for the prediction of detection thresholds for amplitude-symmetric patterns, such as sinewave, squarewave and trapezoid-wave gratings, but results in different responses for disks and single-phase gratings. Fig. 2 shows modulation thresholds of radially symmetric cosine gratings along with model approximations. In the linear summation model four channels, with modulation transfer functions one octave apart (0.3 units in the log frequency domain), were sufficient. The scaling constant between the PSF's of channels A, C, E and G equals therefore 2. Inclusive-OR detection means that a curve is fitted by the envelope of the channel responses. This is approximated by using eight channels, 0.15 units apart in the log frequency domain, in stead of using a continuum of channels. This is accomplished by assuming additional channels B, D, F and H, such that the scaling constant between the PSF's of channels A, B, C, D etc. equals $\sqrt{2}$. Obviously, both these models give comparable and adequate fits to these measured data.

It should be emphasized that all succeeding model predictions for detection thresholds of other spatial patterns are based on the model approximations given in Fig. 2. This means that, in all cases, models are accurately fitted to these data and the simultaneous predictions, with no free parameters except for Fig. 13, in case of other patterns are examined.

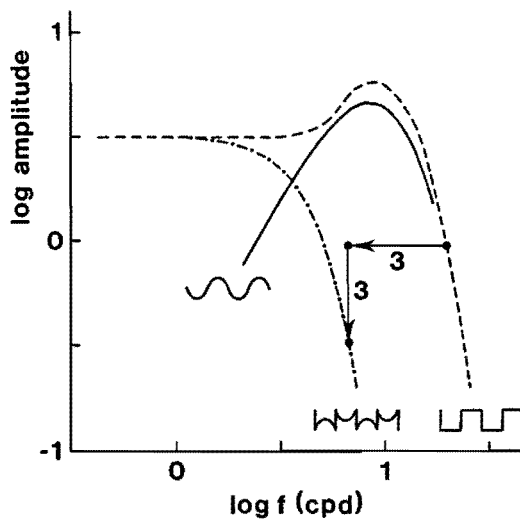


Figure 3: The response of the narrowest channel (labelled A in Fig. 2) to normalized sinewave gratings (solid curve), squarewave gratings (dashed) and to square-wave gratings with missing fundamental (dash-dotted). High-frequency flanks appear horizontally and vertically shifted over 0.48 log units, a factor of 3.

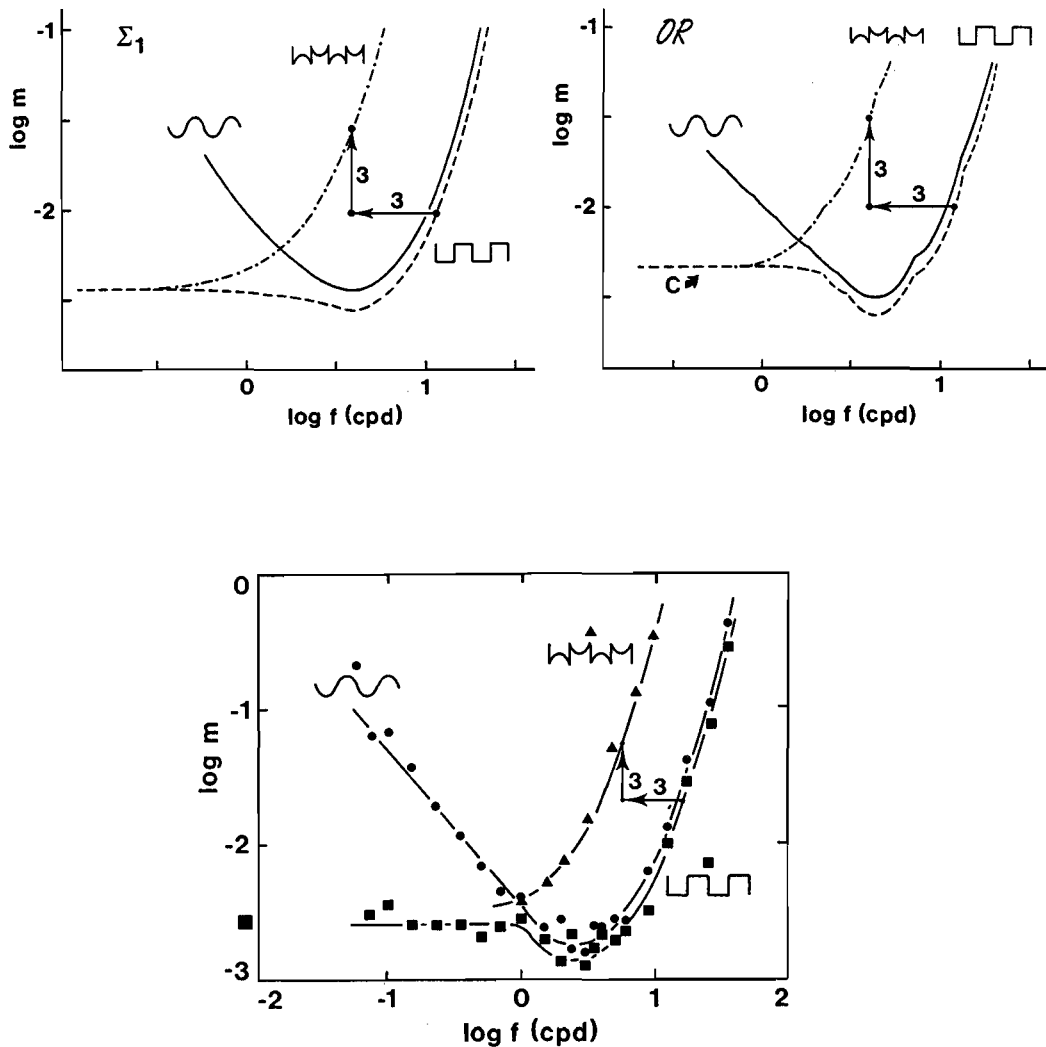


Figure 4: Top panels: Multichannel model predictions for detection thresholds of squarewave gratings (dashed) and squarewave gratings with missing fundamental (dash-dotted). Left panel: linear summation. Right panel: inclusive-OR detection, where detection at low frequencies is governed by channel C only. Bottom panel: Measured detection thresholds for these patterns, adapted from Campbell et al. (1978).

The question arises whether existing data on other periodic stimulus patterns would allow for a quantitative choice between the two models. Convolving a squarewave grating and a squarewave grating with missing fundamental with the PSF or LSF of the narrowest channel, we obtain the amplitude responses given in Fig. 3. These curves, which demonstrate that the responses of a single channel already reflect most properties of measured detection thresholds in question (Campbell et al., 1978), agree with the results of similar computations performed with using different PSF's or LSF's (MacLeod et al., 1974; Legéndy, 1975). Measured data and multichannel model predictions are presented in Fig. 4. Again, both models appear to render comparable predictions, the only difference being the more or less pronounced dip in the predicted curves for squarewave gratings. The question thus shifts towards the significance of this dip with respect to the experimental error. The data supplied by Campbell et al. (1978) do not show a clear dip, while those supplied by Campbell and Robson (1968) do. Since these data are obtained at backgrounds of 15 and 500 cd.m^{-2} respectively, we may conclude that inclusive-OR detection is to be preferred (if the significance of this dip depends on the background level instead of being an experimental artefact; recall that the predictions given in the top panels of Fig. 4 are based on detection thresholds measured against a 300 cd.m^{-2} background as given in Fig. 2). Anyhow, this examination of two extreme cases of nonlinear summation of channel outputs demonstrates that data on sinewave and squarewave gratings can be simultaneously fitted by accurately adjusting the summation exponent at the output of a multichannel model.

A similar observation holds for trapezoid-wave gratings of different ramp widths, see Figs. 5 and 6. The amplitude responses of a single channel reflect the behaviour of measured data (Campbell et al., 1981), and so do the multichannel predictions. The vertical shift of the curves at high spatial frequencies agrees with the ratios of the amplitudes of the fundamental Fourier components. The unit-sloping curves at low frequencies are shifted 0.3 log units if the ramp width is doubled or halved, which brought Campbell et al. (1981) to propose an additional contrast-gradient detection mechanism for ramp widths above 0.5 degrees. Note that only predictions based on linear summation have been computed here; these are presented in the top panels of Fig. 6. Inclusive-OR detection was considered by Jaschinski-Kruza and Cavonius (1984). Their predictions, together with measured data, are presented in the bottom panels of Fig. 6. In conclusion, a choice between the two models is not accomplished by regarding the low- and high-frequency data on trapezoid-wave gratings, since both predict the same behaviour.

The performance of the two models can also be studied by considering our data on detection thresholds of radially symmetric single-phase cosine gratings. The partly asymmetrical response of the narrowest channel to such a pattern was presented in chapter 6. The incorporation of this asymmetry in the models, by

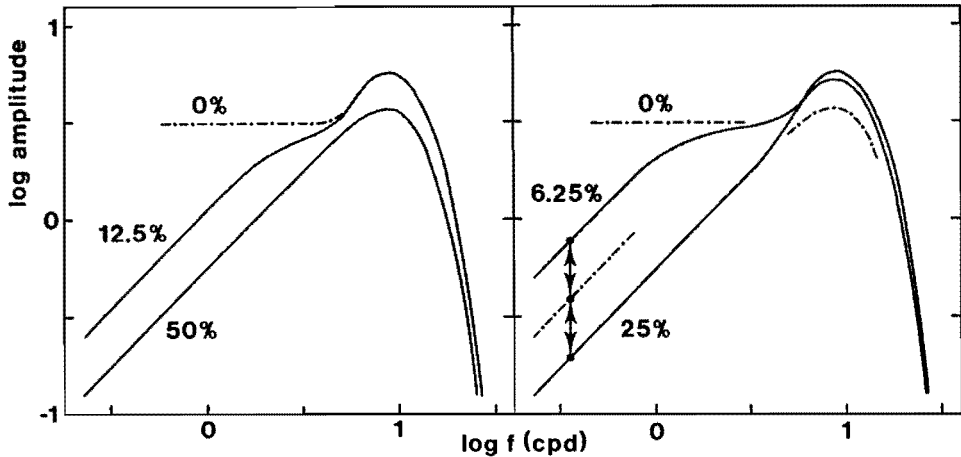


Figure 5: Amplitude responses of the narrowest channel to normalized trapezoid-wave gratings with different ramp widths (0% = square and 100% = triangular). Responses for different ramp widths are given in separated panels to avoid clutter, while parts of the left panel are duplicated in the right panel for comparison (dash-dotted). The unit-sloping asymptotes of low-frequency 25% and 50% gratings coincide. Arrows indicate a difference of 0.3 log unit.

considering not only peak detection but also the difference between maximum and minimum (peak-to-trough value) for each channel, implies four possible combinations: linear summation and inclusive-OR detection, each with peak detection and with peak-to-trough detection within channels. These four predictions are shown in Fig. 7. From Fig. 7 we must conclude that inclusive-OR detection is slightly better, and that inclusive-OR detection on the basis of the peak-to-trough responses is best.

Yet, the ultimate test of the models would be a correct prediction of detection thresholds of aperiodic stimuli, e.g. disks. Convolution of disks of different diameters with the PSF of the narrowest channel, we obtain different response profiles. The response values in the centre reflect a 'band-pass' behaviour, i.e. the centre response becomes zero for large disk diameters, see Fig. 8. As in the frequency domain, this is a consequence of the pure band-pass PSF. The maximum of the response, which is located at the inner edge, shows an asymptotic value for large disks which is smaller than the response for the optimum diameter. The peak-to-trough response curve has a similar appearance. Model predictions of detection thresholds of disks are shown in Fig. 9. None of these predictions confirms the required behaviour for large stimuli, although linear summation on the basis of peak-to-trough detection (bottom left panel) approximates a monotonously decreasing threshold curve best. Furthermore, all predictions have in common that the predicted threshold values are too low when compared to the measured data.

This is noteworthy. The lowest measured detection threshold of disks is about

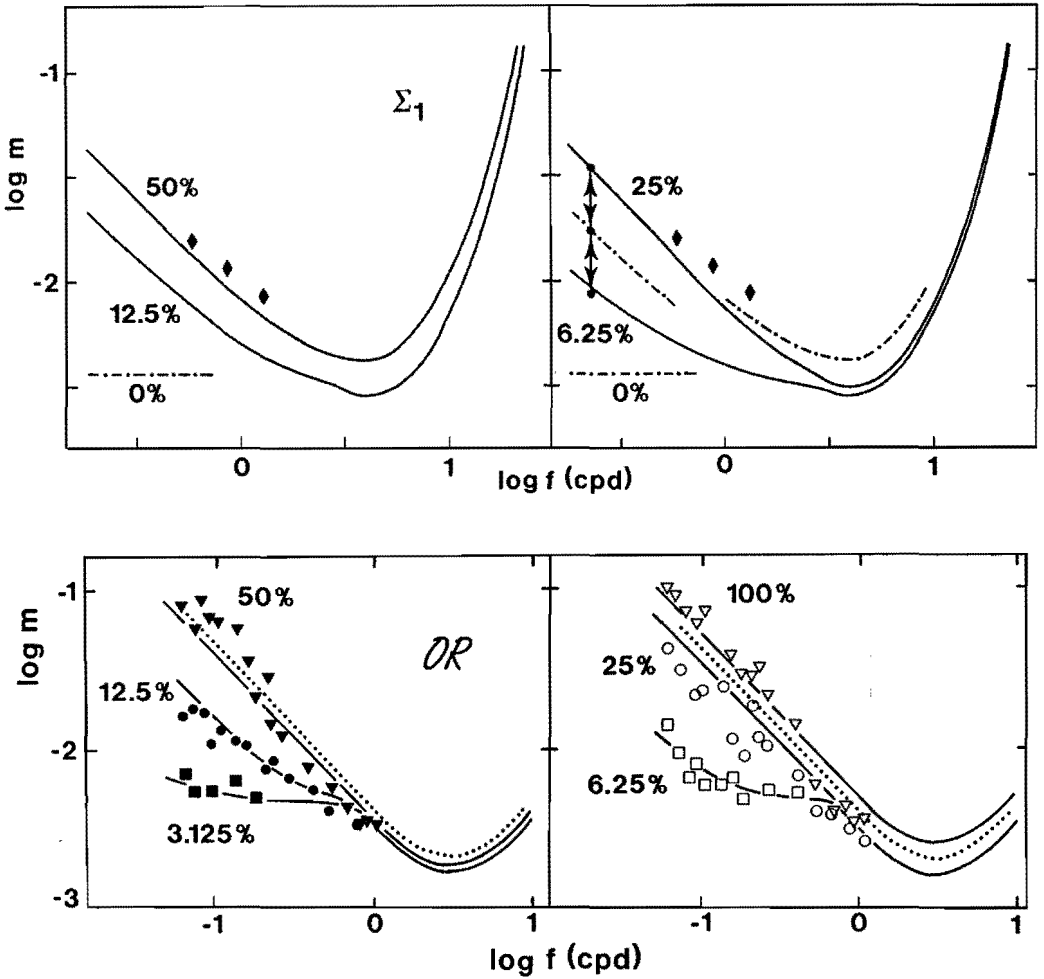


Figure 6: Upper panels: Multichannel model predictions of detection thresholds for trapezoid-wave gratings based on linear summation of channel outputs. Solid diamonds reflect measured detection thresholds of radially symmetric cosine gratings. Bottom panels: Predictions in case of inclusive-OR detection, taken from Jaschinski-Kruza et al. (1984), together with measured data from Campbell et al. (1981); the model was, as for our computations, adjusted to fit detection thresholds of sinewave gratings (dotted curve).

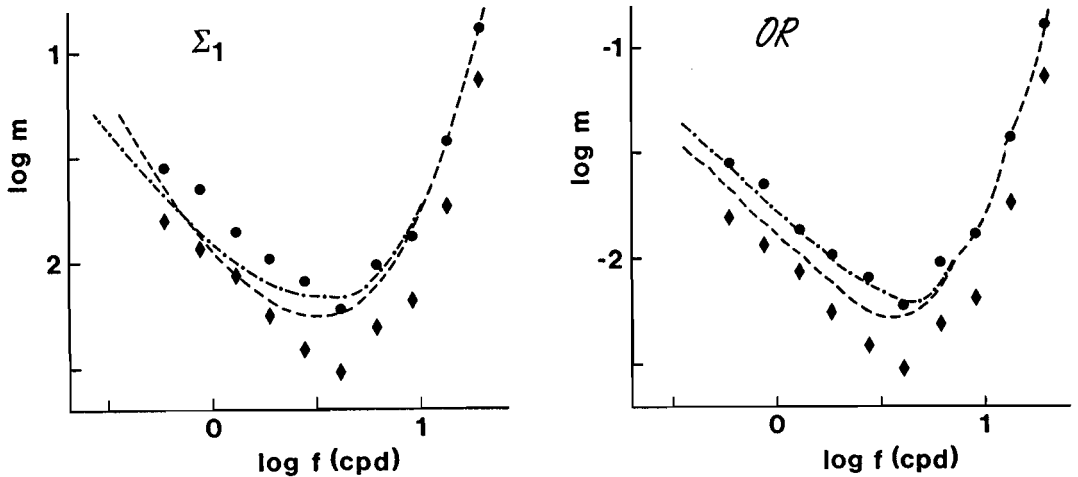


Figure 7: Multichannel model predictions for detection thresholds of radially symmetric single-phase cosine gratings. Linear summation (left panel) and inclusive-OR detection (right panel) were considered with peak detection (dashed) and with peak-to-trough detection (dash-dotted) within channels. Measured data points concern full cosine gratings (solid diamonds) and single-phase gratings (solid circles).

10 cd.m^{-2} (Fig. 9), while the minimum threshold amplitude of cosine gratings is about 1 cd.m^{-2} (Fig. 2). This means that the maximum sensitivity for disks and radially symmetric cosine gratings, both quasistatically presented against a 300 cd.m^{-2} background and measured within one subject who used a 2 mm artificial pupil, differ by 1 log unit. On the other hand, comparing Figs. 3 and 8, the maximum responses of the narrowest channel to normalized sinewave gratings and normalized disks appear to be exactly the same. Consequently, the maximum responses of the broader channels to these patterns will be the same, since they equal those of the narrowest one but for a scaling factor.

A further analysis showed that the introduction of a 3.3 degree window of the grating patterns, which corresponds to the viewing window actually used in the detection experiments, by also considering deviant responses in the centre of radially symmetric cosine gratings and transient phenomena at the edge of this window (see Campbell et al., 1969), can not provide a solution to this problem.

Despite fair predictions for grating stimuli, we must conclude that some other process should be incorporated into the models to explain the disk data. Nonlinear pooling of channel outputs can not provide a solution since both extreme models display the same tendencies. This other process should accomplish two effects. If inclusive-OR detection is assumed, the amplitude response of a single channel to disk-shaped stimuli must increase monotonously with the disk diameter and be independent from the diameter for large disks (a 'low-pass' type response curve).

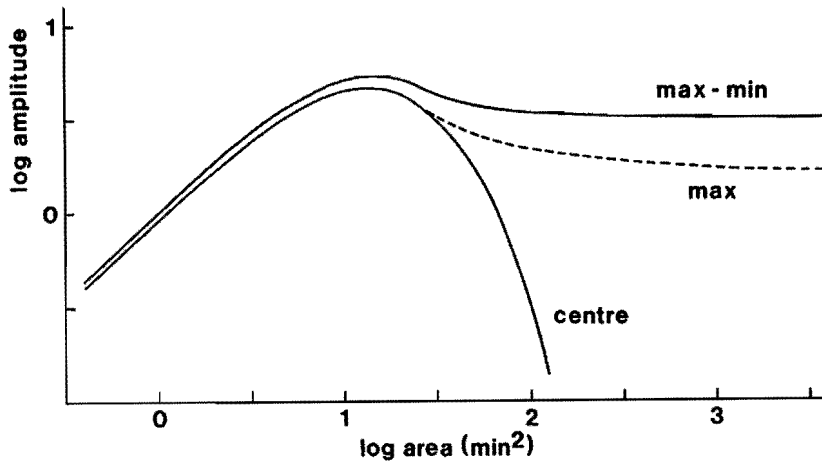


Figure 8: Amplitude responses of the narrowest channel to normalized disks with varying diameter.

In case of linear summation, this response should be somewhat flatter if compared to the maximum-minus-minimum response curve shown in Fig. 8. The second effect should reveal an overall compensation for the predicted curves of Fig. 9. This means that the amplitude response curve of any channel to disks must be relatively lowered with respect to its amplitude response curve to gratings. These two effects may be achieved by local probability summation within channels.

8.3 Local Probability Summation within Channels

Figure 10 shows the general model structure if local probability summation within channels is included. As was done in the foregoing section, only the two extreme cases of response pooling at the output will be considered here: linear summation ($q=1$) and inclusive-OR detection ($q \uparrow \infty$). A luminance pattern is convolved with the PSF of a channel in stage 1. Local probability summation is performed in stages 2-4. In stage 2 the absolute value of the spatial response is raised to the p -th power. In stage 3 the spatial response is locally averaged by sampling over a regular and rectangular grid, the sampled values being integrated over a certain window. This stage can therefore be regarded as an extra low-pass filtering: convolution with a rectangular array of Dirac pulses which is bounded by a circular window. The next two steps consist of taking the p -th root of the spatial response and the determination of the maximum. This model structure agrees with those assumed by Mostafavi et al. (1976) and Wilson et al. (1979), be it that the inhomogeneous retinal sensitivity has been neglected (Mostafavi) and that probability summation is computed over a circularly limited area, instead of over large areas which correspond to the viewing windows used in detection experiments

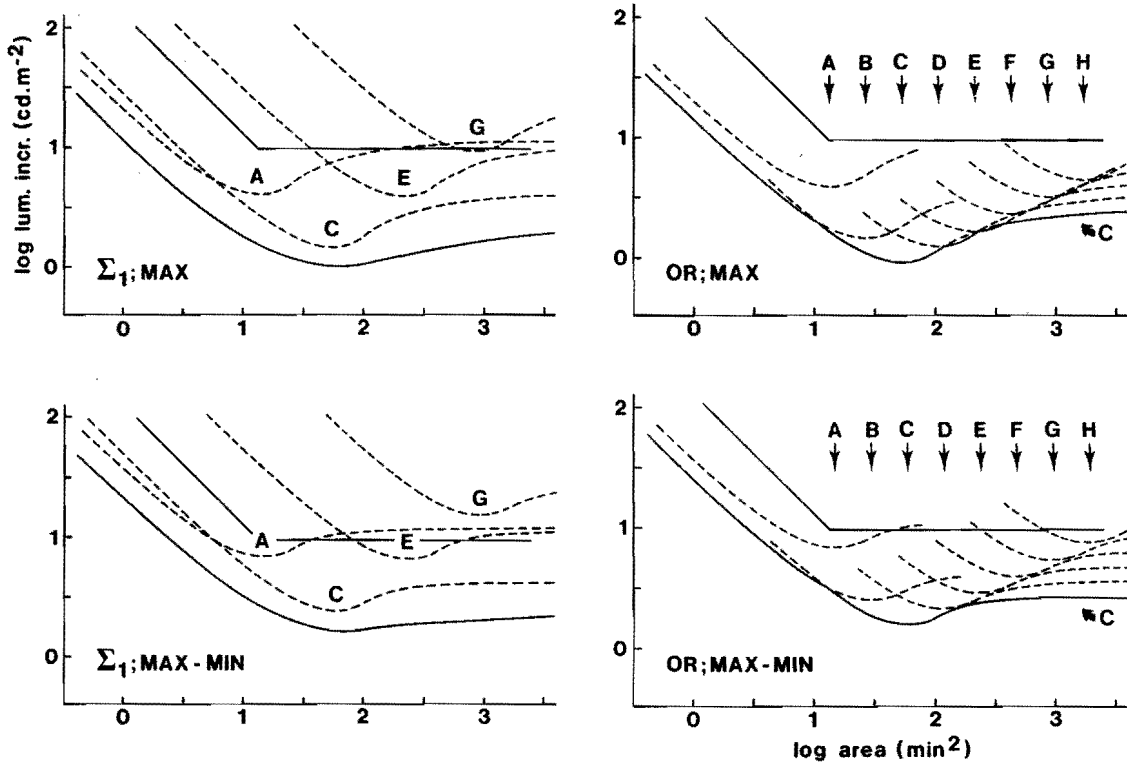


Figure 9: Multichannel model predictions for detection thresholds of disks (lowest solid curves). Left panels: linear summation. Right panels: inclusive-OR detection. Top panels: maximum (peak) responses. Bottom panels: maximum-minus-minimum (peak-to-trough) responses. Straight lines are measured asymptotes of small and large incremental disks. Assuming inclusive-OR detection, it follows that detection of large disks is always governed by channel C.

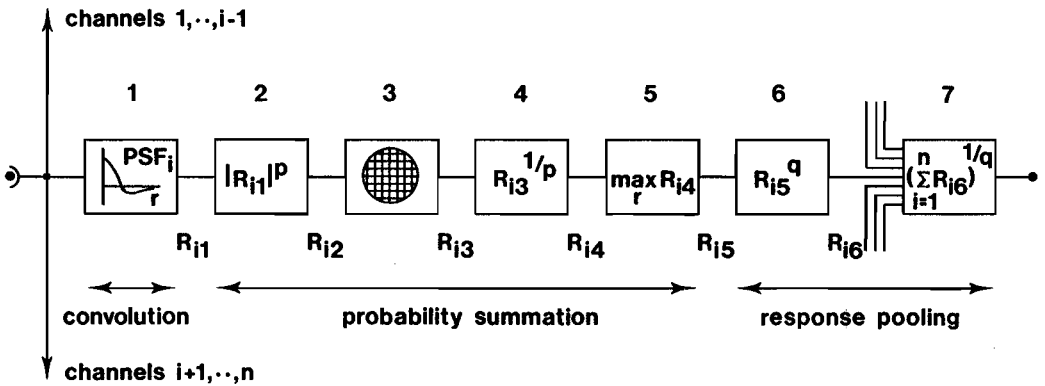


Figure 10: Multichannel model structure with local probability summation included in each channel. Channels are renamed $1, \dots, n$ for convenience. See text for explanation.

(8 degrees horizontally by Wilson, 2×2 degrees by Mostafavi). The parameters of the local probability summation mechanism are not necessarily required to be invariant across channels. Recall that the initial linear stage of a channel is described by a space-invariant PSF, enabling global convolution in stead of local correlation with sensitivity profiles representing receptive fields. Sampling the spatial response over a regular grid means approximating a discrete distribution of receptive fields with similar sensitivity profiles, while local summation between neighbouring receptive fields is accomplished by nonlinear integration within the window. If the mesh size and window are related to the spatial extent of the PSF's of the channels, the overall model structure will resemble the hierarchically organized stack structure as advocated by Koenderink and van Doorn (1978 and 1982), while possible advantages of a recursive neuronal circuitry describing the channel-dependent spatial resolution may be preserved (Hartmann, 1982).

There are three degrees of freedom: the exponent p in stages 2 and 4, the density of the grid and the diameter of the window in stage 3. The grid density and window diameter were expected to have a similar influence on the probability summation result. After a few introductory response computations the density was adjusted to 1.0 min. of arc for the narrowest channel. This means that the spatial response is sampled fairly densely, and variations around this value affect responses to disks and gratings in the same way; see also Wilson et al. (1979). In order to further facilitate modelling, the grid was linearly magnified for the successive broader channels. Since the PSF's of the channels were chosen to be equidistant in the scale space, the same scale constant (2 or $\sqrt{2}$) was applied to the grid density and the window diameter. The important benefit of this procedure is that the amplitude response curves of the narrowest channel can be used for

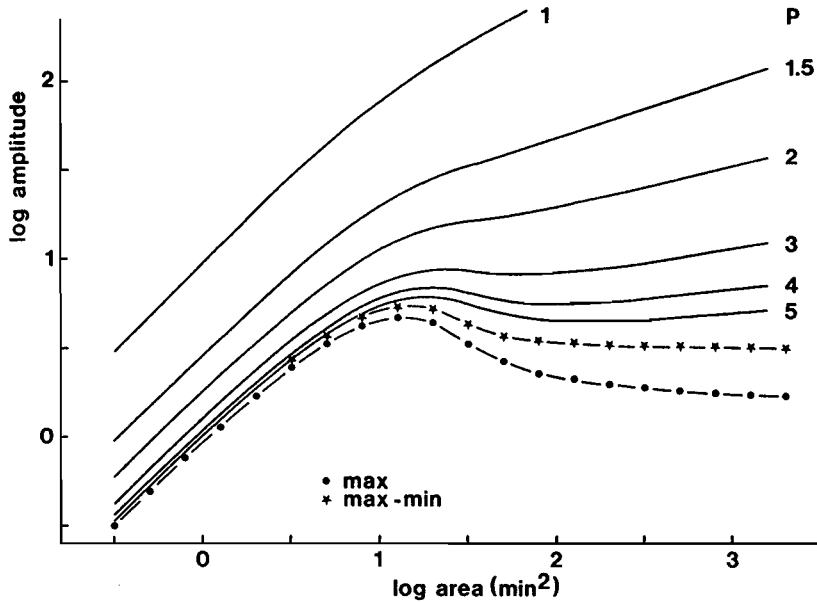


Figure 11: Influence of the probability summation exponent p to the response of the narrowest channel to normalized disks. The diameter of the integrating area is assumed large if compared to the largest disk (nonlinear integration over the entire spatial response). The solid star and solid circle curves are reproduced from Fig. 9.

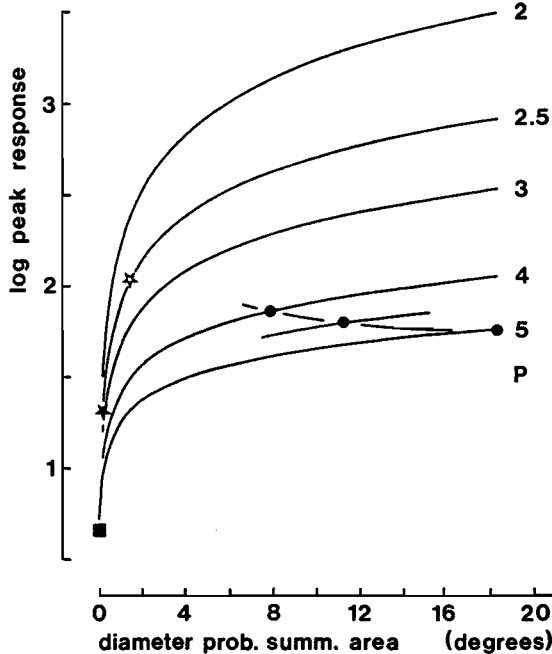


Figure 12: The peak response of the narrowest channel to a normalized 8.5 cpd sinuswave grating, for different values of the probability summation exponent p , as a function of the diameter of the integrating area. The peak response without probability summation is indicated by the solid-square symbol. Solid circles on the $p = 4, 4.5$ and 5 curves indicate necessary choices in case of linear summation,

all channels, if the appropriate scaling factors are considered (isomorphism and equidistant translation of the respective response curves of the narrowest channel in log-log coordinates; see for instance Blommaert and Roufs, 1981).

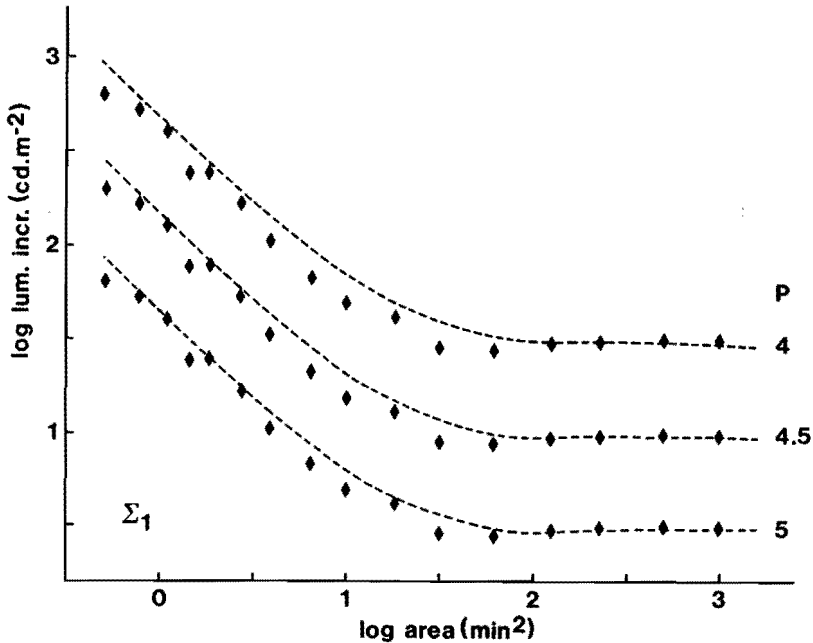


Figure 13: Multichannel model predictions for detection thresholds of disks (dashed curves). Linear summation of channel outputs is assumed and the diameters of the probability summation area of the narrowest channel correspond to the solid-circle symbols in Fig. 12. Curves for $p=4$ and $p=5$ have been shifted over 0.5 log unit to avoid overlap. Solid diamond symbols are (shifted) measured data on incremental disks.

It was concluded before that linear summation at the output requires a flattening of the response curve to disks. Fig. 11 shows the influence of probability summation for different values of the exponent p . The window diameter of the sampling grid was assumed to be much larger than the largest disk (about 1 degree for the narrowest channel A, 2 degrees for channel C, and so on). This means nonlinear integration over the entire (sampled) spatial response. Varying the exponent p between values of 4 and 5 renders suitable curves. The same nonlinear process must be applied to sinewave gratings. It turned out that the shape of the amplitude response curve remains unchanged if the probability summation exponent and the diameter of the integrating area are varied; the only difference is vertical translation of the entire curve. Fig. 12 gives therefore the maximum of the amplitude response of the narrowest channel. This maximum or peak response occurs for a frequency of 8.5 cpd. Both the exponent p and the diameter of the

window affect the peak response.

Multichannel predictions of detection thresholds of disks, which are based on linear summation, are presented in Fig. 13. These predictions appear to be quite reasonable, and $p=5$ proved to be optimal, although a somewhat larger p might also provide a good prediction. However, in order to obtain a correct vertical position, the window diameter had to be adjusted to 18 degrees in case of the narrowest channel instead of 3.3 degrees actually used (data from Fig. 12). Accordingly, the predictions given by the dashed curves in Fig. 13 should be lowered by at least 0.3 log units relative to the measured data.

The other alternative, inclusive-OR detection, requires a monotoneously increasing amplitude response of each channel to small and intermediate sized disks and a constant amplitude to large ones. Fig. 14 shows some examples achieved by varying the exponent p as well as the diameter of the probability summation area. From Fig. 14 it follows that $p=2.5$ and a diameter of the probability summation area of 10.0 min. of arc (10' for channel A, $10\sqrt{2}$ ' for channel B, 20' for channel C etc.) is about the best choice, i.e. renders a constant response for large disks. The solid-star symbol in Fig. 12 indicates the corresponding peak value for sinewave gratings. However, the model prediction shown in Fig. 15 (the dashed curves) remains much too low, about 0.75 log units for large disks. Even if an additional shift of all channel sensitivities is considered, which would introduce an error in the model fit to thresholds of sinewave gratings of course, but such that the prediction for large disks agrees with the measured data (see the dash-dotted curves in Fig. 15; the open-star symbol in Fig. 12) there remains a deviation for small disks. As in case of linear summation, the prediction of disk thresholds appears not quite satisfactory, although correctly shaped threshold curves have been obtained.

The dotted curve in Fig. 15 was included in order to illustrate that a single band-pass channel of narrow bandwidth could be used to model detection thresholds of disks, provided that probability summation is assumed. This is merely done to prove that fitting such a single curve, either by a linear low-pass Gaussian filter (see chapter 6) or a by a single band-pass DOG filter in combination with probability summation, would also do. The prediction of detection thresholds of sinewave gratings, which corresponds to the single channel fit according to the dotted curve in Fig. 15, would be absurd.

The left panel of Fig. 16 gives responses of the narrowest channel to single-phase rectified cosine gratings for the two probability summation alternatives considered for disks and full-wave cosine gratings. It can be observed that probability summation hardly affects the shape of the response curve. The only significant influence is a vertical translation of the entire curve. Multichannel threshold predictions for this stimulus type are shown in the right panel of Fig. 16. In contrast to the multichannel predictions for disks, the prediction on the basis of inclusive-

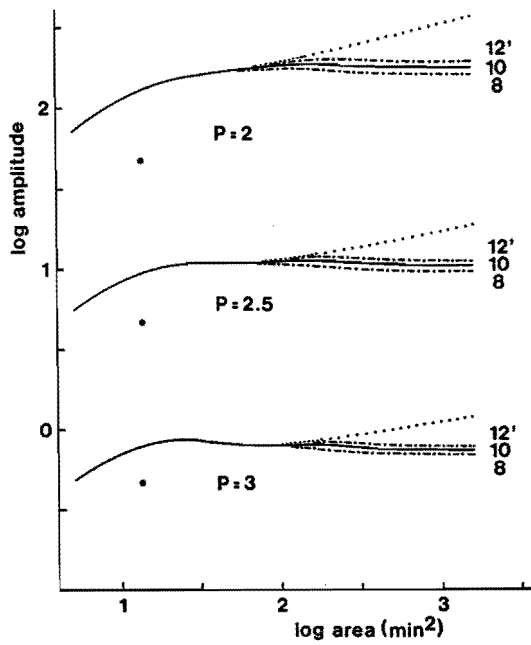


Figure 14: Influence of varying the probability summation exponent p and the diameter of the probability summation area (in min. of arc) upon the response of the narrowest channel to medium and large sized normalized disks. Curves for $p=2$ and $p=3$ have been shifted $+1$ and -1 log unit for clarity. Solid circles indicate the (shifted) maximum of the response without probability summation. Dotted curves denote responses for large probability summation windows.

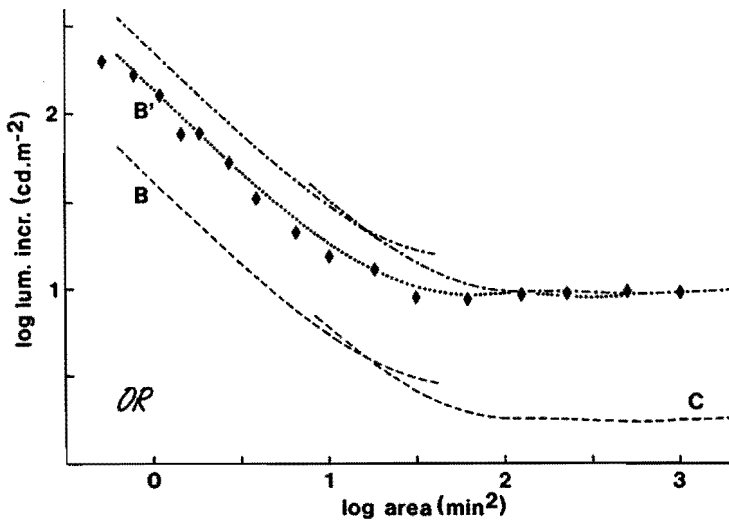


Figure 15: Multichannel model prediction for disk thresholds by assuming inclusive-OR detection, $p=2.5$ and a diameter of the probability summation area of 10 min. of arc in diameter for channel A. Only channels B and C appear to be relevant (dashed curves). Measured detection thresholds of incremental disks are given by solid diamonds. Dash-dotted curves were obtained by applying an additional shift (open star in Fig. 12), while the dotted curve equals the vertically shifted prediction of channel B only. See text for details.

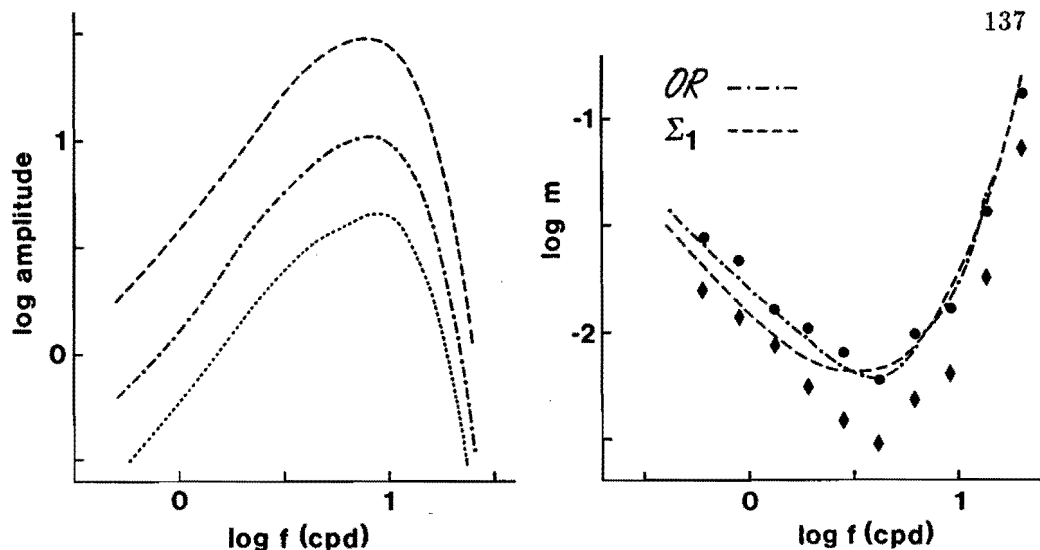


Figure 16: Left panel: Responses of the narrowest channel to single-phase rectified sinewave gratings. Dashed curve: $p=5$ and diameter of probability summation window 18 degrees. Dash-dotted curve: $p=2.5$ and window of 10 min. of arc. The peak-to-trough response without probability summation is shown dotted for comparison. Right panel: Multichannel model predictions for detection thresholds of single-phase gratings. Dashed curve: linear summation, $p=5$ and window of 18 degrees. Dash-dotted curve: inclusive-OR detection, $p=2.5$ and window of 10 min. of arc. Solid symbols are measured values for radially symmetric full-cosine gratings (diamonds) and for single-phase gratings (circles).

OR detection with an exponent $p=2.5$ and a diameter of the summation window of 10 min. of arc for the narrowest channel is quite accurate. The new model predictions with probability summation included are comparable to those given in Fig. 7, which means that the effect of probability summation is largely approximated by taking the peak-to-trough responses of the channels.

The prediction of detection thresholds of more complex aperiodic patterns, e.g. noise gratings, may also raise problems. Because of their stochastic nature, the ensemble mean over repeated response determinations, each with the same spectral distribution of the stimuli, has to be considered (see also chapter 7). Fig. 17 shows such ensemble means of the responses of the narrowest channel to these patterns. Note that somewhat different probability-summation parameters have been used in Fig. 17; this was merely done to yield response curves which do not overlap. Probability summation results in a flattening of the response curves, the vertical position of the curves particularly being affected. Corresponding multichannel predictions, viz. being based on ensemble means as illustrated in Fig. 17, are presented in Fig. 18. The shown tendency is clear: measured as well as predicted curves are flattening with increasing bandwidth, and the minimum \hat{m}

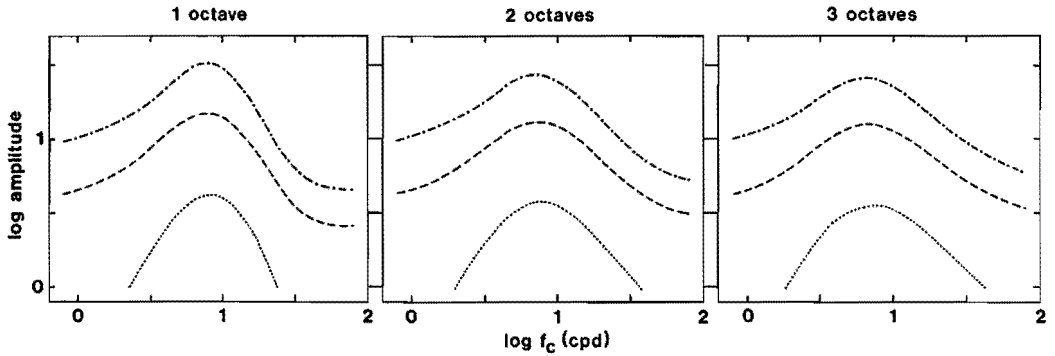


Figure 17: Influence of probability summation on the amplitude response of the narrowest channel to normalized noise gratings. Curves are the ensemble means of 25 computations. Dash-dotted curves: $p=2$ and diameter of probability summation window 10 min. of arc. Dashed curves: $p=5$ and window of 1 degree. Dotted curves: peak responses without probability summation.

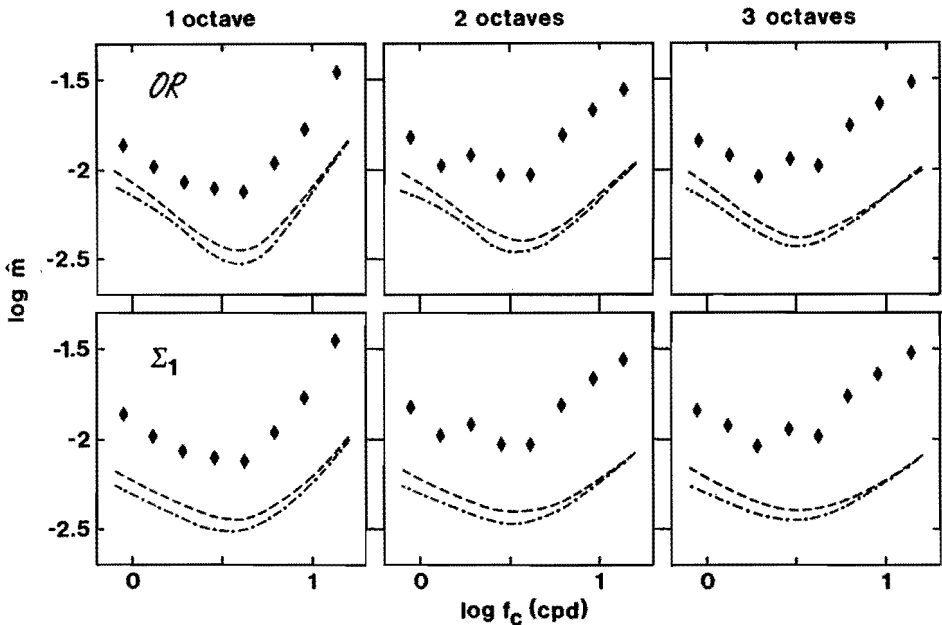


Figure 18: Multichannel model predictions for detection thresholds of noise gratings, which are based upon the ensemble means of the channel responses as illustrated in Fig. 17. Top panels: inclusive-OR detection. Bottom panels: linear summation. Dash-dotted curves: $p=2.5$ and window of 10 min. of arc. Dashed curves: $p=5$ and window of 18 degrees. Solid diamonds are measured values.

slightly increases. But all predictions are significantly below the measured data. This difference is hardly influenced by the choice of the probability-summation parameters: predictions based on linear summation and inclusive-OR detection, both with using the same parameters, display the same tendency.

8.4 Discussion

Simple multichannel models, i.e. those without explicitly assuming spatial probability summation and that on the basis of inclusive-OR detection in particular, enable an excellent fit to the detection threshold curve of sinewave gratings and good predictions of detection thresholds of other gratings. Their predictions of detection thresholds of disk shaped stimuli showed that, even in case of peak-to-trough response evaluation within channels, some other nonlinear process is to be involved. As a first variant local probability summation was incorporated into the channels. This means local nonlinear summation of the spatial response of a channel within a circular window, thereby assuming scaling constants of the channel-dependent summation mechanisms which equal those of the PSF's. This process provides additional and necessary degrees of freedom or parameters for fitting and predicting detection thresholds of quite different types of stimulus patterns. The probability summation parameters, viz. being the nonlinear summation exponent and the diameter of the summation area, can be estimated on the basis of curve-fitting procedures: exactly fitting detection thresholds of sinewave gratings, the linear summation and the inclusive-OR detection models were both shown to be able to predict a 'low-pass' type threshold curve of disks. Moreover, the inclusive-OR model provided an excellent prediction of detection thresholds of single-phase rectified gratings and both models rendered correctly shaped threshold curves of noise gratings.

The choices for the probability summation exponent p , obtained on the basis of curve-fitting procedures, are close to already published values. Mostafavi and Sakrison (1976) also used curve-fitting procedures, thereby assuming that only a single channel governs detection of their noise patterns (independent channels with a summation exponent between channels of $q \uparrow \infty$). Their own data were fitted best for $p = 6 \pm 0.5$, while their predictions of Robson's data on the influence of grating width suggested a value of $p \approx 3.5$. However, most of their data were rather insensitive for values of p between 1 and 16. Watson (1982b) found that subliminal summation of local compound grating patterns depends on the frequency difference: from linear summation to summation with an exponent of about 4 for frequencies more than one octave apart. Wilson and Bergen (1979) used $p = q = 4$, but this is merely the average of values determined by considering the steepness of psychometric functions, which showed extreme values of 2.9 and 5.6. Nachmias (1981) demonstrated that this steepness depends on the test pattern

as well as the psychophysical method applied. Evidence exists that the steepness strongly depends on measurement intervals: fast determinations of psychometric functions yield significantly higher slopes if compared to averaging over long-term data: ≈ 6.5 versus ≈ 3.5 (Roufs, 1973; Watson, 1982a; Blommaert, 1987). This indicates that one should be very cautious in applying a steepness value as a parameter describing nonlinear integration in deterministic models. Koenderink and van Doorn (1978), who emphasized the role of spatial power mediating detection and apparent-contrast constancy at low suprathreshold contrast levels, proposed 'pythagorean' summation over all units in their stack model: $p = q = 2$. Later on (Koenderink and van Doorn, 1982) they concluded that $p\alpha = 2$ if p equals the summation exponent and α equals the exponent in Weber's law on contrast discrimination: $\Delta m \propto m^\alpha$. Legge's (1981) discrimination exponents for two frequencies substituted, i.e. $\alpha = 0.6$ and $\alpha = 0.7$, gives p values of 3.33 and 2.8 respectively. Hence, our present values $p = 2.5$ in case of $q \uparrow \infty$ and $p = 5$ in case of $q = 1$ seem quite acceptable. Besides, since we considered the extreme values of q , it can be expected that some intermediate value of q renders comparable predictions for the various patterns if $2.5 \leq p \leq 5$. Such an intermediate condition renders also a different estimate of the window diameter describing the local probability summation effect. Whether such a model is able to bridge the 1 log unit difference between the lowest detection thresholds as measured for disks and gratings is questionable however.

Suggestions for further modelling

We would like to mention two other possibilities open for further investigation. The first one consists of more local summation between channel responses. This proposal is increasingly suggested by the strictly local character of subliminal summation (Graham et al., 1978; Watson, 1982b) and frequency adaptation (Williams et al., 1982; Perizonius et al., 1985), and supported by the relevant model computations carried out by Koenderink and van Doorn (1978 and 1982). The models used so far are based on independent response evaluation within channels: local probability summation in combination with the determination of the maxima of the respective channel responses somewhere in the visual field. In a second step these maxima are combined by linear summation, the inclusive-OR rule and in the general case nonlinear pooling. This model structure therefore neglects the possibility of local summation between receptive fields which belong to different channels. Restricting ourselves to the one-dimensional case for the sake of simplicity, the steps involved in the models can be described and further generalized. The response R_j of channel j , with a line spread function $LSF_j(x)$, to a luminance pattern $\ell(x)$ is obtained by convolution

$$R_j(x) = \ell(x) \otimes LSF_j(x) \quad (1)$$

successive sampling over a (bounded) regular mesh

$$R_{i,j} = |R_j(x_i)|; \quad x_i = i\Delta x; \quad -N \leq i \leq N \quad (2)$$

where Δx and N may depend on the channel, and nonlinear summation of the sampled values

$$R_j = \left(\sum_i R_{i,j}^p \right)^{1/p} \quad (3)$$

The overall response R of the model is determined by nonlinear summation over different channels

$$R = \left(\sum_j R_j^q \right)^{1/q} = \left[\sum_j \left\{ \left(\sum_i R_{i,j}^p \right)^{1/p} \right\}^q \right]^{1/q} \quad (4)$$

If the summation exponents p and q are equal it follows that

$$R = \left[\sum_j \sum_i R_{i,j}^p \right]^{1/p} \quad (5)$$

This simplified description illustrates the possible equivalence of summation over the location in the visual field and summation over channels, i.e. neighbouring receptive fields within one channel and overlapping fields across channels. The stack model described by Koenderink et al. (1978 and 1982), for instance, is proposed to perform this type of summation over all units. Since the summation over locus and channel is equivalent, eq. (5) can be rewritten as

$$R = \left[\sum_i \sum_j R_{i,j}^p \right]^{1/p} \quad (6)$$

and, going back to the structure of eq. (4), generalized by postulating

$$R = \left[\sum_i \left\{ \left(\sum_j R_{i,j}^q \right)^{1/q} \right\}^p \right]^{1/p} \quad (7)$$

This means that the channel responses at location x_i are summed with an exponent q first, followed by summation over the visual field with an exponent p , the latter possibly being performed by using a local spatial window. Looking at the channel responses to sinewave gratings and to edges (broad bars, large disks), the difference between the implementations of eqs. (4) and (7) can be illustrated. The responses to a sinewave grating are sinusoids with the same frequency and phase. Summation of the maxima of these sinusoids and the maximum of the summed sinusoids are therefore completely equivalent. However, the spatial responses to an edge are

different, with maxima at different distances from the edge. Hence, the response according to eq. (7) will be lower if compared to that according to eq. (4). Accordingly, the model prediction in case of eq. (7) would yield a higher threshold for large disks if the model parameters are established to fit the threshold curve of sinewave gratings.

Interesting would be the extreme case $q = 1$, being linear local response summation. If the distributions of receptive fields approximate a continuum, then

$$R(x) = \sum_j \{\ell(x) \otimes LSF_j(x)\} = \ell(x) \otimes \sum_j LSF_j(x) \quad (8)$$

If

$$R_i = |R(x_i)|; x_i = i\Delta x; -N \leq i \leq N \quad (9)$$

it follows that

$$R = \left(\sum_i R_i^p\right)^{1/p} \quad (10)$$

In this case the nonlinear multichannel model can be replaced by a linear single channel model, followed by probability summation over a (local) window of the spatial response. Although the existence of multiple channels is assumed in order to be able to describe for instance the frequency-selective threshold elevation evoked by preadaptation, the advantage of the simplicity of a single-channel analysis has been gained. Note that this would be a continuation of the Campbell and Robson (1968) approach, be it that the nonlinear process of probability summation has to be considered. This proposal may be justified by regarding the amplitude responses of the narrowest channel to the various spatial patterns presented in sections 8.2 and 8.3. These responses, computed by using a relatively narrow-bandwidth bandpass filter, were shown to display the properties as required by the measured threshold curves, in particular if probability summation was assumed. It may therefore be expected that any (DOG) bandpass filter, even a broad-bandwidth one with a modulation transfer function that corresponds to the contrast sensitivity function as measured with sinewave gratings, will predict threshold curves for other patterns quite close to measured ones. Some data often referred to in order to argue the necessity of independent channels could be easily explained for: Detection of a compound grating, obtained by summing sinusoids of frequencies f and $3f$, does not depend on the phase difference (Graham and Nachmias, 1971). The response in the *peaks-add* situation is narrower, with a higher maximum, if compared to the response in the *peaks-subtract* situation. If both responses are sampled and integrated over a local window, a suitable choice of the probability summation parameters p , N and Δx might cause exactly

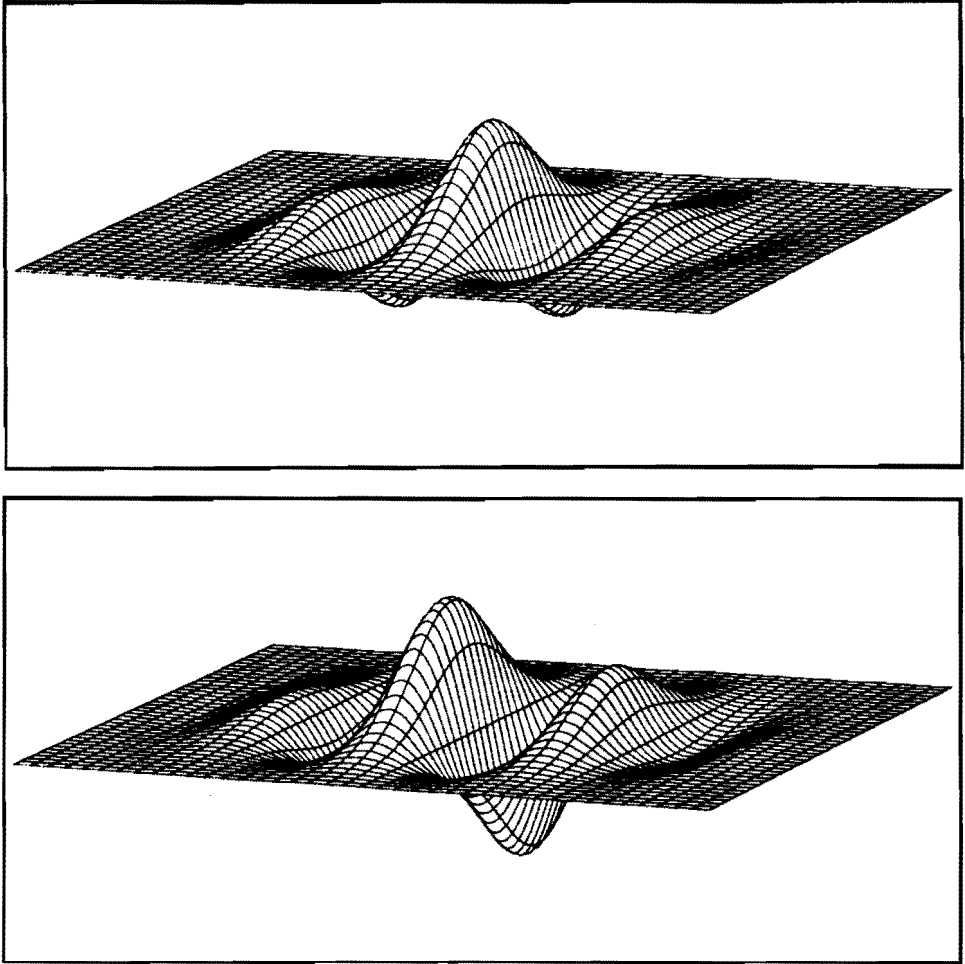


Figure 19: Receptive field profiles of even- and odd-symmetry, orientation-selective simple cells in the visual cortex, freely adopted from Mostafavi et al. (1976) and Marčelja (1980).

equal model responses R . This is confirmed by predictions based on a single space-invariant channel model (Graham et al., 1978) with $p \approx 1.5$. However, it is likely that the extreme case $q = 1$ must be rejected on the basis of other data sets.

A second possibility open for further investigation would be using models that increasingly resemble the neuronal structures as physiologically demonstrated. Images are at the retinal level coded by correlation with radially symmetric, both in space and spatial extent distributed, receptive fields. They are further analyzed in the lateral geniculate nucleus and the visual cortex.

One of the outstanding properties of the visual cortex is the coding by elongated, Gabor-function like, receptive fields having different orientations in different layers (e.g. Marčelja, 1980; Mostafavi et al., 1976). It is even assumed that images are analyzed by complete decomposition into local features, accomplished by still more complex receptive field types (e.g. Hubel and Wiesel, 1979; Marr, 1982; Perrett et al., 1983; Mistlin et al., 1984). Although our present insight into these mechanisms, and the role they play in the reconstruction of images in particular, is far from complete, it is conceivable that a relatively simple model which consists of circular channels followed by orientation-selective ones can explain the present data.

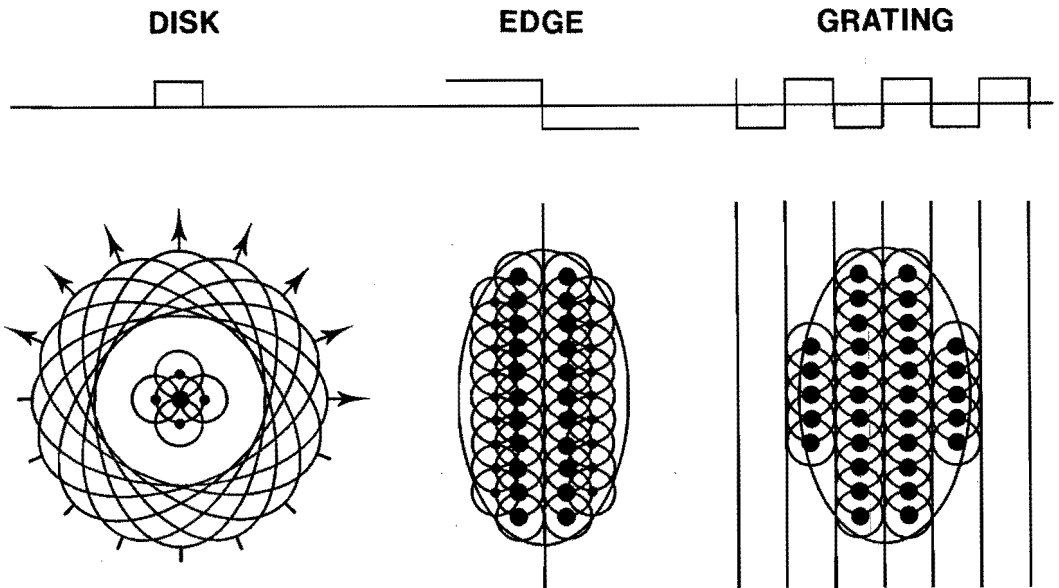


Figure 20: Graphic illustration of simple cells combining neighbouring ganglion cells. The outer extent of a simple cell is indicated by a large ellipse, the excitative centre of a ganglion cell by an open circle. Solid circles denote more (big circles) or less (small circles) responding ganglion cells.

At the retinal level there is no preference of the receptive fields: the maximum of a channel response in case of disks and in case of sinewave gratings are equal; see section 8.2. These maxima occur for a disk diameter that corresponds to the excitative centre diameter (zero crossing) of the PSF, and for a grating frequency with a period approximately twice the excitative centre of the LSF, sometimes called best diameter and best frequency. Going from the retinal level to the cortical level, neighbouring ganglion cells with similar DOG-shaped receptive field profiles are combined into the more complex fields as displayed by so-called 'simple cells', having even or odd symmetry and different orientations; see Fig. 19. Only regarding one receptive field class, viz. being retinal and cortical channels with similar radial bandwidths, the influence of combining retinal ganglion cells could help in explaining the sensitivity difference observed between disks and gratings. An even-symmetry simple cell will roughly respond on the basis of a single ganglion cell if the latter is excited by its best disk, see the left panel of Fig. 20, and all simple cells with different orientations will equally respond. In case of an edge or large disk, see the middle panel of Fig. 20, an odd-symmetry simple cell with an orientation parallel to the edge will be dominant, its response being determined by weighted summation of ganglion cells alongside the edge. The response of such a cell will be maximum in case of a grating, see the right panel of Fig. 20. Hence, the response of a single simple cell to a best-frequency grating is expected to be much higher if compared to its response to a best-diameter disk.

An additional and perhaps useful parameter in bridging the sensitivity difference between disks and gratings is the number or density of ganglion cells which are combined by a simple cell. If the number of contributing ganglion cells increases, the response of a simple cell may increase as well. A problem not yet solved is the coding from ganglion cells to simple cells. If it is assumed that this coding takes place by simple weighted summation, the accordingly weighted sum of the circular receptive fields of ganglion cells should approximate the orientation-selective receptive field of a simple cell. Hartmann (1982) demonstrated such a coding process in case of DOG-shaped profiles. He showed that weighted summation of circular receptive fields can result in also circular but larger receptive fields. He even suggested the recursive application of this coding process between different levels of processing. Hence, the examination of weighted summation of circular receptive fields into orientation-selective ones would be quite interesting.

As for probability summation between neighbouring receptive fields at the retinal level, there may be a cortical equivalent. A rationale for this presumption might be the rather stochastic firing rate of neurons. An isolated firing neuron signalling action in its receptive field may pass unnoticed. Real action, which occurs for larger objects in the visual field and which coincides with the presence of extended, elongated edges for instance, may not be neglected. The importance of an object can be emphasized by local summation: the mutual activation of

neighbouring firing neurons requesting attention.

Accordingly, the possibility of probability summation over neighbouring simple cells, with different orientations located at the same place, with equal directions though lying in line or just in parallel, or even with different radial bandwidths, perhaps involving different summation exponents and spatial windows, may not be rejected in advance. On the other hand, the combination of simple retinal receptive fields into more and more complex cortical fields, resembling high level feature extraction, is already accomplished at any level by the weighted summation of neurons one level lower. This might mean that probability summation, with all the additional and complicating parameters, may not be required to a first approximation.

In conclusion, a model that consists of initial radially symmetric channels followed by orientation-selective channels seems, at first sight, promising in unifying threshold curves of disks and of gratings. Although a relatively simple model structure might do, there are quite some possibilities to be considered and actual prediction computations might become rather laborious.

References

- Arend, L.E. (1973) Spatial factors in the Broca-Sulzer phenomenon. *J. Opt. Soc. Am.* 63, 879-883.
- Arend, L.E. (1976) Temporal determinants of the form of the spatial contrast threshold MTF. *Vision Res.* 16, 1035-1042.
- Arend, L.E. and Lange, R.V. (1980) Narrow-band spatial mechanisms in apparent contrast matching. *Vision Res.* 20, 143-147.
- Arend, L.E., Lange, R.V. and Sandick, B.L. (1981) Nonlocal determination of brightness in spatially periodic patterns. *Perc. and Psychoph.* 29, 310-316.
- Bagrash, F.M. (1973) Size-selective adaptation: psychophysical evidence for size-tuning and the effects of stimulus contour and adapting flux. *Vision Res.* 13, 575-598.
- Bartleson, C.J. and Breneman, E.J. (1967a) Brightness reproduction in the photographic process. *Photographic Science and Engineering* 11, 254-262.
- Bartleson, C.J. and Breneman, E.J. (1967b) Brightness perception in complex fields. *J. Opt. Soc. Am.* 57, 953-957.
- Bartleson, C.J. (1968) Criterion for tone reproduction. *J. Opt. Soc. Am.* 58, 992-995.
- Bartleson, C.J. and Breneman, E.J. (1973) Differences among responses of observers in scaling brightness. *Die Farbe* 22, 200-211.
- Békésy, G. von (1968) Mach- and Hering-type lateral inhibition in vision. *Vision Res.* 8, 1483-1499.
- Bergen, J.R., Wilson, H.R. and Cowan, J.D. (1979) Further evidence for four mechanisms mediating vision at threshold: sensitivities to complex gratings and aperiodic stimuli. *J. Opt. Soc. Am.* 69, 1580-1587.
- Bergström, S.S. (1973) A note on the neural unit model for contrast phenomena. *Vision Res.* 13, 2087-2092.
- Biondini, A.R. and de Mattiello, M.L.F. (1985) Suprathreshold contrast perception at different luminance levels. *Vision Res.* 25, 1-9.
- Björklund, R.A. and Magnussen, S. (1979) Decrement versions of the Broca-Sulzer effect and its spatial analogue. *Vision Res.* 19, 155-157.
- Blakemore, C. and Campbell, F.W. (1969) On the existence of neurones in the human visual system selectively sensitive to the orientation and size of retinal images. *J. Physiol.* 203, 237-260.
- Blakemore, C., Muncey, J.P.J. and Ridley, R.M. (1973) Stimulus specificity in the human visual system. *Vision Res.* 13, 1915-1931.
- Blommaert, F.J.J. and Roufs, J.A.J. (1981) The foveal point spread function as a determinant for detail vision. *Vision Res.* 21, 1223-1233.
- Blommaert, F.J.J. (1987) Vision of details in space and time. Doctoral thesis, University of Technology Eindhoven, The Netherlands.

- Bodmann, H.W., Haubner, P. and Marsden, A.M. (1979) A unified relationship between brightness and luminance. C.R. CIE, Proc. 19th session, Kyoto 1979, 99-102.
- Bowen, R.W. and Pokorny, J. (1978) Target edge sharpness and temporal brightness enhancement. *Vision Res.* 18, 1691-1695.
- Bowen, R.W. and Markell, K.A. (1980) Temporal brightness enhancement studied with a large sample of observers: evidence for individual differences in brightness perception. *Perc. and Psychoph.* 27, 465-476.
- Bowker, D.O. (1983) Suprathreshold spatiotemporal response characteristics of the human visual system. *J. Opt. Soc. Am.* 73, 436-440.
- Bracewell, R.N. (1978) *The Fourier transform and its applications*. McGraw-Hill Kogakusha LTD., Tokyo.
- Brink, G. van den and Keemink, C.J. (1976) Luminance gradients and edge effects. *Vision Res.* 16, 155-159.
- Broca, A. and Sulzer, D. (1902) La sensation lumineuse en fonction du temps. *Journal de Physiologie et de Pathologie Générale* 4, 632-640.
- Bryngdahl, O. (1966) Characteristics of the visual system: psychophysical measurements of the response to spatial sinewave stimuli in the photopic region. *J. Opt. Soc. Am.* 56, 811-821.
- Budrikis, Z.L. (1973) Model approximations to visual spatiotemporal sinewave threshold data. *B.S.T.J.* 52, 1643-1667.
- Burkhardt, D.A., Gottesman, J., Kersten, D. and Legge, G.E. (1984) Symmetry and constancy in the perception of negative and positive luminance contrast. *J. Opt. Soc. Am.* A1, 309-316.
- Campbell, F.W. and Green, D.C. (1965) Optical and retinal factors affecting visual resolution. *J. Physiol.* 181, 576-593.
- Campbell, F.W. and Gubisch, R.W. (1966) Optical quality of the human eye. *J. Physiol.* 186, 558-578.
- Campbell, F.W. and Robson, J.G. (1968) Application of Fourier analysis to the visibility of gratings. *J. Physiol.* 197, 551-566.
- Campbell, F.W., Carpenter, R.H.S. and Levinson, J.Z. (1969) Visibility of aperiodic patterns compared with that of sinusoidal gratings. *J. Physiol.* 204, 283-298.
- Campbell, F.W., Howell, E.R. and Johnstone, J.R. (1978) A comparison of threshold and suprathreshold appearance of gratings with components in the low and high spatial frequency range. *J. Physiol.* 284, 193-201.
- Campbell, F.W., Johnstone, J.R. and Ross, J. (1981) An explanation for the visibility of low frequency gratings. *Vision Res.* 21, 723-730.
- Cannon, M.W. (1979) Visual contrast perception: an approximately linear process. *Proc. Int. Conf. Cybernetics and Society*, Denver, CO-USA, oct. 1979, 444-448.

- Cannon, M.W. (1980) Suprathreshold transfer characteristics of the human visual system. Proc. Int. Conf. Cybernetics and Society, Boston, MA-USA, oct. 1980, 410-414.
- Cannon, M.W. (1985) Perceived contrast in the fovea and periphery. *J. Opt. Soc. Am. A2*, 1760-1768.
- CIE (1981) An analytic model for describing the influence of lighting parameters upon visual performance. Publication CIE No. 19/2.1 (TC-3.1).
- Cohn, T.E. (1974) A new hypothesis to explain why the increment threshold exceeds the decrement threshold. *Vision Res.* 14, 1277-1279.
- Cornsweet, T.N. (1970) *Visual perception*. Academic Press, N.Y.
- Cornsweet, T.N. and Yellott, J.I. (1985) Intensity-dependent spatial summation. *J. Opt. Soc. Am. A2*, 1769-1786.
- Curtis, D.W., Attneave, F. and Harrington, T.L. (1968) A test of a two-stage model of magnitude judgment. *Perc. and Psychoph.* 3, 25-31.
- Curtis, D.W. (1970) Magnitude estimations and category judgments of brightness and brightness intervals: a two-stage interpretation. *J. Exp. Psychol.* 83, 201-208.
- Curtis, D.W. and Rule, S.J. (1972) Magnitude judgments of brightness and brightness difference as a function of background reflectance. *J. Exp. Psychol.* 95, 215-222.
- Davidson, M. (1968) Perturbation approach to spatial brightness interaction in human vision. *J. Opt. Soc. Am.* 58, 1300-1308.
- DePalma, J.J. and Lowry, E.M. (1962) Sinewave response of the visual system. II Sinewave and squarewave contrast sensitivity. *J. Opt. Soc. Am.* 52, 328-335.
- De Valois, R.L. and De Valois, K.K. (1980) Spatial vision. *Ann. Rev. Psychol.* 31, 309-341.
- Drum, B. (1984) Flicker and suprathreshold spatial summation: evidence for a two-channel model of achromatic brightness. *Perc. and Psychoph.* 36, 245-250.
- Ekman, G. (1956) Discriminal sensitivity on the subjective continuum. *Acta Psychologica* 12, 233-243.
- Ekman, G. (1964) Is the power law a special case of Fechner's law? *Perc. and Motor Skills* 19, 730.
- Erning, L. van (1984) On visual percepts related to receptive and perceptive field properties. Doctoral thesis, Nijmegen University, The Netherlands.
- Fagot, R.F. (1963) On the psychophysical law and estimation procedures in psychophysical scaling. *Psychometrika* 28, 145-160.
- Franzén, O. and Berkley, M. (1975) Apparent contrast as a function of modulation depth and spatial frequency. *Vision Res.* 15, 655-660.
- Furukawa, T. and Hagiwara, S. (1978) A nonlinear receptive field model of the visual system. *IEEE BME-25*, 76-83.
- Georgeson, M.A. and Sullivan, G.D. (1975) Contrast constancy: deblurring in human vision by spatial frequency channels. *J. Physiol.* 252, 627-656.

- Georgeson, M.A. and Harris, M.G. (1984) Spatial selectivity of contrast adaptation: models and data. *Vision Res.* 24, 729-749.
- Ginsburg, A.P. and Cannon, M.W. (1980) Suprathreshold processing of complex visual stimuli: evidence for linearity in contrast perception. *Science* 208, 619-621.
- Glezer, V.D. (1965) The receptive fields of the retina. *Vision Res.* 5, 497-525.
- Gottesman, J., Rubin, G.S. and Legge, G.E. (1981) A power law for perceived contrast in human vision. *Vision Res.* 21, 791-799.
- Graham, N. and Nachmias, J. (1971) Detection of grating patterns containing two spatial frequencies: A comparison of single-channel and multiple-channel models. *Vision Res.* 11, 251-259.
- Graham, N., Robson, J.G. and Nachmias, J. (1978) Grating summation in fovea and periphery. *Vision Res.* 18, 815-825.
- Greenlee, M.W. and Magnussen, S. (1985) Third-harmonic adaptation and the perception of squarewave gratings. *Perception* 14, A3.
- Hall, C.F. and Hall, E.L. (1977) A nonlinear model for the spatial characteristics of the human visual system. *IEEE SMC-7*, 161-170.
- Hamada, J. (1984) A multi-stage model for border contrast. *Biol. Cyb.* 51, 65-70.
- Hamerly, J.R., Quick, R.F. and Reichert, T.A. (1977) A study of grating contrast judgment. *Vision Res.* 17, 201-207.
- Hanes, R.M. (1951) Suprathreshold area brightness relationships. *J. Opt. Soc. Am.* 41, 28-31.
- Hartmann, G. (1982) Recursive features of circular receptive fields. *Biol. Cyb.* 43, 199-208.
- Hauske, G., Wolf, W. and Lupp, U. (1976) Matched filters in human vision. *Biol. Cyb.* 22, 181-188.
- Hay, G.A. and Chesters, M.S. (1972) Signal transfer functions in threshold and suprathreshold vision. *J. Opt. Soc. Am.* 62, 990-998.
- Hay, G.A. and Chesters, M.S. (1977) A model of visual threshold detection. *J. Theor. Biol.* 67, 221-240.
- Henning, G.B., Hertz, B.G. and Hinton, J.L. (1981) Effects of different hypothetical detection mechanisms on the shape of spatial frequency filters inferred from masking experiments: I. Noise masks. *J. Opt. Soc. Am.* 71, 574-581.
- Higgins, K.E. and Rinalducci, E.J. (1975) Suprathreshold intensity area relationships: a spatial Broca-Sulzer effect. *Vision Res.* 15, 129-143.
- Higgins, K.E. and Knoblauch, K. (1977) Spatial Broca-Sulzer effect at brief stimulus durations. *Vision Res.* 17, 332-334.
- Hipparchus (150 B.C.) Greek astronomer who lived on Rhodes island. e.g. *The Mitchell Beazley Joy Of Knowledge Library - Fact Index*; Mitchell Beazley Encyclopaedias Limited, London, 1976.
- Hirsch, J. and Hylton, R. (1982) Limits of spatial frequency discrimination as evidence of neural interpolation. *J. Opt. Soc. Am.* 72, 1367-1374.

- Horeman, H.W. (1965) Relations between brightness and luminance under induction. *Vision Res.* 5, 331-340.
- Hubel, D.H. and Wiesel, T.N. (1979) Brain mechanisms of vision. In: *The brain*, Scientific American Book, Freeman and Comp., San Francisco, 84-97.
- Jamar, J.H.T. and Koenderink, J.J. (1985) Contrast detection and detection of contrast modulation for noise gratings. *Vision Res.* 25, 511-521.
- Jaschinski-Kruza, W. and Cavonius, C.R. (1984) A multiple channel model for grating detection. *Vision Res.* 24, 933-941.
- Jaschinski-Kruza, W. (1984b) Detection of luminance gradients: sensitivity to low-frequency trapezoid-wave gratings. *Perception* 13, A29.
- Julesz, B. (1962) Visual pattern discrimination. *IRE Trans. Information Theory* IT-8, 84-92.
- Julesz, B. and Schumer, R.A. (1981) Early visual perception. *Ann. Rev. Psychol.* 32, 575-627.
- Kelly, D.H. and Magnuski, H.S. (1975) Pattern detection and the two-dimensional Fourier transform: circular targets. *Vision Res.* 15, 911-915.
- Kelly, D.H. (1984) Retinal inhomogeneity. I. Spatiotemporal contrast sensitivity. *J. Opt. Soc. Am.* A1, 107-113.
- Kelly, D.H. and Burbeck, C.A. (1984) Critical problems in spatial vision. *Crit. Rev. Biomed. Eng.* 10, 125-177.
- Koenderink, J.J. and Doorn, A.J. van (1978) Visual detection of spatial contrast; influence of location in the visual field, target extent and illuminance level. *Biol. Cyb.* 30, 157-167.
- Koenderink, J.J. and Doorn, A.J. van (1982) Invariant features of contrast detection: an explanation in terms of self-similar detector arrays. *J. Opt. Soc. Am.* 72, 83-87.
- Krüger, J. and Fischer, B. (1975) Symmetry between the visual B- and D-systems and equivalence of center and surround: studies of light increment and decrement in retinal and geniculate neurons of the cat. *Biol. Cyb.* 20, 223-236.
- Kulikowski, J.J. (1976) Effective contrast constancy and linearity of contrast sensation. *Vision Res.* 16, 1419-1431.
- Legéndy, C.R. (1975) Can the data of Campbell and Robson be explained without assuming Fourier analysis? *Biol. Cyb.* 17, 157-163.
- Legge, G.E. (1981) A power law for contrast discrimination. *Vision Res.* 21, 457-467.
- Lowry, E.M. and DePalma, J.J. (1961) Sinewave response of the visual system. I. The Mach phenomenon, 740-746. II. Determination and evaluation of the spread function, 474. *J. Opt. Soc. Am.* 51.
- Luce, R.D. and Edwards, W. (1958) The derivation of subjective scales from just noticeable differences. *Psychol. Rev.* 65, 222-236.
- MacLeod, I.D.G. and Rosenfeld, A. (1974) The visibility of gratings: spatial frequency channels or bar-detecting units. *Vision Res.* 14, 909-915.

- Magnussen, S. and Glad, A. (1975) Brightness and darkness enhancement during flicker: perceptual correlates of neuronal B- and D-systems in human vision. *Exp. Brain Res.* 22, 399-413.
- Mansfield, R.J.W. (1973) Brightness function: effect of area and duration. *J. Opt. Soc. Am.* 63, 913-920.
- Marčelja, S. (1980) Mathematical description of the responses of simple cortical cells. *J. Opt. Soc. Am.* 70, 1297-1300.
- Marks, L.E. (1974) *Sensory processes. The new psychophysics.* Academic Press, New York.
- Marr, D. (1982) *Vision.* Freeman and Comp., San Francisco.
- Matthews, M.L. (1966) Appearance of Mach bands for short durations and at sharply focused contours. *J. Opt. Soc. Am.* 56, 1401-1402.
- Mayhew, J.E.W. and Frisby, J.P. (1978) Suprathreshold contrast perception and complex random textures. *Vision Res.* 18, 895-897.
- McCollough, C. (1955) The variation in width and position of Mach bands as a function of luminance. *J. Exp. Psychol.* 49, 141-152.
- Mistlin, A.J., Potter, D.D., Head, A.S., Perrett, D.I., Milner, A.D. and Jeeves, M.A. (1984) Neuronal sensitivity to body view and posture and type of motion. *Perception* 13, A31.
- Mostafavi, H. and Sakrison, D.J. (1976) Structure and properties of a single channel in the human visual system. *Vision Res.* 16, 957-968.
- Nachmias, J. (1981) On the psychometric function for contrast detection. *Vision Res.* 21, 215-223.
- Nes, F.L. van (1968) *Experimental studies in spatiotemporal contrast transfer by the human eye.* Doctoral thesis, Utrecht University, The Netherlands.
- Olzak, L.A. and Thomas, J.P. (1986) Seeing spatial patterns, 7.1-7.56. In: *Handbook of perception and human performance*; Vol. 1: *Sensory processes and perception*, K.R. Boff, L. Kaufman and J.P. Thomas Editors, Wiley-Interscience, New York.
- Onley, J.W. (1961) Light adaptation and the brightness of brief foveal stimuli. *J. Opt. Soc. Am.* 51, 667-673.
- Oppenheim, A.V., Schafer, R.W. and Stockham, T.G. (1968) Nonlinear filtering of multiplied and convolved signals. *Proc. IEEE*, Vol. 56, 1264-1291.
- Patel, A.S. (1966) Spatial resolution by the human visual system: the effect of mean retinal illuminance. *J. Opt. Soc. Am.* 56, 689-694.
- Perizonius, E., Schill, W., Geiger, H. and Röhler, R. (1985) Evidence on the local character of spatial frequency channels in the human visual system. *Vision Res.* 25, 1233-1240.
- Perrett, D.I., Smith, P.A.J., Milner, D. and Jeeves, M.A. (1983) Visual cells sensitive to face orientation and direction of eye gaze in the macaque monkey. *Perception* 12, A13.

- Pollehn, H. and Roehrig, H. (1970) Effect of noise on the modulation transfer function of the visual channel. *J. Opt. Soc. Am.* 60, 842-848.
- Poulton, E.C. (1968) The new psychophysics: six models for magnitude estimation. *Psychol. Bulletin* 69, 1-19.
- Poulton, E.C. (1979) Models for biases in judging sensory magnitude. *Psychol. Bulletin* 86, 777-803.
- Pratt, W.K., Faugeras, O.D. and Gagalowicz, A. (1978) Visual discrimination of stochastic texture fields. *IEEE Vol. SMC-8*, 796-804.
- Quick, R.F. (1974) A vector-magnitude model of contrast detection. *Kybernetik* 16, 65-67.
- Quick, R.F., Hamerly, J.R. and Reichert, T.A. (1976) The absence of a measurable critical band at low suprathreshold contrasts. *Vision Res.* 16, 351-355.
- Quinn, P.C. (1985) Suprathreshold contrast perception as a function of spatial frequency. *Perc. and Psychoph.* 38, 408-414.
- Ratliff, F. (1965) Mach bands: quantitative studies on neural networks in the retina. Holden-Day Inc., San Francisco, California.
- Richardson, L.F. (1929) Quantitative mental estimates of light and colour. *British J. Psychol. (General Section)* 20, 27-37.
- Ridder, H. de (1987) Dynamic properties of human brightness perception. Doctoral thesis, in preparation.
- Rinalducci, E.J. and Higgins, K.E. (1971) An investigation of the effective intensity of flashing lights at threshold and suprathreshold levels. In: *The perception and application of flashing lights*; Int. Symp. London, E.D. Wright Editor, Adam Hilger, London, 113-125.
- Roufs, J.A.J. (1963) Perception lag as a function of stimulus luminance. *Vision Res.* 3, 81-91.
- Roufs, J.A.J. (1973) Dynamic properties of human vision. Doctoral thesis, Eindhoven University of Technology, The Netherlands.
- Roufs, J.A.J. (1974) Dynamic properties of vision. IV. Thresholds of decremental flashes, incremental flashes, and doublets in relation to flicker fusion. *Vision Res.* 14, 831-851.
- Roufs, J.A.J. and Blommaert, F.J.J. (1981) Temporal impulse and step responses of the human eye obtained psychophysically by means of a drift-correcting perturbation technique. *Vision Res.* 21, 1203-1221.
- Saunders, J.E. (1972) The validity of magnitude estimations of luminosity and the measurement of the relative effects of preadaptation and contrast. *Vision Res.* 12, 689-698.
- Schade, O.H. (1948) Electro-optical characteristics of television systems. I. Characteristics of vision and visual systems. *RCA Rev.*, 5-7.
- Schade, O.H. (1956) Optical and photoelectric analog of the eye. *J. Opt. Soc. Am.* 46, 721-739.

- Selwyn, E.W.H. (1948) The photographic and visual resolving power of lenses. Part I. Visual resolving power. *Phot. J.* 88B, 6-12.
- Semmelroth, C.C. (1970) Prediction of lightness and brightness on different backgrounds. *J. Opt. Soc. Am.* 60, 1685-1689.
- Shapley, R. (1974) Gaussian bars and rectangular bars: the influence of width and gradient on visibility. *Vision Res.* 14, 1457-1462.
- Simonds, J.L. (1961) A quantitative study of the influence of tone-reproduction factors on picture quality. *Photographic Science and Engineering* 5, 270-277.
- Springer, R.M. (1978) Suprathreshold information transfer in the visual system: brightness match profiles of high contrast gratings. *Vision Res.* 18, 291-300.
- Stevens, S.S. and Stevens, J.C. (1960) Brightness function: parametric effects of adaptation and contrast. *J. Opt. Soc. Am.* 50, 1139.
- Stevens, S.S. (1961) To honor Fechner and to repeal his law. *Science* 133, 80-86.
- Stevens, S.S. (1966) A metric for the social consensus. *Science* 151, 530-541.
- Stevens, S.S. (1975) *Psychophysics*. Wiley-Interscience, New York.
- Stewart, M.R., Fagot, R.F. and Eskildsen, P.R. (1967) Invariance tests for bisection and fractionation scaling. *Perc. and Psychoph.* 2, 323-327.
- Stockham, T.G. (1972) Image processing in the context of a visual model. *Proc. IEEE* 60, 828-842.
- Stromeyer, C.F. and Julesz, B. (1972) Spatial frequency masking in vision: critical bands and spread of masking. *J. Opt. Soc. Am.* 62, 1221-1232.
- Swanson, W.H., Wilson, H.R. and Giese, S.C. (1984) Contrast matching data predicted from contrast increment thresholds. *Vision Res.* 24, 63-75.
- Teghtsoonian, R. (1973) Range effects in psychophysical scaling and a revision of Stevens' law. *Am. J. Psychol.* 86, 3-27.
- Thomas, J.P. and Kovar, C.W. (1965) The effect of contour sharpness on perceived brightness. *Vision Res.* 5, 559-564.
- Toet, A. (1987) Visual perception of spatial order. Doctoral thesis, Utrecht University, The Netherlands.
- Valeton, J.M. and van Meeteren, A. (1986) Masking effects of pictorial noise. In: *First quinquennial review; Dutch Society for Pattern Recognition and Image Processing*; Editors E. Backer et al.; D.E.B. Publishers, Pijnacker, The Netherlands, 107-123.
- Vos, J.J., Walraven, J. and van Meeteren, A. (1976) Light profiles of the foveal image of a point source. *Vision Res.* 16, 215-219.
- Vrolijk, P.C. (1986) Propagating inhibition. Doctoral thesis, Rotterdam University, the Netherlands.
- Wagenaar, W.A. (1975) Stevens vs Fechner: a plea for dismissal of the case. *Acta Psychologica* 39, 225-235.
- Warren, R.M. (1976) Measurement of loudness and brightness: scaling a chimera. In: *Advances in Psychophysics*, Geissler and Zabrodin (Eds.), VEB, Berlin, 215-237.

- Watanabe, A., Mori, T., Nagata, S. and Hiwatashi, K. (1968) Spatial sinewave responses of the human visual system. *Vision Res.* 8, 1245-1263.
- Watson, A.B. (1982a) Derivation of the impulse response: comments on the method of Roufs and Blommaert. *Vision Res.* 22, 1335-1337.
- Watson, A.B. (1982b) Summation of grating patches indicates many types of detector at one retinal location. *Vision Res.* 22, 17-25.
- White, T.W., Irvin, G.E. and Williams, M.C. (1980) Asymmetry in the brightness and darkness Broca-Sulzer effects. *Vision Res.* 20, 723-726.
- Williams, D.W., Wilson, H.R. and Cowan, J.D. (1982) Localized effects of spatial-frequency adaptation. *J. Opt. Soc. Am.* 72, 878-887.
- Wilson, H.R. and Bergen, J.R. (1979) A four mechanism model for threshold spatial vision. *Vision Res.* 19, 19-32.

Summary

The research presented in this thesis is restricted to achromatic spatial vision of stimuli (mostly) quasistatically presented against a fixed photopic background. The key problem addressed concerns the difference and the relation between local brightness perception and global apparent-contrast perception. Local brightness means the brightness as perceived at a specific point of a stimulus pattern while global apparent contrast involves the contrast impression of a pattern as a whole. The difference between the perception of luminance increments and decrements on the one hand, and periodic and aperiodic patterns on the other, has also been investigated.

The nonlinear relation between brightness and luminance is commonly described by a Stevens power function, the stimulus-dependent exponent being determined by scaling methods. Comparing different scaling methods (chapter 2) it was found that magnitude estimation, where the brightness of a test stimulus is rated proportional to that of a fixed reference stimulus, is less reliable on account of the number handling and strategy of the subject. Brightness exponents can be determined also by means of bisection and fractionation: here the subject has to indicate whether the brightness of a test stimulus is halfway a given brightness interval. In case of bisection this interval is defined by two reference stimuli, while fractionation makes use of only one reference stimulus and the background, where the stimuli are superimposed on, serves as the second reference. Exponents for two stimuli determined by bisection and fractionation differed by a constant factor, which also relates to the strategy of the subject: the handling of an interval scale and a ratio scale. But exponent ratios for different stimulus combinations agreed fairly well with ratios determined by directly matching them. Besides, the transitivity of matching results, a premise often taken for granted, appeared to be quite reasonable. This means that the influence of stimulus properties, such as duration and area, upon Stevens exponents can be studied also by performing matching experiments. The established brightness exponents, their significance thus being confirmed by matching results, indicate that the nonlinear relation between brightness and luminance depends on stimulus dimensions (area and duration), on background level (if compared with published results obtained at a dark background), and on retinal position.

Subsequent studies on the brightness perception of incremental and decremental sharp disks (chapters 3 and 4) revealed that the Stevens exponent also depends on the polarity of a stimulus, as well as edge blur (chapter 5). However, for radially symmetric cosine gratings (chapter 5) significant deviations from a power function were found in the low-frequency low-contrast situation. This implies that Stevens' empirical law with simple threshold correction, which was confirmed in case of all disk-shaped stimuli, is inadequate in describing perception of periodic gratings.

Exploring the differences between local brightness and global apparent-contrast perception, it was found again that a distinction must be made with regard to disk-shaped stimuli and circular cosine gratings (chapters 3, 4 and 5). In case of large disks the brightness difference with the background and the apparent contrast with the surround increase differently with the luminance increment and decrement (chapter 3). This asymmetry also strongly depends on the disk diameter: matching either incremental or decremental disks with varying diameter yields iso-brightness and apparent iso-contrast curves showing a larger Ricco (integration) area for decrements (chapter 4). This is confirmed by the corresponding threshold curves. Moreover, curves obtained by matching the brightness in the centre, the maximum brightness near the edge (in case of increments only) or apparent contrast were different. The spatial Broca-Sulzer effect is the phenomenon that the brightness of disk-shaped stimuli, with varying diameter though constant luminance, is maximum for a specific diameter. For smaller diameters the brightness decreases while for larger ones it declines to a constant level. This effect appeared to be maximum for brightness in the centre, less pronounced for maximum brightness near the edge, and it vanished completely for apparent contrast. Detection and centre iso-brightness curves of sharp disks with varying diameter suggest that the visual system behaves like a lowpass filter at threshold and like a bandpass filter at suprathreshold levels (see page 69 Fig. 14).

Further investigating the difference between brightness and apparent contrast, it was found that the centre brightness of an incremental large disk is slightly influenced by the shape of the edge (degree of blur) while apparent contrast rapidly decreases if the disk is blurred (chapter 5). These data would support the conjecture that apparent-contrast perception is strongly related to the maximum brightness gradient at the edge.

However, circular cosine gratings behave quite differently (chapter 5). The asymmetry as found for incremental and decremental small disks was not confirmed for cosine gratings: matching either brightness maxima or brightness minima of gratings with varying spatial frequency revealed no asymmetry at all. Furthermore, the difference between brightness and apparent contrast as found for sharp and blurred disks was confirmed neither: apparent iso-contrast curves exactly equalled curves obtained by matching the brightness extremes. Hence, the results for this stimulus configuration point towards the difference between brightness extremes as a determinant for apparent-contrast perception. Opposite to the disk data, the curves suggest that the visual system behaves like a bandpass filter at threshold and like a lowpass filter at suprathreshold levels (see page 79 Fig. 5).

Detection of circular noise gratings, defined by the central frequency and bandwidth of Gaussian spectral distributions, appeared to require an increasing luminance amplitude and RMS value if the bandwidth increases while the central frequency is kept constant (chapter 7). In this situation apparent contrast is un-

affected by the bandwidth. Varying the central frequency, detection curves and apparent iso-contrast curves flatten for larger bandwidths. Apparent contrast is even independent from the frequency distribution for bandwidths larger than one octave if the RMS value is large enough. The fact that a univocal magnitude of the apparent contrast is perceived in case of these stochastic patterns emphasizes the importance of this visual percept.

The detection asymmetry found for incremental and decremental small disks, which somehow relates to the threshold curve of circular cosine gratings, was further examined by considering other stimuli (chapter 6). If disks are not quasistatically presented but dynamically (briefly pulsed), threshold curves become exactly symmetric, with a larger Ricco area as compared to the quasistatic case. This is new evidence for spatiotemporal inseparability and explains the controversy in the literature with respect to detection (a)symmetry. Threshold curves measured for single-phase rectified circular cosine gratings, which consist of either periodic luminance increments or decrements, were also symmetric: no differences were observed in the quasistatic and in the dynamic situations if the spatial phase for low frequencies is adjusted to obtain mirrored patterns. All quasistatic threshold curves display a bandpass behaviour and the dynamic ones display a lowpass behaviour, but the amplitude required for detection of a single-phase rectified grating appears to be twice that of a full cosine grating. The discrepancy between quasistatic threshold curves of incremental and decremental disks (asymmetry) and single-phase rectified circular cosine gratings (symmetry) can be explained by assuming a multiple channel model with asymmetrical amplitude transfer functions of the narrowest channel(s) and a symmetrical threshold mechanism.

The pronounced differences between data sets measured for the various patterns seem to obstruct a unification by means of a two-stage model, in which a luminance pattern is converted into a brightness pattern by the first stage and apparent contrast is deduced from the brightness pattern in the second stage. The similarity of the brightness and apparent-contrast curves obtained for disks with varying diameter (chapter 4), which raises the conjecture that apparent-contrast perception is strongly related to some property of the perceived brightness profile, would point towards such a two-stage model. However, the different conclusions established in case of blurred disks and circular cosine gratings (chapter 5), being the maximum brightness gradient respectively the difference between brightness extremes, suggest that apparent-contrast perception is highly stimulus specific, thus complicating a general description of the second stage.

Similar problems are encountered in describing the first stage which converts luminances into brightnesses. Although simple nonlinear single channel models can be devised to fit centre iso-brightness data of disks with varying diameter and to accurately predict maximum iso-brightness data (chapter 4), such models can not simultaneously cope with data on the brightness extremes of circular cosine

gratings. Moreover, more complicated though still simple nonlinear multichannel models, which consist of a limited number of bandpass filters each being combined with a nonlinear amplitude transfer function, appeared incapable to unify brightness perception of disks and gratings (chapter 5). Again, the difficulties met would support the idea of a pattern-specific visual processing.

However, considering only vision at threshold level, multichannel model computations performed for various spatial patterns indicated that a unification of disk and grating data might not be impossible (chapter 8). Assuming local probability summation within channels, correctly shaped threshold curves can be obtained, but the difference between the maximum sensitivities for disks and gratings could not yet be bridged. These model computations are based on radially symmetric point spread functions of channels, which actually is a simulation of the processing at retinal level by receptive fields. A more accurate simultaneous description of threshold curves may be achieved by considering also orientation-selective channels which simulate the cortical processing by simple cells. Such an extension of multichannel models might be advantageous, not only for the description of detection but also for the description of suprathreshold perception.

Samenvatting

Het onderzoek dat in dit proefschrift beschreven is heeft als onderwerp de achromatische visuele waarneming van spatiale patronen die (doorgaans) quasistatisch op een vaste, fotopische achtergrond gepresenteerd worden. Met name gaat het over het verschil en de relatie tussen lokale helderheid en globaal subjectief contrast. Hiermee wordt bedoeld de helderheid zoals die op een specifiek punt van een stimuluspatroon wordt ervaren en de globale contrastindruk van een stimuluspatroon als geheel. Het verschil tussen de waarneming van luminantie-incrementen en -decrementen enerzijds, en periodieke en aperiodieke patronen anderzijds, is eveneens onderzocht.

De nietlineaire relatie tussen helderheid en luminantie wordt gewoonlijk beschreven door een Stevens machtsfunctie, waarbij de stimulusafhankelijke exponent bepaald wordt middels schaling. Bij het vergelijken van verschillende schalingsmethoden (hoofdstuk 2) bleek dat magnitudeschatting, waarbij de helderheid van een teststimulus geschat wordt in verhouding tot die van een vaste referentiestimulus, minder betrouwbaar is vanwege de getalshantering en de strategie van de proefpersoon. Helderheidsexponenten kunnen ook bepaald worden middels bisectie en fractionering: hierbij moet de proefpersoon aangeven of de helderheid van een teststimulus halverwege een gegeven helderheidsinterval ligt. Bij bisectie wordt dit interval gedefinieerd door twee referentiestimuli, terwijl bij fractionering slechts een referentiestimulus gegeven wordt en de achtergrond, waarop de stimuli gesu-

perponeerd worden, als tweede referentie dient. Middels bisectie en fractionering bepaalde exponenten van twee stimuli verschilden echter een konstante faktor, hetgeen ook aan de strategie van de proefpersoon kan worden toegeschreven, namelijk het hanteren van een interval- en een ratioschaal. Maar de exponentverhoudingen voor diverse stimuluskombinaties kwamen redelijk goed overeen met verhoudingen die bepaald werden door de helderheden van deze stimuli direkt aan elkaar gelijk te stellen. De gelijkstellingsresultaten bleken ook redelijk te voldoen aan de vaak veronderstelde transitiviteit. Dit betekent dat de invloed van stimuluseigenschappen, zoals oppervlakte en duur, op de grootte van de Stevens exponent ook door het uitvoeren van gelijkstellingsexperimenten bepaald kan worden. De middels gelijkstelling bevestigde helderheidsexponenten laten zien dat de nietlineaire relatie tussen helderheid en luminantie afhangt van de stimulus dimensies (oppervlakte en duur), van het niveau van de achtergrond (als de gevonden waarden worden vergeleken met literatuurwaarden gemeten bij een donkere achtergrond), en de retinale positie.

Uit verdere experimenten op het gebied van de helderheidswaarneming van incrementele en decrementele scherpe schijven (hoofdstukken 3 en 4) bleek dat de Stevens exponent ook afhangt van de polariteit van een stimulus, en van de randscherpte (hoofdstuk 5). Voor laagfrequente rotatiesymmetrische cosinusroosters met een kleine modulatie diepte werden echter significante afwijkingen van een machtsfunctie gevonden (hoofdstuk 5). Dit impliceert dat de empirische wet van Stevens met een eenvoudige drempelcorrectie, die voldeed voor alle schijfvormige stimuli, niet goed in staat is om de waarneming van periodieke roosters te beschrijven.

Met betrekking tot het verschil tussen de waarneming van lokale helderheid en globaal subjectief contrast werd opnieuw gevonden dat een onderscheid gemaakt moet worden tussen schijfvormige stimuli en rotatiesymmetrische cosinusroosters (hoofdstukken 3, 4 en 5). Voor grote schijven neemt het helderheidsverschil met de achtergrond en het subjectieve contrast met de omgeving op verschillende wijze toe met het luminantie-increment en -decrement (hoofdstuk 3). Deze asymmetrie hangt ook sterk af van de schijfdiameter: gelijkstelling van incrementele schijven of decrementele schijven met variërende diameter resulteert in krommen van gelijke helderheid en van gelijk subjectief contrast met een groter interval waarover luminantie wordt geïntegreerd (Ricco-gebied) voor decrementen (hoofdstuk 4). Deze tendens wordt bevestigd door de betreffende drempelkrommen. Bovendien bleken krommen verkregen door gelijkstelling van de helderheid in het centrum, het helderheidsmaximum in de buurt van de rand (alleen voor incrementen) of het subjectieve contrast niet aan elkaar gelijk. Het spatiale Broca-Sulzer effect is het verschijnsel dat de helderheid van schijfvormige stimuli, bij variërende diameter doch gelijkblijvende luminantie, maximaal is voor een zekere diameter. Voor kleinere diameters neemt de helderheid af terwijl voor grotere diameters de helder-

heid een konstant niveau bereikt dat lager ligt dan het maximum. Dit effect was maximaal voor de helderheid in het centrum, ietwat minder geprononceerd voor de maximum helderheid bij de rand, en het was volledig afwezig voor het subjektieve contrast. De detektiedrempels en de krommen van een gelijke centrumhelderheid voor scherpe schijven suggereren dat het visuele systeem zich gedraagt als een laagdoorlaat filter op drempelniveau en als een banddoorlaat filter voor bovendrempelige niveaus (zie pagina 69 Fig. 14).

Verder onderzoek naar het verschil tussen helderheid en subjektief contrast liet zien dat de helderheid in het centrum van grote schijven nauwelijks beïnvloed wordt door de randscherpte terwijl het subjektieve contrast juist sterk daarvan afhangt (hoofdstuk 5). Deze gegevens bevestigen het vermoeden dat de waarneming van subjektief contrast sterk gerelateerd is aan de maximale helderheidsgradient op de rand.

Voor rotatiesymmetrische cosinusroosters wordt iets totaal anders gevonden (hoofdstuk 5). De asymmetrie zoals gevonden voor incrementele en decrementele kleine schijven werd niet bevestigd voor cosinusroosters, d.w.z. gelijkstelling van helderheidsmaxima of -minima van roosters met variërende spatiale frequentie resulteerde niet in een asymmetrie. Bovendien werd het verschil tussen helderheid en subjektief contrast, zoals gemeten voor scherpe en onscherpe schijven, niet bevestigd: krommen van een gelijk subjektief contrast zijn identiek aan krommen van gelijke helderheidsextremen. De resultaten voor deze stimulusconfiguratie wijzen er daarom op dat het verschil tussen helderheidsextremen bepalend is voor de contrastwaarneming. In tegenstelling tot de schijfresultaten suggereren de krommen dat het visuele systeem zich op drempelniveau als een banddoorlaat filter gedraagt en bovendrempelig als een laagdoorlaat filter (zie pag. 79 Fig. 5).

Voor detektie van rotatiesymmetrische ruisroosters, welke in het frequentiedomein gedefinieerd worden middels centrale frequentie en bandbreedte van een Gaussische amplitudeverdeling, blijkt bij toenemende bandbreedte een grotere amplitude en RMS waarde nodig te zijn indien de centrale frequentie ongewijzigd blijft (hoofdstuk 7). In deze situatie wordt het subjektieve contrast niet beïnvloed door de bandbreedte. Indien ook de centrale frequentie gevarieerd wordt dan worden drempelkrommen en krommen van gelijk subjektief contrast vlakker als de bandbreedte vergroot wordt. Het subjektieve contrast blijkt zelfs onafhankelijk van de frequentiedistributie voor bandbreedtes groter dan een oktaaf indien de RMS waarde maar groot genoeg is. Het feit dat een eenduidige sterkte van het subjektief contrast wordt waargenomen bij deze stochastische patronen onderstreept het belang van dit visueel percept.

De asymmetrische detektie van incrementele en decrementele kleine schijven, die op de een of andere manier gerelateerd is aan de drempelkromme voor rotatiesymmetrische cosinusroosters, is verder onderzocht aan de hand van andere stimuli (hoofdstuk 6). Als schijven in plaats van quasistatisch dynamisch, d.w.z.

kortdurend geflitst, aangeboden worden dan worden hun drempels exact symmetrisch, met een groter Ricco-gebied in vergelijking tot de quasistatische situatie. Dit is een nieuwe aanwijzing voor spatiotemporele insepareerbaarheid en verklaart de controverse met betrekking tot detektie(a)symmetrie in de literatuur. Drempelkrommen van enkelfasig gelijkgerichte rotatiesymmetrische cosinusroosters, welke bestaan uit periodieke luminantie-incrementen of -decrementen, waren ook symmetrisch: er werden geen verschillen gevonden in zowel de quasistatische als ook dynamische situatie indien de spatiale fase van laagfrequent roosters zodanig wordt veranderd dat de patronen gespiegeld zijn. Alle quasistatische drempelkrommen laten een banddoorlaat gedrag zien terwijl de dynamische een laagdoorlaat gedrag vertonen, maar de amplitude van enkelfasig gelijkgerichte cosinusroosters nodig voor detektie blijkt twee keer zo groot als die van volledige cosinusroosters. De discrepantie tussen de quasistatische drempelkrommen van incrementele en decrementele schijven (asymmetrie) en die van enkelfasig gelijkgerichte cosinusroosters (symmetrie) kan verklaard worden door een meerkanaals model aan te nemen met asymmetrische amplitude-overdrachtsfuncties voor de smalste kanalen en een symmetrisch drempelmechanisme.

De uitgesproken verschillen tussen de gegevens verkregen met de diverse stimuluspatronen belemmeren de konstruktie van een model dat bestaat uit twee deelsystemen in serie, waarin een luminantiepatroon wordt omgezet in een helderheidspatroon door het eerste systeem, en subjektief contrast wordt afgeleid van het helderheidspatroon door het tweede. De sterke gelijkenis van de krommen van gelijke helderheid en van gelijk subjektief contrast zoals gemeten met scherpe schijven (hoofdstuk 4), welke doet vermoeden dat subjektief contrast sterk gerelateerd is aan een of ander kenmerk van het waargenomen helderheidspatroon, wijst in de richting van zo'n model. De verschillende conclusies getrokken op grond van de onscherpe schijven en cosinusroosters, namelijk de maximale helderheidsgradient enerzijds en het verschil tussen helderheidsextremen anderzijds, wijzen er echter op dat de waarneming van subjektief contrast sterk afhangt van het stimulustype, en dat een algemene beschrijving van het tweede deelsysteem moeilijk wordt.

Soortgelijke problemen ontstaan bij de beschrijving van het eerste deelsysteem dat luminanties omzet in helderheden. Eenvoudige nietlineaire enkelkanaalsmodellen kunnen geformuleerd worden om de helderheid in het centrum van schijven te beschrijven. Deze zijn ook in staat om de maximum helderheid korrekt te voorspellen (hoofdstuk 4). Zulke modellen kunnen de waarneming van de helderheidsextremen van rotatiesymmetrische cosinusroosters echter niet simultaan voorspellen. Meer gecompliceerde maar nog steeds redelijk eenvoudige meerkanaalsmodellen, die bestaan uit een beperkt aantal bandfilters in combinatie met nietlineaire amplitude overdrachtsfuncties, bleken echter ook niet in staat om de helderheidswaarneming van schijven en cosinusroosters simultaan te beschrijven (hoofdstuk 5). Ook hier zouden de ondervonden problemen er op kunnen wijzen

dat de visuele verwerking sterk stimulusspecifiek is.

Als alleen de waarneming op drempelniveau beschouwd wordt, dan laten meerkanaals modelberekeningen voor diverse spatiale patronen zien dat een modelmatige vereniging van schijf- en roostergegevens niet onmogelijk hoeft te zijn (hoofdstuk 8). Drempelkrommen met een korrekte vorm kunnen verkregen worden door lokale waarschijnlijkheidssommatie binnen de kanalen te veronderstellen. Maar het verschil tussen de maximale gevoeligheid voor schijven en roosters kon nog niet overbrugd worden. Deze modelbeschouwingen zijn gebaseerd op rotatiesymmetrische puntspreidfuncties van de kanalen, hetgeen een simulatie is van de verwerking op retinaal niveau d.m.v. receptieve velden. Een betere simultane beschrijving van drempelkrommen kan bereikt worden door tevens oriëntatie-selektieve kanalen in overweging te nemen, wat aansluit bij de verwerking op corticaal niveau middels z.g. 'simple cells'. Een dergelijke uitbreiding van meerkanaalsmodellen zou voordelig kunnen zijn, niet alleen voor de beschrijving van detektie maar wellicht ook voor de beschrijving van de bovendrempelige waarneming.

Curriculum vitae

- 1951 Geboren te Venlo.
- 1963 - 1967 MULO-B te Venlo.
- 1967 - 1973 HTS-Venlo Elektrotechniek, incl. voorbereidend jaar.
- 1973 - 1981 TH-Eindhoven Elektrotechniek, onderbroken door militaire dienst (kanonnier LUA Harskamp!).
Afstudeeronderwerp: digitale beeldverbetering in de echografie, Biofysisch Lab van de afdeling Oogheelkunde, Radboud Ziekenhuis (KUN) Nijmegen.
- 1982 - 1986 Wetenschappelijk medewerker in dienst van de Stichting Biofysica van de Nederlandse Organisatie voor Zuiver Wetenschappelijk Onderzoek (ZWO), gedetacheerd op het IPO voor het verrichten van onderzoek op het gebied van de bovendrempelige contrastwaarneming.
- 1987 - Wetenschappelijk medewerker van de Ecole Polytechnique Federale de Lausanne, Laboratoire de Traitement des Signaux, Zwitserland.



Da steh' ich nun, ich armer Tor,
und bin so klug als wie zuvor.

Busch & Goethe

STELLINGEN

1. De wet van Stevens, welke zegt dat de sterkte van een waargenomen sensatie een machtsfunctie is van de daaraan ten grondslag liggende (drempelgekorrigeerde) fysische grootheid, moet beschouwd worden als een niet verifieerbare aanname.
2. Een kwantitatieve vergelijking van meetresultaten gebaseerd op de gelijkstelling van de helderheid van schijven enerzijds en die van het helderheidscontrast van sinusroosters anderzijds wordt belemmerd door het feit dat helderheid en helderheidscontrast wezenlijk van elkaar verschillende perceptieve attributen zijn.
Dit proefschrift.
3. Het feit dat een stochastisch luminantiepatroon in een eenduidig helderheidscontrast resulteert onderstreept het bijzondere belang van dit perceptief attribuut.
Dit proefschrift.
4. Het toepassen van helderheidscontrastformules in termen van luminanties moet gezien worden als een wetenschappelijk ongefundeerde en daarom overbodige gegevenstransformatie.
D.A. Burkhardt et al. (1984), J.O.S.A. A1, 309-316.
5. De omvang van het bovendrempelig visueel onderzoek staat in geen verhouding tot haar relevantie voor de normale visuele waarneming.
6. Het publiceren van psychofysische modellen door systeemtheoretisch geschoolde wetenschappers die niet over enig psychofysisch inzicht beschikken is slechts bij uitzondering een zinvolle zaak.
Z.L. Budrikis (1973), B.S.T.J. 52, 1643-1667.
H. Marko (1979), in: Biomedical Pattern Recognition and Image Processing, eds. K.S. Fu and T. Pavlidis, Berlin Dahlem Konferenzen 1979, Verlag Chemie GmbH, Weinheim, 269-296.
7. Het verdient aanbeveling om, alvorens het ensemble gemiddelde van een grote groep proefpersonen te meten, eerst het systeemgedrag van een enkele proefpersoon te bestuderen.
E.J. Bartleson and E.J. Breneman (1973), Die Farbe 22, 200-211.
R.W. Bowen et al. (1981), Perception and Psychophysics 30, 587-593.

8. De eenheid retinale verlichtingssterkte [Trolands], zijnde het produkt van luminantie [$cd.m^{-2}$] en pupilgrootte [mm^2], heeft vanwege de verwaarlozing van de filterwerking van het optische deel van het oog een beperkte geldigheid. M. Alpern (1978), in: Handbook of Optics, eds. W.G. Driscoll and W. Vaughan, McGraw-Hill, New York, 12.1-12.39.
9. Histogram hyperbolisatie en homomorf filteren kunnen weliswaar nuttige beeldverbeteringstechnieken in de digitale beeldverwerking zijn, elke argumentatie als zouden deze technieken psychofysisch verantwoord zijn is echter zeer kwestieus.
W. Frei (1977), C.G.I.P. 5, 286-294.
T.G. Stockham (1972), Proc. IEEE 60, 828-842.
10. Het middels supercomputers inkleuren van klassieke zwart-wit films getuigt van een grenzeloze minachting van ons kulturele erfgoed.
11. Ondertiteling van films, hoe storend dan ook, is gelet op het behoud van de authenticiteit veruit te prefereren boven nasynchronisatie.
12. De lijfspreuk van het IPO¹ krijgt, gelet op het even redundante als overvloedig gekonsumeerde Nederlandse televisie-aanbod, een wel heel bijzondere betekenis ten aanzien van de geestelijke volksgezondheid.

Stellingen bij het proefschrift: Spatial characteristics of brightness and apparent-contrast perception. Hans du Buf, Eindhoven, 3 november 1987.

¹PERCEPTIO AGITAT MENTEM